Theoretical and Observational Windows into the Dark Sector

by

Robert X. Sims

M.Sc. in Physics, Dartmouth College, Hanover, NH, 2017
B.S. in Physics, University of Rochester, Rochester, NY, 2014
B.S. in Mathematics, University of Rochester, Rochester, NY 2014

Submitted in partial fulfillment of the requirements
for the degree of Doctor of Philosophy
in the Department of Physics at Brown University

Providence, Rhode Island

May 2019

This dissertation by Robert X. Sims is accepted in its present form
by the Department of Physics as satisfying the
dissertation requirements for the degree of Doctor of Philosophy.

Date: _____ _____

Stephon Alexander, Advisor

Recommended to the Graduate Council

Date: _____ _____

Savvas Koushiappas, Reader

Date: _____ _____

David Lowe, Reader

Approved by the Graduate Council

Date: _____ _____

Andrew Campbell, Dean of the Graduate School

Vitae

Robert X. Sims was born in Canton, Massachusetts in 1992. He obtained his Bachelor of Science in both Mathematics and Physics from the University of Rochester in May 2014. As an undergraduate student, Robert worked on the neutrino scattering experiment, MINERνA, with advisor Arie Bodek. He obtained his Master of Science in Physics from Dartmouth College in June 2017, beginning research in Cosmology with Stephon Alexander in June 2015. Robert continued his graduate student research with Stephon Alexander at Brown University in August 2016.

Acknowledgments

First and foremost, I would like to thank my advisor Stephon Alexander, whose continuous support and belief in me has been crucial to my success. On countless occasions, he has provided optimal challenges within research, accelerating my intellectual growth as a physicist, while also giving me a degree of autonomy. Furthermore, he frequently went out of his way to introduce me to, and include me in collaborations, with renown physicists. I am grateful the time and patience he has given through the past few years, and am thankful for the unique experiences as his graduate student.

I am thankful to my numerous collaborators. Whether the project is completed, current, or cut-short, every collaborator has given me invaluable advice and provided unique perspectives on the problem at hand. In particular, I would like to thank my officemates Jatan Buch, Shing Chau Leung, and Kyriakos Vattis for the numerous insightful conversations, leading to the refinement of many research ideas.

Finally, I would like to thank the late Martin Badoian. As my high school mathematics teacher and coach of the math team, he was the central figure in my high school life. Academically, he would strive for all his students to achieve a deep level of understanding and engrained in his students the importance of hard work, both of which were crucial to my studies as a graduate student. His passion and dedication to his students was evident in every interaction, and inspired us all to be better both academically and personally. I a sincerely lucky to have spent these formative years with such a model and advisor, and I truly would not be here if it were not for all he has done.

Contents

List of Tables

List of Figures

Chapter 1

Introduction

The standard cosmological paradigm of a universe with a cosmological constant (Λ) and cold dark matter (CDM), contains six independent parameters, for which the theory gives no definite predictions of their values. Typically, the Cosmic Microwave Background auto- and cross-correlation spectra are used to find best-fit values for these six parameters [1], which can then be tested against other cosmological observables, such as Baryonic Acoustic Oscillations [2]. Thus far, ΛCDM has proven robust against many observational tests, with few discrepancies found[1].

Furthermore, inflationary models can be used to calculate the initial conditions for the ΛCDM model. While such theories (typically in tandem with assumptions about reheating dynamics) can provide theoretical motivation for some cosmological parameters, such as the scalar spectral index and the tensor-to-scalar ratio described in Section 1.3.1, these expected values of parameters are model dependent. The problem of theoretically explaining these parameters are then diverted to properly embedding inflationary models into a self-consistent, high energy field theory.

Worse still, two of the critical components of ΛCDM, the cosmological constant and the cold dark matter, dominate the evolution of the universe at late times, yet continue to evade consistent theoretical models [4] or experimental probes [5, 6, 7, 8, 9]. In particular, a combination of large scale structure, CMB power spectrum, and Big Bang nucleosynthesis differentiate dark matter from the Standard model. While hope remains for detection of beyond Standard model particles in future direct and indirect detection

[1] Recently, much attention has been given the apparent discrepancy between measurements of the Hubble parameter between the CMB and Type Ia supernova data [3].

experiments, including colliders [10], at present we are left to infer the structure of the dark sector from its gravitational interactions. This provides a vast playground to explore new theoretical and observational probes of the dark sector.

In particular, this thesis will consider primordial circular polarization, the electron's electric dipole moment, and modified gravitational waveforms as probes of the dark sector. As we will see, with recent experimental advances, these probes can provide powerful constraints on the dark sector.

1.1 Axions and Axion-like particles

Historically, axions were introduced into the literature as the pseudo-Nambu-Goldstone mode associated with breaking the $U(1)$ Peccei-Quinn symmetry [11, 12, 13]. This additional symmetry to the Standard model is imposed in order to cancel the anomalous chiral current arising from the nontrivial QCD vacuum [14, 15]. The phenomenological use of the QCD axion in resolving the Strong CP problem heavily restricts the number of free parameters of the model. In particular, the mass of the axion can be related to the symmetry breaking scale f_a as

$$m_a = \frac{m_\pi f_\pi}{f_a} \frac{\sqrt{m_u m_d}}{m_u + m_d} \approx \left(6 \times 10^{-6} \text{ eV}\right) \left(\frac{10^{12} \text{ GeV}}{f_a}\right), \tag{1.1}$$

where f_π is the pion decay constant and m_u, m_d, m_π are the masses of the up quark, down quark, and pion, respectively.

While research has continued with the QCD axion, in particular investigating the DFSZ [16, 17] and KSVZ [18, 19] models, much of the interest in cosmology comes from a generalized version of the axion. To make direct connection with the Peccei-Quinn axion described above, one may consider further modifications of the Standard model by introducing additional anomalous $U(1)$ symmetries [20]. Each broken symmetry can result in a new pseudo-scalar with axion-like interactions. More generally, these axion-like particles (ALP) can arise from a variety of high energy theories, including the compactification of higher dimensions in string theory [21, 22].

The properties of the ALP may contain physical quantities which are currently not observed, such as the energy scale f_a in Eq. (1.1), which significantly expands the allowed parameter space of the "low" energy theory. Instead, the ALP interactions are treated

as an effective field theory, with the phenomenological goal of constraining particular interactions at a given energy scales. This perspective endows ALP with tremendous versatility in cosmological settings, such as models of inflation [23] and dark matter [24, 25, 26, 27].

1.2 The Horizon Problem and Inflation

Current observations [28] of the Cosmic Microwave Background (CMB) verifies the cosmological principle that the early universe was nearly homogeneous and isotropic. Furthermore, the redshifting of light from supernova [29] provides strong evidence for the expansion of space. With these observations, the universe is well described by the Friedmann-Lemaitre-Robertson-Walker (FLRW) metric, given in comoving Cartesian coordinates as

$$g_{\mu\nu} = \begin{pmatrix} -1 & 0 & 0 & 0 \\ 0 & a(t)^2 & 0 & 0 \\ 0 & 0 & a(t)^2 & 0 \\ 0 & 0 & 0 & a(t)^2 \end{pmatrix}, \tag{1.2}$$

where $a(t)$ is the scale factor. For a given stress-energy tensor $T_{\mu\nu}$, the Einstein equations can be used to find evolution equations for the scale factor.

If the only matter content of the universe is a collection of perfect fluids, each with energy density ρ_i and pressure p_i, the nonzero components of the Einstein equations can be written explicitly as the Friedmann equations:

$$H^2 = \frac{1}{3M_p^2} \sum_i \rho_i, \tag{1.3}$$

$$\dot{H} + H^2 = -\frac{1}{6M_p^2} \sum_i \rho_i + 3p_i, \tag{1.4}$$

where dots represent time derivatives, $H \equiv \dot{a}/a$ is the Hubble parameter, and the Planck mass is given by $M_p^{-2} = 8\pi G$. When the universe is dominated by a single fluid with equation of state $w = p/\rho$, the Friedmann equations can be solved to give the scale

factor as a function of time as

$$a(t) = \begin{cases} a_0(\frac{t}{t_0})^{\frac{2}{3(1+w)}} & w \neq -1, \\ a_0 e^{H(t-t_0)} & w = -1, \end{cases} \tag{1.5}$$

where t_0 is the some initial time, and the initial scale factor is given by $a_0 = a(t_0)$.

The comoving particle horizon can be used to find regions which was, at some time, in causal contact. The particle horizon is given as the conformal time

$$\eta(t) = \int_0^t \frac{\mathrm{d}t'}{a(t')} \propto t^{\frac{1+3w}{3(1+w)}}, \tag{1.6}$$

for $\omega \neq -1$. For a universe dominated by either matter or radiation (or $w > -1/3$), the particle horizon monotonically increases in time. Thus, the largest scales observed today could not have been in causal contact at the surface of last scattering. Furthermore, using the physical size of the particle horizon $d = a(t)\eta(t)$, the observed angular scale of the causal patches in the CMB should be approximately $2°$. The homogeneity across the entire sky manifests as an initial condition problem, called the horizon problem [30].

One possibility for alleviating the horizon problem is to have in initial era where the dominant form of energy density had an equation of state $w < -1/3$. At sufficiently early times, large length scales were inside the Hubble radius $(aH)^{-1}$ and thus in causal contact. Eventually, these modes will leave the horizon due to the decreasing Hubble radius. Radiation and matter dominated epochs follow this period, where the Hubble radius increases and modes begin reentering the horizon. Because these scales were in causal contact in the early universe, one expects the CMB to be homogeneous.

Inflation [31] was the first model to address the horizon problem[2] using an exponentially growing scale factor. Generally, models of inflation rely on a homogeneous scalar field ϕ with a potential $V(\phi)$. The equation of state for the field can be written as

$$w = \frac{\frac{1}{2}\dot{\phi}^2 - V(\phi)}{\frac{1}{2}\dot{\phi}^2 + V(\phi)}. \tag{1.7}$$

When the potential term dominates the kinetic energy, $\dot{\phi}^2 \ll 2V(\phi)$, the equation of state is approximately $w = -1$, resulting in an exponentially growing scale factor in Eq. (1.5).

[2] As well as the flatness and monopole problems.

In order to exit this deSitter phase, without considering interactions, the rolling of the scalar field must eventually decrease the potential energy such that the equation of state in the universe $w \geq -1/3$, and the Hubble radius begins to increase again. In order to guarantee that the all observed length scales were in causal contact during inflation, the scalar field must not be accelerating rapidly. In terms of the equation of motion

$$\ddot{\phi} + 3H\dot{\phi} + V_{,\phi} = 0, \tag{1.8}$$

we must additionally require $|\ddot{\phi}| \ll |3H\dot{\phi}|, |V_{,\phi}|$. Typically these conditions are written in terms of two slow-roll parameters

$$\epsilon = \frac{3}{2}(1+w) = \frac{\dot{\phi}^2}{2M_p^2 H^2}, \qquad \eta = -\frac{\ddot{\phi}}{H\phi}. \tag{1.9}$$

Inflation continues as long as the slow-roll conditions $\epsilon, \eta \ll 1$ are valid.

We note, in order to obey the slow-roll conditions, the potential must be extremely flat,

$$V \gg M_p V_{,\phi} \text{ and } M_p^2 V_{,\phi\phi}, \tag{1.10}$$

which requires a weakly interacting scalar field theory. These small couplings are rare in particle physics, unless fine tuning is introduced. One important exception is the use of Nambu-Goldstone bosons in models with high symmetry breaking scale [23]. Thus, one can use axions as a natural inflationary model, with a potential typically given by

$$V(\phi) = \Lambda^4 \left[1 \pm \cos\left(\frac{\phi}{f_a}\right)\right], \tag{1.11}$$

where Λ is a mass scale associated with the nonperturbative gauge field configuration.

After the slow-roll conditions are violated, the universe undergoes a period of reheating, where the energy density of the inflaton scalar field is deposited into other degrees of freedom. In axion-inflation models, the inflaton retains the axion-like interaction to CP-odd combinations to fermions and gauge fields, which can provide a rich phenomenology during reheating. We will discuss these possibilities in chapter 2.

1.3 Previous Detection Methods

We now review methods applied for detecting axions and their interactions with Standard model particles. In particular, we will consider constraints on (axionic) inflationary models from the CMB, cosmological constraints on axion-photon couplings, as well as laboratory experiments for axions.

1.3.1 Inflationary Perturbations

Using a deSitter background, we consider the theory of metric perturbations during inflation. In the comoving gauge, the scalar ($\mathcal{R}$) and tensor (h_{ij}) metric perturbations are given by

$$g_{ij} = a^2 \left[(1 - 2\mathcal{R})\delta_{ij} + h_{ij}\right], \tag{1.12}$$

where the tensor perturbations are transverse and traceless. To first order in perturbation theory, the equations of motion for the scalar and tensor fluctuations can be written as

$$v_k'' + \left(k^2 - \frac{z''}{z}\right) v_k = 0, \qquad u_k'' + \left(k^2 - \frac{a''}{a}\right) u_k = 0, \tag{1.13}$$

where primes denote derivatives with respect to conformal time, k-subscripts denote a Fourier transform, $z = a\dot{\phi}/H$, and the scalar and tensor perturbations are given by $v = z\mathcal{R}$ and $u = aM_p h_s$, for each polarization s of tensor perturbations. When the wavelength of the Fourier mode exceed the Hubble radius, the modes are called superhorizon with $k \ll aH$, and the metric perturbations cease to evolve. Due to this "freeze-out", calculating properties of modes as they leave the horizon act as initial conditions for the same modes that reenter the horizon in the late universe. In particular, the power spectra of fluctuations as they leave the horizon are calculated.

In terms of the two-point correlation function, the power spectrum $P_{\mathcal{O}}(k)$ can be written as

$$\langle \mathcal{O}\mathcal{O} \rangle = \int P_{\mathcal{O}}(k) \mathrm{d} \log k \,. \tag{1.14}$$

Typically, the power spectra will be power law functions of the scale k, the exponent given in terms of the spectral indices

$$P_{\mathcal{R}}(k) \propto k^{n_s - 1}, \qquad P_T(k) \propto 2P_h(k) = k^{n_T}, \tag{1.15}$$

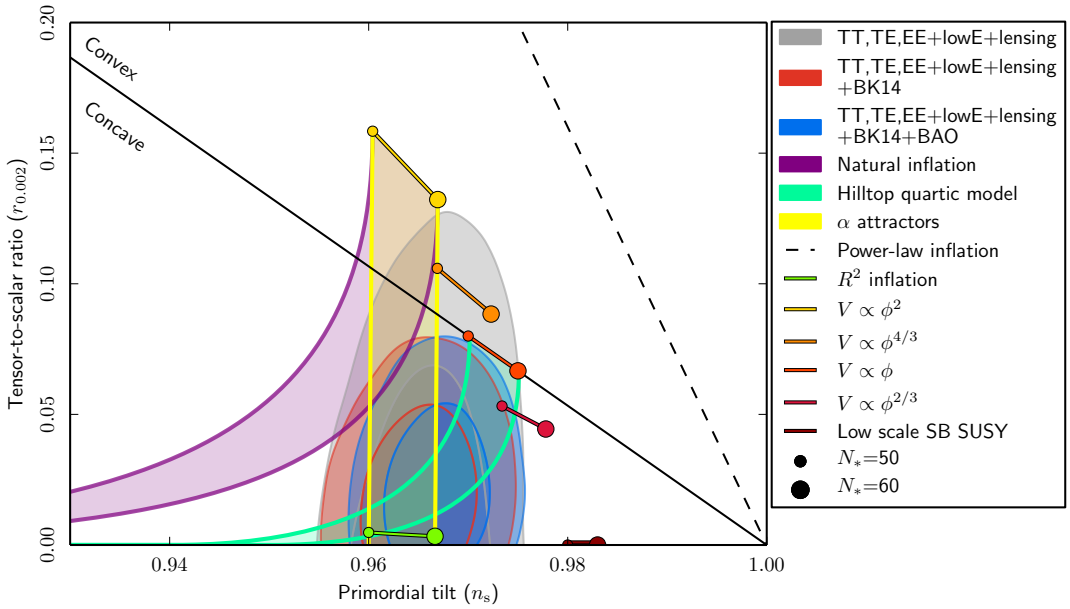

Figure 1.1: Marginalized joint 68% and 95% CL constraints on tensor-to-scalar ratio at $k = 0.002$ Mpc^{-1} and primordial (scalar) spectral tilt, reproduced from Planck 2018 [33]. For comparison, various theoretical predictions for inflationary models are also displayed.

where the factor of two in the tensor power spectra comes from the two polarizations of gravitational waves. Promoting the Fourier modes v_k, u_k to quantum operators, these scalar and tensor fluctations acquire a nonzero variance. The power spectra of scalar and tensor modes can be calculated by defining the vacuum such that, in the asymptotic past, the energy of sub-horizon modes is minimized [32]:

$$P_{\mathcal{R}} = \frac{1}{8\pi^2}\frac{H^2}{\epsilon M_p^2}\bigg|_{k=aH}, \qquad P_T = \frac{2}{\pi^2}\frac{H^2}{M_p^2}\bigg|_{k=aH}, \tag{1.16}$$

and the spectral indices can be found as

$$n_s - 1 = \frac{\mathrm{d}\log P_{\mathcal{R}}}{\mathrm{d}\log k} = 2\eta - 4\epsilon, \qquad n_T = -2\epsilon, \tag{1.17}$$

where ϵ, η are the slow-roll parameter given by Eq. (1.9). Finally, the tensor-to-scalar ratio is defined as the ratio of power spectra:

$$r = \frac{P_T}{P_{\mathcal{R}}} = 16\epsilon. \tag{1.18}$$

Typically different inflationary models will result in different spectral tilts and r, thus measurements and constraints of these parameters provides valuable constraints for the inflationary model. The scalar spectral index and tensor-to-scalar ratio can be rewritten in terms of the potential as

$$n_s - 1 = 2M_p^2 \left[\frac{V_{,\phi\phi}}{V} - \frac{3}{2} \left(\frac{V_{,\phi}}{V} \right)^2 \right], \qquad r = 8M_p^2 \left(\frac{V_{,\phi}}{V} \right)^2. \tag{1.19}$$

The most sensitive measurements of these parameters by [33] are then used to constrain the inflationary potential and particular models. From Fig. 1.1, the predictions of Natural inflation [23] are disfavored on length scales $k = 0.002$ Mpc^{-1}, posing a $2-3\sigma$ deviation from observation.

1.3.2 Axion-Photon Coupling

One of the most constrained axion interactions is an effective couplings to photons through the Lagrangian term

$$\frac{g_{a\gamma\gamma}}{4} \phi F_{\mu\nu} \tilde{F}^{\mu\nu} \subset \mathcal{L}, \tag{1.20}$$

where $\tilde{F}^{\mu\nu} = \frac{1}{2}\epsilon^{\mu\nu\rho\sigma} F_{\rho\sigma}$ and the coupling $g_{a\gamma\gamma} \propto f_a^{-1}$ has inverse mass dimension. With this coupling, the axion acquires a decay into two photons and in the presence of off-shell photons (Primakoff process), an axion and photon can interconvert.

The decay timescale of the axion can be calculated as

$$\tau = \frac{64\pi}{g_{a\gamma\gamma}^2 m_a^3} = 10^{25}\ \text{s} \left(\frac{g_{a\gamma\gamma}}{10^{-10}\ \text{GeV}^{-1}} \right)^{-2} \left(\frac{m_a}{1\ \text{eV}} \right)^{-3}. \tag{1.21}$$

If the decay timescale corresponds to the periods between the onset of BBN and last scattering, the injection of photons will manifest in the abundance of elements, spectral distortions, or the dimishment of number of neutrinos in the CMB [35][3]. These cosmological constraints are shown as blue shaded regions in Fig. 1.2. Theories with decays timescales shorter than the age of the universe will not correspond to the observed dark matter [36], although these constraints remain important for particle physics searches for axions. Thus, axionic dark matter models must be either very light or very weakly coupled.

[3] For light axions decaying during BBN, the additional photons produce more subtle effects [35], such as a difference in baryon-to-photon ratio at BBN and CMB.

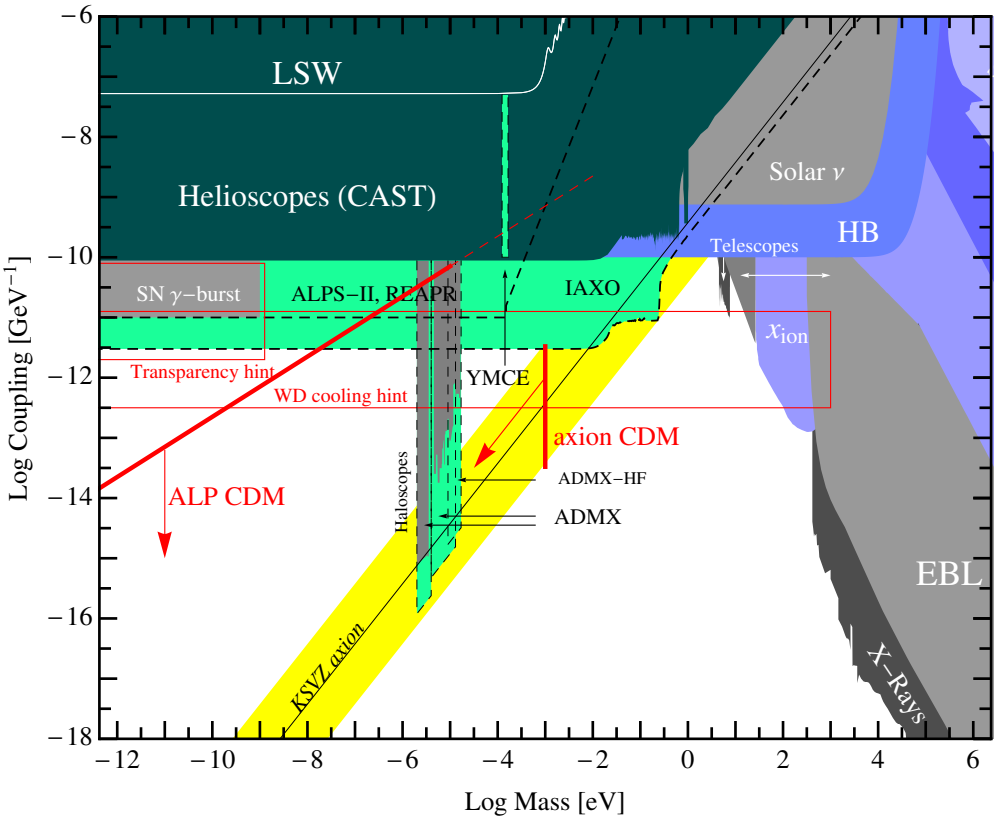

Figure 1.2: Constraints on axion and ALP couplings to the photon as a function of the mass of the axion from cosmological (blue), astronomical observations (gray), and experimentally excluded regions (green), reproduced from [34]. The yellow region corresponds to QCD axion models, including the DFSZ and KSVZ models.

We note, the QCD axion is guaranteed to couple to photons [37], due to the interaction with quarks. This coupling can be written as

$$g_{a\gamma\gamma} \sim \left(1.45 \times 10^{-10}\ \text{GeV}^{-1}\right)\left(\frac{m_a}{1\ \text{eV}}\right). \tag{1.22}$$

For masses less than $\mathcal{O}(10\ \text{eV})$, or $f_a \geq 10^7$ GeV, the QCD axion will not could not decay into photons within the age of the universe, and remains a viable dark matter candidate.

One particular experimental probe of the axion-photon coupling is the microwave resonant cavity experiment, ADMX, which can be seen in Fig. 1.2 as the only low mass experiment probing the QCD axion. In this experiment, the application of an external magnetic field allows the Primakoff process to interconvert axions into resonant electromagnetic modes of the cavity. Since the axionic dark matter should be nonrelativistic

(cold), the resonant frequency of the cavity must closely match the mass of the axion. Under this resonant condition, the power associated with the microwave signal can be written as [38]

$$P_{\rm sig} \approx \frac{1}{2} g_{a\gamma\gamma}^2 \left(\frac{\rho_a}{m_a}\right) B_0^2 V C Q_L, \tag{1.23}$$

where ρ_a is the local density of axions, B_0 is the external magnetic field, V is the volume of the cavity, Q_L is the loaded quality factor, and C is some mode-dependent form factor. Crucial to this experiment is the large quality factor needed to improve sensitivity to low axion-photon couplings, at the cost of probing only a narrow window (for a particular cavity configuration) in the axion mass range.

1.4 Outline

This thesis attempts to fill in some of the void left by ΛCDM on the nature of the dark sector. It explores the theoretical application of ALP on new observational windows into the dark sector though circular polarization [39], electron electric dipole moments [40], and modifications to the gravitational waveform [41].

In Chapter 2, we begin with a review of the reheating epoch after inflation. Applying these dynamics to a generic axion inflation, we predict the electromagnetic spectrum following reheating and decompose these modes into Stokes parameters. In particular, we find the primordial power spectrum for circular (V-mode) polarization and resulting in a blue-tilted spectral index.

We then turn to axionic dark matter models where the axion has an effective coupling to fermions. Chapter 3 calculates the non-relativistic effects manifesting from this coupling. In particular, for a reasonable laboratory setup, the dominant effect for an axion-electron is an oscillating electric dipole moment (EDM). We show that for an idealized spin-precession experiment, this oscillating EDM can be measured by a SQUID magnetometer.

Chapter 4 considers a generic dark matter model where the (charged) dark matter has accumulated within compact objects, such as neutron stars or a black holes. The build-up of dark charge will manifest in a violation of Keplar's laws. Beginning with an overview of gravitational wave physics, we derive the corrections to the gravitational waveform due to the accumulation of dark charge. Using a Fisher matrix analysis, we

are able to constrain generic properties of the dark sector, including axionic dark matter models.

We conclude with Chapter 5, where we discuss future work to be done on each of the aforementioned theoretical and observational probes.

Chapter 2

Circular Polarization

2.1 Introduction

One of the cornerstones of CMB physics is the prediction of linear polarization of the E-modes (gradient-type) from the intrinsic quadrupole temperature anisotropy, which has been measured in the CMB [42]. Inflationary models also predict B-mode (curl-type) polarization which is generated from tensor metric perturbations and induces non-vanishing off-diagonal components of the polarization matrix. This greatly increases the amount of 'fundamental physics' that can be extracted from the CMB, for example, in the simplest models of inflation, a detection of primordial B-modes will probe the energy scale of inflation.

While often forgotten, the final Stokes parameter, V-modes, can contain a wealth of information about early universe, in particular parity violation. In the chiral polarization basis, these V-mode describe a net circular polarization of the photons [43] as

$$V = \frac{1}{a^4}\left(|A'_+|^2 - |A'_-|^2\right), \tag{2.1}$$

where $A_\pm$ are the projections of the photon into chiral polarization basis, and $'$ is the derivative with respect to conformal time, and the corresponding brightness temperature perturbation can then be constructed in an analogous manner to E and B [44, 45]. The V-mode polarization is usually assumed to be zero because Thomson scattering does not intrinsically source V, unless a magnetic field is present [45].

In this chapter, we will consider the generation of circular polarization in the context

of axion inflation [23, 46, 47, 48, 49]. The inflationary (and reheating) generation of circular polarization could be quite a general phenomenon provided that the inflaton field sources chiral symmetry breaking either directly in the photon sector [50, 51, 52] or indirectly through coupling to fermions [53][1], and we will study both these scenarios. In the former case, there is a direct production of one polarization state during inflation, while in the latter case, the pseudoscalar sources a left-right asymmetry in a charged fermion which is subsequently transferred to circularly polarized photons [55]. These mechanisms for generating CMB circular polarization are qualitatively different from the generation of E- and B-mode polarization, as well as the generation of V by background magnetic fields [45], as in the former case the polarization is generated *during* inflation and reheating, while in the latter cases the polarization is only generated upon horizon re-entry of primordial scalar and tensor modes.

2.2 Circular Polarization Preliminaries

We have expressed V in Eq. (2.1) as a difference in the photon polarization states; this will be the most useful definition for our analysis. This definition is related to the more conventional definition $V = 2\,\mathrm{Im}[E_x^* E_y]$ by the change of basis to $\{x_+, x_-\}$ coordinates, $\sqrt{2}\hat{x}_+ = \hat{x} + i\hat{y}$, $\sqrt{2}\hat{x}_- = \hat{x} - i\hat{y}$ [2]. This can also be expressed in terms of components of the 'polarization matrix' as

$$V = -i(\rho_{12} - \rho_{21}) \tag{2.2}$$

where ρ_{ij} is the polarization matrix defined by [44]

$$\rho = \frac{1}{2}\begin{pmatrix} I+Q & U-iV \\ U+iV & I-Q \end{pmatrix} \tag{2.3}$$

$$= I\,\mathbb{I} + Q\,\sigma_3 + U\,\sigma_1 + V\sigma_2\,, \tag{2.4}$$

where in the second line we have used the Pauli matrices σ_i.

The V defined above has units of intensity. Anisotropies in V can be converted to a

[1] Note that our analysis differs from that of [54], which studied Majorana fermions. These are not useful for generating gauge fields, since the vector current J^μ vanishes identically for Majorana fermions.

[2] In this basis, $\sqrt{2}E_x = E_+ + E_-$ and $\sqrt{2}E_y = i(E_+ - E_-)$, which gives $V = 2\,\mathrm{Im}[E_x^* E_y] = E_+^2 - E_-^2$. In an FRW spacetime, this is precisely Eq. (2.1).

fractional temperature fluctuation, which we denote Θ_V, via the rescaling [56, 57, 58],

$$\Theta_V \equiv \frac{\delta V_T}{T} = \frac{\delta V}{I}, \tag{2.5}$$

where V_T is the V stokes parameter in units of temperature, $I \equiv \frac{1}{a^4}\left(|A'_+|^2 + |A'_-|^2\right)$ is the intensity stokes parameter, and T is the background blackbody temperature. One can then construct the C_l^{VV} as the coefficients in the multipole expansion of the two-point function $\langle \delta V_T \delta V_T \rangle$.

The quantity we compute in this paper is the polarization present at the end of inflation and reheating, which serves as the initial condition for the subsequent evolution to last scattering. In the case of E and B, the initial polarization is ignored, for good reason: it is heavily suppressed by scatterings and is negligible compared to the polarization produced by primordial scalar and tensor perturbations. In contrast, for V (in the absence of a magnetic field) there is no signal generated by primordial scalar and tensor fluctuations, so the only inflationary V will be a relic of that produced *during* inflation. However, a mechanism is still required to circumvent the suppression from scatterings. We will not fully develop this mechanism here, but will discuss possibilities in Section 2.6.

Analogous to the primordial scalar spectrum, the (dimensionless) primordial power spectrum of V-mode polarization is given by

$$P_{\Theta_V}(k) = \frac{1}{I^2}\frac{k^3}{2\pi^2}|\delta V_k|^2. \tag{2.6}$$

This can be parametrized in a similar way to the primordial scalar spectrum [28, 59] as

$$P_{\Theta_V}(k) = \mathcal{A}_V \left(\frac{k}{k_0}\right)^{n_V - 1} \tag{2.7}$$

where $\mathcal{A}_V$ is the amplitude of primordial V-mode anisotropies at a reference scale k_0, and n_V is the spectral index.

2.3 Background Dynamics: Axion Inflation

We will study axion inflation coupled to a low energy U(1) gauge-fermion system with a triangle anomaly cancelling term. The action for this model is given by

$$S = \int \mathrm{d}^4x\sqrt{-g}\left[\frac{M_{\rm Pl}^2}{2}R - \frac{1}{2}(\partial\phi)^2 - V(\phi) + \overline{\psi}(i\gamma^\mu D_\mu - m_\psi)\psi \right. \\ \left. -\frac{1}{4}F_{\mu\nu}F^{\mu\nu} + A_\mu J^\mu + \frac{C}{f}\partial_\mu\phi J^{\mu 5} + \frac{\alpha}{f}\phi F_{\mu\nu}\tilde{F}^{\mu\nu}\right]. \tag{2.8}$$

In the above, $F_{\mu\nu}$ is the usual field strength tensor of the photon, D_μ is the covariant derivative with respect to the spin connection, and the vector current J_μ and axial vector current $J^{\mu 5}$ are given by

$$J^\mu = g\,\overline{\psi}\gamma^\mu\psi \quad , \quad J^{\mu 5} = \overline{\psi}\gamma^\mu\gamma_5\psi. \tag{2.9}$$

The fermion ψ is a 4-component Dirac spinor charged under the standard model gauge group, though we will only consider the effective coupling to $U(1)_{\rm EM}$.

The background cosmology of this model is dictated by the Friedman equation,

$$H^2 = \frac{1}{3M_{Pl}^2}\left[\rho_\phi + \rho_A + \rho_\psi\right], \tag{2.10}$$

where ρ_ϕ is the inflaton energy density, which we will assume is dominant during inflation, while ρ_A and ρ_ψ are the effective background energy density in the gauge field A_μ and the fermion ψ respectively. This is in addition to the equation of motion of the inflaton, given by

$$\ddot{\phi} + 3H\dot{\phi} + V_{,\phi} = -\frac{C}{f}\partial_\mu J^{\mu 5} + \frac{\alpha}{f}F_{\mu\nu}\tilde{F}^{\mu\nu}. \tag{2.11}$$

While the mechanism we consider here is independent of the choice of inflationary potential, for concreteness we will consider the classic example of

$$V(\phi) = \frac{1}{2}m_\phi^2\phi^2, \tag{2.12}$$

with a benchmark value for the mass of $m_\phi = 10^{-6}M_{Pl}$. Similar potentials for an axion arises in monodromy models, such as the F-term axion monodromy model of [60].

Provided that backreaction is not significant during inflation, such that we can ignore

the source terms on the RHS of (2.11), inflation ends once the slow-roll conditions are violated. For $m^2\phi^2$ inflation [61] this occurs at $\phi_{end} = \sqrt{2}M_{Pl}$. At this point $(1/2)\dot{\phi}^2 = M_{Pl}^2 H^2$, which follows from $\epsilon = (1/2)\dot{\phi}^2/(M_{Pl}^2 H^2)$, and hence the value of $\dot{\phi}$ is given by

$$\dot{\phi}_{end} = m_\phi M_{Pl} = \frac{1}{\sqrt{2}} m_\phi \phi_{\rm end}. \tag{2.13}$$

After inflation, and in the absence of expansion and backreaction, the field ϕ begins to oscillate, triggering the 'preheating' phase. In this phase the field is described by,

$$\phi(t) = \phi_{end} \sin(m_\phi t). \tag{2.14}$$

The maximum field velocity in this phase is thus $\dot{\phi}_{pre} = m_\phi \phi_{end}$, which is roughly a factor of $\sqrt{2}$ larger than the maximum value of the field velocity during inflation.

During inflation there will be production of fermions and gauge fields due to the interactions in the Lagrangian. The relative strength of these interactions is controlled by the ratio of parameters C/α. We will consider the regimes $|C/\alpha| \gg 1$ and $|C/\alpha| \ll 1$ separately.

2.3.1 Charged Fermion and Gauge Field Production during Inflation with $\partial_\mu \phi J^{\mu 5}$

In the region of parameter space $|C| \gg |\alpha|$, the dominant interaction for ϕ is with fermions. To describe the fermion dynamics, it will be convenient to decompose the 4-component Dirac spinor ψ into two 2-component Weyl spinors φ and η, via

$$\psi = \begin{pmatrix} \varphi \\ \eta^\dagger \end{pmatrix}, \tag{2.15}$$

in terms of which the fermion currents take the form

$$J^\mu = g\left(\varphi^\dagger \overline{\sigma}^\mu \varphi - \eta^\dagger \overline{\sigma}^\mu \eta\right) \quad , \quad J^{\mu 5} = \varphi^\dagger \overline{\sigma}^\mu \varphi + \eta^\dagger \overline{\sigma}^\mu \eta. \tag{2.16}$$

Working in the comoving time FRW metric, we can reduce the covariant derivative to a partial derivative by rescaling the fermion fields by $a^{-3/2}$ to absorb the factor of $\sqrt{-g}$,

as in [53]. The fermionic action then takes the form:

$$S_{\rm f} = \int {\rm d}^4x \Big[i\varphi^\dagger \bar{\sigma}^\mu \partial_\mu \varphi + i\eta^\dagger \bar{\sigma}^\mu \partial_\mu \eta - m_\psi(\varphi\eta + \varphi^\dagger\eta^\dagger) + \frac{C}{f}\partial_\mu\phi(\varphi^\dagger\bar{\sigma}^\mu\varphi + \eta^\dagger\bar{\sigma}^\mu\eta) + gA_\mu(\varphi^\dagger\overline{\sigma}^\mu\varphi - \eta^\dagger\overline{\sigma}^\mu\eta)\Big]. \tag{2.17}$$

Neglecting the $\phi F\tilde{F}$ interaction, the dynamics of the gauge-fermion system are dictated by the gauge field equation of motion,

$$\partial_\nu\left(\sqrt{-g}F^{\mu\nu}\right) = J^\mu, \tag{2.18}$$

and the fermion equation of motion,

$$i\bar{\sigma}^\mu\partial_\mu\varphi + \left(\frac{C}{f}\partial_\mu\phi + gA_\mu\right)\bar{\sigma}^\mu\varphi = m_\psi\eta^\dagger, \tag{2.19}$$

$$i\bar{\sigma}^\mu\partial_\mu\eta + \left(\frac{C}{f}\partial_\mu\phi - gA_\mu\right)\bar{\sigma}^\mu\eta = m_\psi\varphi^\dagger. \tag{2.20}$$

During inflation the time-variation of ϕ leads to a violation of adiabaticity for the fermions, leading to non-perturbative particle production wherein one helicity of the fermions is preferentially produced [53]. The results of [53], which did not include gauge fields, apply to our case at times when gauge field production on the fermion equation of motion is negligible, or more precisely $\frac{C}{f}\dot{\phi} \gg gA_0\,,\, gA_i$. This assumption eventually breaks down and the analysis must be done numerically. For our purposes, we will use their results for the fermion production and study the corresponding gauge field production.

The fermions can be expanded in mode functions as

$$\varphi_\alpha(x,t) = \sum_\lambda \int \frac{{\rm d}^3k}{(2\pi)^3}\left[x^\lambda_{\alpha k}(t)a^\lambda_k e^{ikx} + y^\lambda_{\alpha k}(t)b^{\lambda\dagger}_k e^{-ikx}\right], \tag{2.21}$$

$$\eta_\alpha(\mathbf{x},t) = \sum_\lambda \int \frac{{\rm d}^3k}{(2\pi)^3}\left[x^\lambda_{\alpha k}(t)b^\lambda_k e^{ikx} + y^\lambda_{\alpha k}(t)a^{\lambda\dagger}_k e^{-ikx}\right],$$

and further decomposed into a helicity basis via the definition

$$x^\lambda_k(t) = X^\lambda_k(t)\xi_\lambda(\mathbf{k}) \quad , \quad y^{\lambda\dagger}_k(t) = Y^{\lambda *}_k(t)\xi_\lambda(\mathbf{k}). \tag{2.22}$$

where $\lambda = \pm$ denotes the (+) and (–) helicity states. Explicit expressions for the helicity eigenspinors ξ_λ can be found in [62].

The particle number is then defined in terms of these mode functions as [53],

$$n_k^\lambda = \frac{1}{\omega_\lambda(\tilde{k}_\lambda + \omega_\lambda)}\left[|\dot{X}_k^\lambda|^2 + \omega_\lambda^2|X_k^\lambda|^2 - 2\omega_\lambda\,\mathrm{Im}(X_k^\lambda \dot{X}_k^\lambda)\right], \tag{2.23}$$

where the modified dispersion relations are,

$$\omega_\lambda^2(t) = \tilde{k}_\lambda(t)^2 + m_\psi^2, \;\; \tilde{k}_\lambda(t) = \left(\frac{k}{a}\lambda + \frac{C}{f}\dot{\phi}\right). \tag{2.24}$$

After matching to the Bunch-Davies vacuum, the mode functions have the form[3],

$$\begin{aligned}
X_k^+(k\tau) &= -\frac{im_\psi}{H}\frac{e^{i\theta}e^{\frac{\pi}{2}\vartheta}}{\sqrt{2k\tau}}W_{-\frac{1}{2}-i\vartheta,\mu}(2ik\tau), \\
X_k^-(k\tau) &= \frac{e^{i\theta}e^{-\frac{\pi}{2}\vartheta}}{\sqrt{2k\tau}}W_{\frac{1}{2}+i\vartheta,\mu}(2ik\tau), \\
Y_k^{+*}(k\tau) &= \frac{e^{i\theta'}e^{\frac{\pi}{2}\vartheta}}{\sqrt{2k\tau}}W_{\frac{1}{2}-i\vartheta,\mu}(2ik\tau), \\
Y_{ik}^{-*}(k\tau) &= -\frac{im_\psi}{H}\frac{e^{i\theta'}e^{-\frac{\pi}{2}\vartheta}}{\sqrt{k\tau}}W_{-\frac{1}{2}+i\vartheta,\mu}(2ik\tau),
\end{aligned} \tag{2.25}$$

where $W_{x,y}(z)$ are Whittaker functions, and we have defined,

$$\vartheta = -\frac{C}{f}\frac{\dot{\phi}}{H} \;\;,\;\; \mu^2 = -\left(\frac{m_\psi^2}{H^2} + \vartheta^2\right), \tag{2.26}$$

and θ, θ', are arbitrary phases. The particle number on large scales is then given by

$$n_k^\pm = e^{-\pi\left(\mp\vartheta + \sqrt{\frac{m_\psi^2}{H^2}+\vartheta^2}\right)}\frac{\sinh\left[\pi\left(\sqrt{\frac{m_\psi^2}{H^2}+\vartheta^2} \pm \vartheta\right)\right]}{\sinh\left[2\pi\left(\sqrt{\frac{m_\psi^2}{H^2}+\vartheta^2}\right)\right]}. \tag{2.27}$$

At strong coupling $\vartheta \gg m_\psi/H$ this simplifies to

$$n_k^+ \approx 1 \;\;,\;\; n_k^- \approx 0. \tag{2.28}$$

There is thus a large asymmetry in the helicity states. This is similar to inflation with the coupling $\phi F\tilde{F}$, wherein one polarization of the gauge fields is amplified and other is

[3] Where we have corrected for a typo in the normalization stated in [53].

negligible.

Finally, the helicity asymmetry in the fermions will be transferred to the photon via perturbative processes, namely Bremsstrahlung. In the case of single-Bremsstrahlung, this process allows a $(+\frac{1}{2})$ spin fermion to convert to a $(-\frac{1}{2})$ fermion via the emission of near-collinear $(+1)$ spin photon, and a $(-\frac{1}{2})$ spin fermion will convert to a $(+\frac{1}{2})$ fermion via the emission of near-colinear (-1) spin photon. In our case, inflation and preheating will produce a large number of $(+)$ helicity fermions, leading to production of $(+)$ photons. The modern theoretical framework to describe this process is the spinor-helicity formalism for gauge theories, as reviewed in e.g. [63, 64]. The emission of Bremsstrahlung in this framework was first studied in [65, 66], where the amplitudes for all relevant processes were computed. In our work we will take m_ψ/H small but finite, such that helicity is approximately conserved on large scales and $V/I \sim \mathcal{O}(1)$ for the produced photons[4].

2.3.2 Gauge Field Production during Inflation from $\phi F\tilde{F}$

If instead $|\alpha| \gg |C|$, the dominant interaction term is that between the inflaton and the gauge field, $\phi F\tilde{F}$. This mechanism for the production of gauge fields from the coupling has been considered in many work [49, 50, 67]. The equation of motion for A_μ is

$$\frac{d^2 A_{k\pm}}{d\tau^2} + \left(k^2 \pm 2k\frac{\xi}{\tau}\right) A_{k\pm} = 0\,, \tag{2.29}$$

where ξ is given by

$$\xi = \frac{2\alpha\dot{\phi}}{fH}\,. \tag{2.30}$$

The parameter ξ plays a similar role to ϑ in the fermionic case, and there is production of one of the polarization states on scales with k less than a critical value set by ξ. In this case, A_{k+} modes which satisfy

$$\frac{k}{aH} < 2\xi, \tag{2.31}$$

[4]Where I is the intensity stokes parameter, which determines $T_{\rm CMB}$ and the TT power spectrum.

experience a tachyonic instability and are amplified during inflation, while A_{k-} is unaffected. The mode function prepared by inflation is

$$A_{k+}^{(0)} = \frac{2^{-1/4}}{\sqrt{2k}} \left(\frac{k}{\xi a H}\right)^{1/4} e^{\pi\xi - 4\xi\sqrt{k/2\xi aH}} \qquad (2.32)$$
$$A_{k-}^{(0)} \approx 0,$$

where the + mode on large scales is amplified by a factor of $e^{\pi\xi}$.

Current CMB observations bound the value of ξ at the moment the CMB pivot scale $k_\star$ exits the horizon to be $\xi_\star \leq 2.2$ [59], which corresponds to a (model-dependent) bound on the coupling $(\alpha/f) \lesssim 110 M_{Pl}^{-1} - 125 M_{Pl}^{-1}$ for $m^2\phi^2$ inflation [50]. When we refer to the 'strong coupling' regime of this model, we mean the range $1 M_{Pl}^{-1} \lesssim (\alpha/f) \lesssim \mathcal{O}(10^2) M_{Pl}^{-1}$.

2.4 Preheating

After inflation, the oscillatory behaviour of the inflaton can lead to instabilities and explosive particle production for fields directly coupled to the inflaton. This phenomenon is known as "preheating", originally discovered in [68, 69, 70, 71, 72, 73]. For both the couplings $\partial_\mu\phi J^{\mu 5}$ and $\phi F\tilde{F}$, the physical origin of non-zero V is the definite sign of $\dot{\phi}$ during inflation, which produces a net circular polarization on super-Hubble scales. However, after inflation, the field ϕ oscillates and both polarizations are produced, making the predictions for V-mode polarization sensitive to the detailed dynamics of preheating. This is in contrast to most other CMB observables, for example n_s and r, which are largely decoupled from the details of (p)reheating. With this in mind, we will undertake an analysis of preheating which seeks to uncover the extent to which circular polarization produced during inflation will survive preheating.

For the case of the direct coupling $\phi F\tilde{F}$ between the axion and gauge fields, the preheating dynamics are straightforward. It was shown in [50, 51] that gauge fields are copiously produced and preheating terminates quickly provided that the coupling is sufficiently large. Preheating into fermions via Yukawa couplings was originally studied in [74], and subsequently analyzed in many works, including [53, 75]. However, preheating into charged fermions via $\partial_\mu\phi J^{\mu 5}$, which then produces photons, is more subtle, and has not been studied thus far. We dedicate the following section to this issue. That is, we

will work in the regime, $\left|\frac{C}{\alpha}\right| \gg 1$. More details of the competition between inflationary interactions will be discussed in Section 2.4.2.

2.4.1 The Structure of Preheating into Charged Fermions

In this section, the basic mechanism we would like to consider is the non-perturbative production of fermions, which is instantaneous and occurs once an inflaton oscillation, and the subsequent perturbative production of photons. The simplest scenario is that preheating terminates after one half-oscillation of the inflation, such that $\dot{\phi}$ never switches sign, and the maximal helicity asymmetry of fermions, and consequently circularly polarization of photons, is achieved.

We will show that this occurs provided that the requisite 'new physics' (as measured by $(C/f)^{-1}$) occurs near the GUT scale, but at a sufficiently high scale that backreaction does not prevent preheating from occurring. For smaller values of the coupling (i.e. a higher energy scale for new physics), preheating lasts for multiple or many cycles allowing for production of both helicity states, which suppresses the circular polarization. In all cases, the conversion to photons then takes place via perturbative processes, occurring within a single Hubble time. Perturbative reheating continues after this point, operating on sub-Hubble scales, until the universe reaches near-thermal equilibrium and the radiation phase of standard big bang cosmology begins.

Before we proceed with preheating, let us recall that if the dominant interaction is between the gauge field and fermion current, the general solution of the gauge field is:

$$A_k^{\pm}(\tau) \sim i \int \frac{\mathrm{d}\eta}{a(\eta)} G_k(\eta, \tau) J^{\pm}(X_k^{\lambda}, Y_k^{\lambda}), \tag{2.33}$$

where $J^{\pm}$ is the $(+/-)$ helicity piece of the vector current, and G_k is the Green's function of A_k. We can define the relative chirality to be

$$\frac{A_+ - A_-}{A_{tot}} = A_{rel}. \tag{2.34}$$

So as long as there is some linear polarization present the total amount of gauge fields will be non-vanishing, $A_{tot} \neq 0$. We can express the relative photon chirality as:

$$A_{rel}(X_k^{\lambda}, Y_k^{\lambda}; \tau) = i A_{tot}^{-1} \int \frac{\mathrm{d}\eta}{a(\eta)} G_k(\eta, \tau)[J_k^+ - J_k^-]. \tag{2.35}$$

Note that during preheating, we can construct the chiral currents $J^{\pm}$ as a quadratic form of the eigenmodes produced during preheating, X_k^{λ} and Y_k^{λ}. We immediately see that if inflation produced a preponderance of left handed photons, then as long as the difference between left and right handed current are $\mathcal{O}(1)$ of the total current, then the chirality of the photons will be non-vanishing. Therefore under reasonable assumptions, the backreaction of the fermion production during preheating will not wash out the initially large photon helicity produced during inflation from potential lepton chirality flipping transitions. To get an explicit computation of the percentage of chirality that is retained during reheating detailed numerical analysis is necessary and we plan to pursue this in a future work.

The structure of preheating is revealed by comparing time-scales in the problem. The time-scale for fermion production is the oscillation period of the inflaton, which is smaller than the Hubble time by roughly a factor of 10. Meanwhile, the time-scale for the production of photons is given by,

$$\tau_\gamma = 1/\Gamma_\gamma \tag{2.36}$$

where Γ_γ is the usual rate of QED-like interactions at finite temperature, given by

$$\Gamma = n\sigma v = g^2 T, \tag{2.37}$$

where T is the effective temperature of the QED-like sector, which is roughly given by $T \approx \rho_\psi^{1/4}$. The time-scale for production of photons is then given by

$$\tau_\gamma = \frac{1}{g^2 \rho_\psi^{1/4}}. \tag{2.38}$$

The relevant scale for comparison is the Hubble-time, which after the first production event is given by $\tau_H = M_{Pl}/\sqrt{\rho_\psi}$. Hence the ratio of the time-scales is given by

$$\frac{\tau_\gamma}{\tau_H} = \frac{\rho_\psi^{1/4}}{g^2 M_{Pl}} = \mathcal{O}(1), \tag{2.39}$$

where the second equality follows from the expressions and numerical values already used, in addition to $g \sim \alpha_{EM} \sim 10^{-2}$. Thus the production of photons takes place in

roughly a Hubble time after the fermions are produced and preheating is terminated. Smaller values of g will lead to a longer time-scale for photon production, which will not substantially alter the structure of preheating.

With this in mind, we now study the production of fermions during preheating. The inflationary solution for the fermion mode functions is no longer valid during preheating, as the background is no longer adiabatically varying. These solutions were studied in the past and we will make some general remarks about the following WKB solutions for the different helicity eigenmodes:

$$X_k^\lambda(t) = \sqrt{1+\frac{\tilde{k}_\lambda}{\omega_\lambda}}e^{i\int\omega_\lambda dt} \quad , \quad Y_k^\lambda(t) = -\sqrt{1-\frac{\tilde{k}_\lambda}{\omega_\lambda}}e^{i\int\omega_\lambda dt} \tag{2.40}$$

where $\tilde{k}_\lambda$ and ω_λ are given in Eq. (2.24).

During preheating the inflaton field oscillates about its potential minimum and adiabaticity can be violated. A simple calculation reveals that this occurs when the effective wave-number $\tilde{k}_\lambda$ vanishes

$$\frac{k}{a}\lambda + \frac{C}{f}\dot{\phi} = 0. \tag{2.41}$$

Adiabaticity is violated for every k-mode twice an oscillation, once when $\dot{\phi}$ is positive (which produces (+) helicity fermions) and once when $\dot{\phi}$ is negative (which produces (–) helicity fermions). This violation of adiabaticity leads to the production of particles.

The fields produced by preheating depend sensitively on the time at which preheating ends. This occurs once the 'preheat fields' disrupt the inflaton equation of motion or else become comparable in energy density to the inflaton and thus take over the background dynamics. This provides two conditions for non-termination of preheating,

$$V_{,\phi} \gg -\frac{1}{a^3}\frac{C}{f}\langle\partial_\mu J^{\mu 5}\rangle, \tag{2.42}$$

and

$$\rho_\phi \gg \rho_\psi + \rho_A. \tag{2.43}$$

We will focus on the second condition, as this suffices to provide a lower bound on C/f such that preheating terminates after one production event (i.e. one half-oscillation).

The energy density in fermions is given by

$$\rho_\psi = \sum_\lambda \int \mathrm{d}^3k \; n_k^\lambda \omega_\lambda(k), \tag{2.44}$$

where n_k^λ is the number density and $\omega_\lambda(k)$ is the energy-per-particle. After one production event, and before conversion into photons, the number density in (–) helicity states vanishes while the number density in (+) helicity states is given by

$$n_k^+ = \begin{cases} \exp\left(-\pi \frac{m_\psi}{\sqrt{k_c^2 - k^2}}\right) & , k < k_c \\ 0 & , k > k_c. \end{cases} \tag{2.45}$$

where the 'critical wave number' k_c is defined by

$$k_c \equiv \frac{C}{f} |\dot{\phi}_{pre}|. \tag{2.46}$$

The same number density applies at the end of inflation, with $\dot{\phi}_{pre}$ being replaced by $\dot{\phi}_{end}$.

The above expressions simplify in the limit $\vartheta \gg m_\psi/H$. In this case, the energy density in fermions can be computed explicitly and is given by

$$\rho_\psi = \frac{\pi k_c^4}{3}\left(1 - \pi(3\pi - 8)\frac{m_\psi}{k_c} + \mathcal{O}(m_\psi/k_c)^{3/2}\right), \tag{2.47}$$

where terms of $\mathcal{O}(m_\psi/k_c)$ will be neglected. Meanwhile the energy density in the inflaton during preheating is given by

$$\rho_\phi \approx \frac{3}{4} m_\phi^2 \phi_{\mathrm{end}}^2. \tag{2.48}$$

One can now easily compute the lower bound on C/f such that backreaction does not shut off preheating before it begins. Using the value of k_c during inflation, the condition (2.43) can be rewritten as a constraint on C/f, as

$$\frac{C}{f} < \frac{1}{\sqrt{m_\phi \phi_{end}}} \left(\frac{9}{\pi}\right)^{1/4}. \tag{2.49}$$

For C/f violating this bound, backreaction is already significant during inflation and preheating does not occur. During the first half-cycle of preheating the critical wave

number changes by a factor of $\sqrt{2}$, which modifies this condition to

$$\frac{C}{f} < \frac{1}{\sqrt{m_\phi \phi_{end}}} \left(\frac{9}{4\pi}\right)^{1/4}. \tag{2.50}$$

For C/f violating this bound, preheating terminates after one production event. Putting in the canonical values for m and ϕ, and re-interpreting C/f as a scale of new UV physics, $C/f \equiv 1/\Lambda_{UV}$, we then find that preheating will terminate either before or immediately after one production event provided Λ_{UV} is below an upper bound given by

$$\Lambda_{UV} < 10^{-3} M_{Pl} \sim 10^{15} \text{ GeV}. \tag{2.51}$$

In this regime there are no (–) helicity fermions produced, giving a maximal helicity asymmetry. This can be rephrased as the condition $\vartheta > 10^3$ during preheating.

In the opposite regime, $\Lambda_{UV} > 10^{15}$ GeV, preheating lasts for many cycles and the number density is modified from the expression (2.45). The key difference from the previous regime is that there is now a production of (–) helicity fermions, and hence gauge fields, which occurs when $\dot{\phi}$ is negative. In this case, the expansion of the universe causes k_c to redshift, which not only changes the maximum k which is populated but also decreases the efficiency of particle production on large scales.

A thorough study of this regime must rely on numerics, as was done by [53]. However, we can make some analytic progress. The particle number on large scales following the i^{th} production event is roughly

$$n_k^i = e^{-\pi \frac{m_\psi}{k_c(t_0)} \left(\frac{a(t_i)}{a(t_0)}\right)^{3/2}}, \tag{2.52}$$

where the helicity (±) of the produced particles is dictated by the sign of $\dot{\phi}$ at the i^{th} event. The impact of the redshift factor, and the remaining helicity asymmetry on large scales $k \ll k_c$, depends sensitively on the ratio m_ψ/k_c.

For $\Lambda_{UV} > 10^{15}$GeV and $m_\psi/k_c \ll 1$, the redshift factor $(a(t_i)/a(t_0))^{3/2}$ (which for the first complete oscillation is roughly 2) is irrelevant and the production of (–) fermions is just as efficient as the production of (+) fermions. The residual asymmetry present after the subsequent oscillations is thus expected to be small, though a quantitative estimate requires numerical analysis. If instead $m_\psi/k_c \sim \mathcal{O}(1)$, the production of (–) is

much less efficient but the initial n_k^+ is only $e^{-\pi} \sim .04$. From this we conclude that the regime $\Lambda_{UV} > 10^{15}$GeV will not lead to a helicity asymmetry on large scales.

There does however remain a spatially averaged *net* helicity asymmetry in this regime, as computed in [53], which occurs due to modes with $k \sim k_c$ at the beginning of preheating which decouple once k_c becomes larger than k. However, for $\Lambda_{UV} \sim 10^{-4} M_{Pl}$ these modes are on a much smaller length scale than is of interest for CMB observations.

2.4.2 Competition of couplings

We would like to argue that there exists a regime in which the inflaton-fermion interaction is dominant for the production of circular polarization, while inflaton-gauge preheating has a subleading role.

Consider the gauge field with the usual QED interaction in addition to a Pontryagin coupling with the inflaton. There is also a derivative coupling between the chiral fermion current and the axion. The action for the gauge field is given by

$$S = \int \mathrm{d}^4x\sqrt{-g}\left[-\frac{1}{4}F_{\mu\nu}F^{\mu\nu} + A_\mu J^\mu + \frac{\alpha}{f}\phi F_{\mu\nu}\tilde{F}^{\mu\nu}\right]. \tag{2.53}$$

Then, the equation of motion for the gauge field with different helicities can be written as

$$\left(\partial_\tau^2 + k^2 \pm \frac{\alpha}{f}\frac{\dot{\phi}}{a(\tau)}k\right) A_k^\pm(\tau) = -\frac{1}{a(\tau)}J_k^\pm(\tau) \tag{2.54}$$

where the fermions have been rescaled, as in [53]. We are interested in the magnitude of the contributions of the two interaction term with the gauge field. By defining $\xi = \frac{\alpha}{f}\frac{\dot{\phi}}{H}$, then we can rewrite the equation of motion as

$$\left(\partial_\tau^2 + k^2\right) A_k^\pm(\tau) = -\frac{1}{a(\tau)}\left(J_k^\pm(\tau) \pm \xi H k A_k^\pm(\tau)\right) \tag{2.55}$$

and we are interested in calculating the relative magnitudes of the two terms on the right side.

If we impose that the QED interaction between the gauge field and fermions dominates during inflation, we have the general solution to the gauge field equation of motion as

$$A_k^\pm(\tau) \sim i\int \frac{\mathrm{d}\eta}{a(\eta)}G_k(\eta,\tau)J_k^\pm(\eta) \tag{2.56}$$

where G_k is the Green's function and we omit the background solution as it is assumed small. The Green's function has been found [55] to be

$$G_k(\eta, \tau) = \frac{-i}{k} \sin\left(k(\tau - \eta)\right) \theta(\tau - \eta) \tag{2.57}$$

Then, the condition we must satisfy becomes

$$|J_k^{\pm}(\tau)|^2 \geq \xi^2 H^4 \left| \int \mathrm{d}\eta \, \eta \sin\left(k(\tau - \eta)\right) J_k^{\pm}(\eta) \right|^2 \tag{2.58}$$

To find an upper bound on the integral, we assume that the growth of the current is slower than the change in comoving Hubble radius aH. Then, the integrand has an envelope that is monotonically decreasing, so the integral is dominated when the current is turned on at the initial time, some τ_i. Hence,

$$|J_k^{\pm}(\tau)|^2 \geq \xi^2 H^4 \tau_i^2 \tau^2 |J_k^{\pm}(\tau_i)|^2 \tag{2.59}$$

We then have the condition on the coupling strength for the $\phi F \tilde{F}$ term as

$$|\xi| \leq a(\tau_i) a(\tau) \frac{|J_k^{\pm}(\tau)|}{|J_k^{\pm}(\tau_i)|} \ll 1. \tag{2.60}$$

The direct coupling between the axion and the gauge field must remain small. The initial time cannot be small (near the end of inflation) as this would contradict the statement that the background gauge field is small, since the field would evolve under the Pontryagin term for a long period of time during inflation. Intuitively, this is a statement that the direct decay rate of the axion into the photons must be small so that the preferred decay mode is through fermions.

Then, if the Pontryagin term is to dominate after the end of inflation, we need to satisfy the equation

$$|J_k^{\pm}(\tau)|^2 \leq (\xi H k)^2 |A_k^{\pm}(\tau)|^2. \tag{2.61}$$

Here, we know the field will grow due to tachyonic instabilities, and have generally exponential growth from some initial value.

$$|A_k^{\pm}(\tau)|^2 = \exp(\lambda \tau) |A_k^{\pm}(\tau_0)|^2 \tag{2.62}$$

where τ_0 is given at the end of inflation. We have already that the gauge field at the end of inflation should behave as

$$|A_k^{\pm}(\tau_0)|^2 = \left(\frac{H}{k}\right)^2 \tau_i^2 \tau_0^2 |J_k^{\pm}(\tau_i)|^2. \tag{2.63}$$

The condition that needs to be satisfied becomes:

$$|J_k^{\pm}(\tau)|^2 \leq \left(\frac{\xi}{a(\tau_i)a(\tau_0)}\right)^2 |J_k^{\pm}(\tau_i)|^2 e^{\lambda\tau}. \tag{2.64}$$

Since the previous condition on ϑ, given by Eq. (2.60), should be saturated around the end of inflation, the new condition becomes

$$|J_k^{\pm}(\tau)|^2 \leq |J_k^{\pm}(\tau_0)|^2 e^{\lambda\tau} \tag{2.65}$$

Hence, the exponential growth factor has a bound given by

$$\lambda \geq \frac{2}{\tau} \ln\left(\frac{|J_k^{\pm}(\tau)|}{|J_k^{\pm}(\tau_0)|}\right) \tag{2.66}$$

Note, although τ is defined to be the time since the end of inflation, there should be some finite time for the phase transition near the end of inflation. Therefore, these considerations must take place some finite τ after the end of inflation.

The weak coupling of ξ may end up complicating this calculation. For weak coupling, there should be an extended period of reheating where the axion will undergo many oscillation in its potential. This will cause the ratio of circular polarization to total intensity of light to diminish after each successive oscillation. Furthermore, the exponential factor λ will generally depend on the k value that is being amplified. As a result, there will be some cutoff in k where this condition will no longer be satisfied. In general, this will favor the large k values, where we do not expect a large generation of circular polarization. Taking the solution for λ from [51],

$$\lambda_k = (3.6 \times 10^{-3}) \left(\frac{k}{\Lambda}\right)^{\frac{1}{2}} m_{pl} \tag{2.67}$$

where $\frac{1}{\Lambda} = \frac{\xi}{4\sqrt{6}m_{pl}}$. From this, Eq. (2.66) becomes a constraint on the amount of time

needed for the phase transition, given by the minimum allowed value of

$$\tau_{min} \geq \frac{2}{\lambda_k} \ln \left(\frac{|J_k^{\pm}(\tau)|}{|J_k^{\pm}(\tau_0)|} \right) \sim (10^9 \text{ s}) \left(\frac{m_{pl}}{\xi k} \right)^{\frac{1}{2}} \tag{2.68}$$

The minimum desired value of k then sets the transition time. The smaller value the k, the longer the transition will take and the assumption that the Pontryagin term will dominate during reheating no longer becomes valid. Therefore, it is not valid to produce circular polarization during inflation through a fermion chiral current and amplify the gauge field during reheating though the Pontryagin term. Based on these arguments, we will consider separately the case of preheating where the fermion-inflaton interaction dominates and when the Pontryagin-inflaton interaction dominates.

2.5 The Spectrum of Circular Polarization on Large Scales

Now we come to the primary goal of this paper: to compute the large scale circular polarization, and in particular, the spectrum. For both production channels we work in the 'strong coupling regime', such that preheating terminates before any (–) helicity particles can be produced.

2.5.1 Indirect production via $\partial_\mu \phi J^{\mu 5}$

This computation of V is in principle a tedious calculation involving integrals over fermion mode functions (which we indeed compute in the supplemental Section 2.7), but there is a intuitive shortcut that can be used to extract the spectral tilt of the V-mode spectrum: provided that the helicity asymmetry in the fermions is efficiently transferred to the gauge field, then the energy density in the gauge fields is precisely equal to the V-mode polarization, i.e.

$$\rho_A = |\dot{A}_+|^2 + |\dot{A}_-|^2 \approx |\dot{A}_+|^2, \tag{2.69}$$

and

$$V = |\dot{A}_+|^2 - |\dot{A}_-|^2 \approx |\dot{A}_+|^2 = \rho_A. \tag{2.70}$$

Moreover, at linear order in energy density perturbations and metric perturbations, and provided the energy transfer from fermions to photons is via perturbative processes (as

opposed to, say, a parametric resonance instability), the spectrum of energy density fluctuations $\delta\rho$ will be unchanged as energy is transferred from the fermions to the gauge fields. This follows from the lack of mode-mixing in linear perturbation theory. It follows from this that (up to an overall normalization) we can equate the Fourier modes of the energy density in fermions and gauge fields:

$$\delta\rho_{\psi k} \propto \delta\rho_{Ak}, \tag{2.71}$$

where the proportionality is up to a time-dependent normalization describing the transfer of energy from the fermions to gauge fields.

The spectrum of fermion energy density fluctuations is encoded in the number density and effective frequency, as the fermion energy density in a given Fourier mode is, up to a random phase, given by

$$\delta\rho_{\psi k} = \sum_{\lambda} n_{k\lambda}\omega_{k\lambda}. \tag{2.72}$$

As per our previous discussions, the number density at large coupling and on large scales is k-independent, as is $\omega_{k\lambda} \sim (C/f)\dot{\phi}$. From this it follows that $|\delta\rho_{Ak}|^2$ on large scales is independent of k, and the V-mode Fourier modes are given by

$$|\delta V_k| = \mathcal{N}, \tag{2.73}$$

for a time-dependent constant $\mathcal{N}$. This result is confirmed via explicit computation in Section 2.7, where we find the result,

$$|\delta V_k|^2 = \frac{16 g^4 f_h^2}{a^8(\tau)} (\vartheta a H)^9 \mathcal{I}(\tau), \tag{2.74}$$

which applies for scales $k \ll k_c$. The coefficient $f_h \equiv 1 - (|A_-|/|A_+|)^2$, while $\mathcal{I}(\tau)$ is a time-dependent function which is an integral over the photons Green's functions.

The power spectrum of V-mode polarization is then

$$P_{\Theta_V}(k) = \frac{1}{I^2}\frac{1}{2\pi^2}k^3|\delta V_k|^2 = \frac{\mathcal{N}^2}{I^2 2\pi^2}k^3, \tag{2.75}$$

corresponding to a spectral index of V-modes n_V, defined by $P_V \propto k^{n_V - 1}$, given by $n_V = 4$ Thus we find a deeply blue spectrum of V-mode polarization. The amplitude of

the power spectrum depends sensitively on the parameters g, ϑ, f_h, and the numerical value of the integral $\mathcal{I}(\tau)$. For an estimate of the amplitude, we turn to the other production mechanism: the coupling $\phi F\tilde{F}$.

2.5.2 Direct production of photons via $\phi F\tilde{F}$

The preheating production of gauge fields via $\phi F\tilde{F}$ was studied by one of the authors in [51]. The mode functions prepared by inflation are amplified, with the production occurring on a characteristic scale. For modes on much larger length scales, the (scalar) energy density fluctuation after the first oscillation is k-independent, with an amplitude that is proportional to the effective background energy density $\langle\rho_A\rangle$ deposited in the gauge field,

$$|\delta\rho_{Ak}|^2 \simeq \frac{\langle\rho_A\rangle^2}{(2\xi a_{end}H_{end})^3}\,. \tag{2.76}$$

The value of $\langle\rho_A\rangle$ is in turn bounded by backreaction considerations, which ultimately gives for the fluctuations, in the strong-coupling regime,

$$\delta\rho_{Ak} \sim \frac{V(\phi_{end})}{(2\xi a_{end}H_{end})^{3/2}}\frac{\Lambda_{UV}}{M_{Pl}} \quad \text{for} \quad \Lambda_{UV} \equiv (\alpha/f)^{-1} < M_{Pl}\,.$$

As in the fermionic preheating scenario, this region of parameter space causes preheating to terminate after one production event, such that a maximum polarization asymmetry is achieved.

In this case the spectrum of super-Hubble V-mode polarization is identical to the spectrum of energy density fluctuations,

$$\delta V_k = \delta\rho_{Ak}. \tag{2.77}$$

The power spectrum of V-mode anisotropies at the end of reheating [5] is given by

$$P_{\Theta_V}(k) = \frac{1}{2\pi^2}\left(\frac{\Lambda_{UV}}{M_{Pl}}\right)^2\left(\frac{k}{2\xi a_{end}H_{end}}\right)^3. \tag{2.78}$$

This is again blue-tilted with a spectral index $n_V = 4$, where $n_V = 1$ corresponds to a

[5] We assume that reheating occurs instantaneously after preheating, and that the photons produced during reheating are unpolarized. The total I at the culmination of reheating is proportional to the total energy density of the universe $\rho = 3M_{Pl}^2H^2$, and this growth in the intensity I is not accompanied by a growth in δV_k, as the tachyonic instability is no longer present during perturbative reheating.

scale-invariant spectrum.

The above expression can be written in the parametrized form (2.7) as,

$$P_{\Theta_V}(k) = \mathcal{A}_V \left(\frac{k}{k_0}\right)^{n_V - 1} \quad , \quad n_V = 4, \tag{2.79}$$

where $\mathcal{A}_V \equiv \mathcal{A}_V(k_0)$ is the amplitude at a reference scale k_0 [6]. For k_0 that exits the horizon sometime during inflation, such that $k_0 = a_0 H_0$, the amplitude $\mathcal{A}_V$ is given by

$$\mathcal{A}_V = \frac{1}{16\pi^2 \xi^3} \left(\frac{\Lambda_{UV}}{M_{Pl}}\right)^2 \left(\frac{a_0 H_0}{a_{end} H_{end}}\right)^3. \tag{2.80}$$

Due to the severe blue-tilt about $k_{end} = a_{end} H_{end}$, the amplitude is suppressed on large scales by a factor $(a_0/a_{end})^3 = e^{-3N_0}$, where N_0 is the number of e-folds of inflation remaining when the mode k_0 exits the Hubble radius. For the benchmark values of $\xi = \mathcal{O}(1)$, $\Lambda_{UV} \equiv f/\alpha = 10^{-2} M_{Pl}$, the amplitude is given by

$$\mathcal{A}_V \approx 10^{-7} e^{-3N_0}. \tag{2.81}$$

From this we see that the severe blue-tilt guarantees a majority of the integrated power will reside in modes that exit the horizon in the last e-fold of inflation. Choosing the reference scale at $k_0 = k_{end}$, the amplitude is given as $\mathcal{A}_V \approx 10^{-7}$.

2.6 Discussion

In this work we have found that axion inflation with the standard $\partial_\mu \phi J^{\mu 5}$ and $\phi F \tilde{F}$ couplings produces circular polarization with a spectral index $n_V = 4$. Currently, there has been no detection of V, and only upper limits on C_l^{VV} exist, e.g. as reported by the SPIDER collaboration [76] and MIPOL [77]. Given this, our work is in a similar spirit to computations of the tensor spectral index n_T, as primordial tensor perturbations are in a similar position of not having been observed at all, let alone their spectral index. However, n_T is a remarkably powerful tool for distinguishing models of the early universe: simple single-field inflation models predict $n_T < 0$, while String Gas Cosmology

[6] Note that the choice of k_0 is arbitrary and does not change the physical amplitude of a given k-mode. This is analogous to the pivot scale used in the power spectra for scalar and tensor fluctuations [59]

predicts $n_T > 0$ [78][7]. Here we have found that $n_V = 4$ is a generic prediction of axion inflation. It would be interesting to construct inflationary models with different values of n_V, and in particular $n_V = 1$, corresponding to a scale-invariant spectrum of V-mode polarization. It was shown in [45] that a nearly scale-invariant spectrum of V-modes can be generated by large-scale magnetic fields; it will be very interesting to connect this with models of inflationary magnetogenesis (as reviewed in [81], and analysed in [52] for axion inflation with the $\phi F\tilde{F}$ coupling we consider here).

The polarization computed here is present at the end of inflation/reheating. However, we have not touched upon the evolution from the end of reheating to the CMB. The evolution to last scattering is described by the Boltzmann equation [82],

$$\dot{V}_{A_l} + \frac{4}{3}\Theta V_{A_l} - \frac{l}{2l+1} D_{\langle a_l} V_{A_{l-1}\rangle} + D^b V_{bA_l} = -n_e \sigma_T (V_{A_l} - \frac{1}{2} V_{a_1} \delta^1_l), \tag{2.82}$$

where σ_T is the Thomson cross section, n_e is the free electron density, $\Theta \equiv \nabla_a u^a$ is the volume expansion, and A_l is a string of indices $a_1..a_l$. We refer the reader to [82] for further details on the notation. The above equation (or rather, scalar multipole moments of the above equation) must be incorporated into a CMB Boltzmann solver, such as CAMB, in order to make precise predictions for the C_l^{VV} observed by CMB experiments. Our results serve as the initial conditions for this analysis. It will be interesting to see if the existing upper limits on V set by MIPOl [77] or SPIDER [76] can already place constraints on the mechanism discussed here.

The evolution of circular polarization after horizon re-entry was discussed in [55], where it was found that there is an exponential suppression of V due to QED interactions. At a temperature scale below the mass of the electron, Thomson scattering washes out any net photon helicity due to the large optical depth at this scale. Even with an initial $V/I \simeq 1$, the standard cosmological treatment of the radiation Boltzmann equation could potentially render primordial circular polarization undetectable in the CMB.

There are, however, potential mechanisms to subvert this exponential decay. As the universe expands, the efficiency at which Thomson scattering can suppress circular polarization diminishes. Hence, there is a temperature scale T_c below which circular po-

[7] Blue-tilted super-horizon tensor modes can also be realized in certain non-minimal inflation models, see e.g.[79], and also in axion inflation coupled to gauge fields [80].

larization will receive negligible corrections due to Compton scattering, and a window is provided between T_c and last scattering during which sources of circular polarization may be present and detectable in the CMB. As an example, [45] shows that magnetic fields present in the plasma at last scattering can source circular polarization. Alternatively, a more direct late time production can be found if the axion's velocity, $\dot{\phi}$, is nonzero at late times. Finally, work on cosmic birefringence [83] has suggested that a rotation angle between E and B-mode polarization can arise from a Chern-Simons term. This rotation angle relies on late time dynamics of the pseudo-scalar field, hence one should also expect a late time production of circular polarization.

Each of these three mechanisms for preventing the decay of V can be described in terms of physical phenomena in the plasma at last scattering. For a constant magnetic field, the dielectric constant becomes dependent on the helicity of the propagating photon. The Chern-Simons term causes a relative change in the dispersion relation of the photons. Finally, the chemical potential in fermions will induce different plasma frequencies for each photon helicity. In each case, if the mechanism is present in the plasma sufficiently early, the full Compton cross section can conserve photon helicity in interactions, preserving some primordial V-mode polarization. We leave a more detailed description of these phenomena for future work.

There are many other directions for future work that we have not touched upon here. Foremost among this is the analysis of cross-correlation of V with other CMB observables. For example, it is known that $\phi F\tilde{F}$ yields a characteristic tensor mode signal [80]; it will be interesting to study the cross-correlation of V and B in this model. Such a complete analysis will maximize the information that can be extracted from future CMB experiments, and the constraints on axion inflation that can derived.

2.7 Appendix: Computation of δV_k

We want to study Fourier modes of the stokes parameter V. However, since $V \sim \dot{A}^2 \sim \psi^4$ is a composite operator, we have to be careful in how we proceed.

Let's first consider a general (real) operator $\mathcal{O}(x,t)$. This can be split into a background and fluctuation piece via the definition

$$\mathcal{O}(x,t) = \langle \mathcal{O} \rangle (t) + \delta\mathcal{O}(x,t), \tag{2.83}$$

where $< .. >$ denotes a classical ensemble average or quantum vacuum expectation value, on super- and sub-Hubble scales respectively. The fluctuation piece can be expanded into plane waves as

$$\delta\mathcal{O}(x,t) = \int \frac{\mathrm{d}^3k}{(2\pi)^3}\delta\mathcal{O}_k\,\alpha_k\,e^{ikx}, \tag{2.84}$$

where α_k are classical random variables, or quantum mechanical annihilation/creation operators, with $\alpha_k = \alpha^*_{-k}$ (which allowed us in the above to combine the positive and negative frequency modes into one term). The mode functions $\delta\mathcal{O}_k$ are then given

$$|\delta\mathcal{O}_k|^2 = \int \mathrm{d}^3x e^{-ikx}\,\left[\,\langle\mathcal{O}(x)\mathcal{O}(0)\rangle - \langle\mathcal{O}\rangle^2\right]. \tag{2.85}$$

As an illustrative example, one can consider $\mathcal{O} = \phi^2$ for a scalar field ϕ. In this case, (2.85) leads to

$$|\delta(\phi\phi)_k|^2 = 2\int \frac{\mathrm{d}^3k'}{(2\pi)^3}|\phi_{k'}|^2|\phi_{k-k'}|^2. \tag{2.86}$$

For the case of interest for the current work, the mode functions are given by

$$|\delta V_k|^2 = 2\int \mathrm{d}^3x\, e^{-ikx}\,\left[\,\langle V(x)V(0)\rangle - \langle V\rangle^2\right] \tag{2.87}$$

Using the expressions of the previous sections, a two-point function $\langle V(x)V(y)\rangle$ is given in terms of a 4-point function of fermion currents [8],

$$\langle V(x)V(y)\rangle = \frac{f_h^2}{a^8}\int\left(\prod_{j=1}^{4}\mathrm{d}\eta_j\,a(\eta_j)G'(\eta_j,\tau)\right)\langle J^\mu(x,\eta_1)J^\dagger_\mu(x,\eta_2)J^\nu(y,\eta_3)J^\dagger_\nu(y,\eta_4)\rangle. \tag{2.88}$$

where $f_h \equiv 1-(|A_-|/|A_+|)^2$ is the efficiency of helicity transfer from the $(\pm)$ fermions to the $(\pm)$ circularly polarized photons: if $f_h = 1$, then helicity is conserved at every interaction, and only + photons are produced. This, in turn, is an 8-point function of fermions (note that $(\overline{\psi}\gamma_\mu\psi)^\dagger = \overline{\psi}\gamma_\mu\psi$):

$$\begin{aligned}&\langle J^\mu(x,\eta_1)J^\dagger_\mu(x,\eta_2)J^\nu(y,\eta_3)J^\dagger_\nu(y,\eta_4)\rangle \\ &\qquad = g^4\langle(\overline{\psi}\gamma^\mu\psi)_{x,\eta_1}(\overline{\psi}\gamma_\mu\psi)_{x,\eta_2}(\overline{\psi}\gamma^\nu\psi)_{y,\eta_3}(\overline{\psi}\gamma_\nu\psi)_{y,\eta_4}\rangle\end{aligned} \tag{2.89}$$

[8] Note: this expression already implicitly assumes that only one photon polarization is amplified

This 8-point function can be computed using the fermionic version of Wick's theorem, keeping track of factors of (-1) from shuffling the fermions. We can begin by decomposing it into 4-point functions:

$$\begin{aligned}\frac{1}{g^4}\langle J^\mu(x,\eta_1)J^\dagger_\mu(x,\eta_2)J^\nu(y,\eta_3)J^\dagger_\nu(y,\eta_4)\rangle \\ = \langle(\overline{\psi}\gamma^\mu\psi)_{x,\eta_1}(\overline{\psi}\gamma_\mu\psi)_{x,\eta_2}\rangle\cdot\langle(\overline{\psi}\gamma^\nu\psi)_{y,\eta_3}(\overline{\psi}\gamma_\nu\psi)_{y,\eta_4}\rangle \\ + \langle(\overline{\psi}\gamma^\mu\psi)_{x,\eta_1}(\overline{\psi}\gamma^\nu\psi)_{y,\eta_3}\rangle\cdot\langle(\overline{\psi}\gamma_\mu\psi)_{x,\eta_2}(\overline{\psi}\gamma_\nu\psi)_{y,\eta_4}\rangle \\ + \langle(\overline{\psi}\gamma^\mu\psi)_{x,\eta_1}(\overline{\psi}\gamma_\nu\psi)_{y,\eta_4}\rangle\cdot\langle(\overline{\psi}\gamma_\mu\psi)_{x,\eta_2}(\overline{\psi}\gamma^\nu\psi)_{y,\eta_3}\rangle\end{aligned} \tag{2.90}$$

The first term is precisely $\langle V\rangle^2$, leaving only the last two terms to determine δV_k. Additionally, since the integral is invariant under the exchange $\eta_3 \leftrightarrow \eta_4$, the last two terms will give identical contributions. Returning to our expression for δV_k, we now have

$$\begin{aligned}|\delta V_k|^2 = 4g^4 f_\hbar^2 \int \mathrm{d}^3x e^{-ikx}\,\frac{1}{a^8}\int\left(\prod_{j=1}^4 \mathrm{d}\eta_j\, a(\eta_j)G'(\eta_j,\tau)\right) \\ \times\langle(\overline{\psi}\gamma^\mu\psi)_{x,\eta_1}(\overline{\psi}\gamma^\nu\psi)_{y,\eta_3}\rangle\langle(\overline{\psi}\gamma_\mu\psi)_{x,\eta_2}(\overline{\psi}\gamma_\nu\psi)_{y,\eta_4}\rangle.\end{aligned} \tag{2.91}$$

The remaining four-point function can be split into two-point functions using Wick's theorem. However it is convenient to decompose the four-component fermion ψ into two-component spinors φ, η since

$$\frac{1}{g}\langle J^\mu(x,\eta_1)\rangle = \frac{1}{g}\overline{\sigma}^{\mu ab}\langle J_{ab}\rangle = \overline{\sigma}^{\mu ab}\left(\langle\varphi^\dagger_a\varphi_b\rangle - \langle\eta^\dagger_a\eta_b\rangle\right) = 0 \tag{2.92}$$

becomes automatically imposed. The product of four-point functions appearing on the second line of (2.91) can be written as

$$\begin{aligned}\langle(\overline{\psi}\gamma^\mu\psi)_{x,\eta_1}(\overline{\psi}\gamma_\nu\psi)_{y,\eta_3}\rangle\langle(\overline{\psi}\gamma_\mu\psi)_{x,\eta_2}(\overline{\psi}\gamma^\nu\psi)_{y,\eta_4}\rangle \\ = \frac{1}{g^4}\langle J^\mu(x,\eta_1)J^\nu(y,\eta_3)\rangle\langle J_\mu(x,\eta_2)J_\nu(y,\eta_4)\rangle\end{aligned} \tag{2.93}$$

and the remaining four-point function has the form

$$\begin{aligned}\frac{1}{g^2}\overline{\sigma}^{\mu ab}\overline{\sigma}^{\nu cd}\langle J_{ab}(x,\eta_1)J_{cd}(y,\eta_3)\rangle \\ &= \overline{\sigma}^{\mu ab}\overline{\sigma}^{\nu cd}\langle\Big(\varphi_a^\dagger\varphi_b-\eta_a^\dagger\eta_b\Big)_{x,\eta_1}\Big(\varphi_c^\dagger\varphi_d-\eta_c^\dagger\eta_d\Big)_{y,\eta_3}\rangle \\ &= \overline{\sigma}^{\mu ab}\overline{\sigma}^{\nu cd}\Big(\langle\varphi_a^\dagger\varphi_b\varphi_c^\dagger\varphi_d\rangle-\langle\eta_a^\dagger\eta_b\varphi_c^\dagger\varphi_d\rangle-\langle\varphi_a^\dagger\varphi_b\eta_c^\dagger\eta_d\rangle+\langle\eta_a^\dagger\eta_b\eta_c^\dagger\eta_d\rangle\Big).\end{aligned} \tag{2.94}$$

Again, Wick's theorem can be used to split the fermion four-point function into two-point functions as

$$\langle\varphi_a^\dagger\varphi_b\varphi_c^\dagger\varphi_d\rangle=\langle\varphi_a^\dagger\varphi_b\rangle\cdot\langle\varphi_c^\dagger\varphi_d\rangle-\langle\varphi_a^\dagger\varphi_d\rangle\cdot\langle\varphi_b\varphi_c^\dagger\rangle \tag{2.95}$$

$$\langle\eta_a^\dagger\eta_b\varphi_c^\dagger\varphi_d\rangle=\langle\eta_a^\dagger\eta_b\rangle\cdot\langle\varphi_c^\dagger\varphi_d\rangle+\langle\eta_a^\dagger\varphi_c^\dagger\rangle\cdot\langle\eta_b\varphi_d\rangle \tag{2.96}$$

$$\langle\varphi_a^\dagger\varphi_b\eta_c^\dagger\eta_d\rangle=\langle\varphi_a^\dagger\varphi_b\rangle\cdot\langle\eta_c^\dagger\eta_d\rangle+\langle\varphi_a^\dagger\eta_c^\dagger\rangle\cdot\langle\varphi_b\eta_d\rangle \tag{2.97}$$

$$\langle\eta_a^\dagger\eta_b\eta_c^\dagger\eta_d\rangle=\langle\eta_a^\dagger\eta_b\rangle\cdot\langle\eta_c^\dagger\eta_d\rangle-\langle\eta_a^\dagger\eta_d\rangle\cdot\langle\eta_b\eta_c^\dagger\rangle. \tag{2.98}$$

The first term on the right hand side of these four-point functions will factor to $\langle J_{ab}\rangle\langle J_{cd}\rangle$. The fluctuation piece of the four-point function can then be written as

$$\begin{aligned}\frac{1}{g^2}\langle J^\mu(x,\eta_1)J^\nu(y,\eta_3)\rangle = 2\overline{\sigma}^{\mu ab}\overline{\sigma}^{\nu cd}\Big(&\langle\varphi_a^\dagger(x,\eta_1)\varphi_d(y,\eta_3)\rangle\cdot\langle\varphi_c^\dagger(y,\eta_3)\varphi_b(x,\eta_1)\rangle \\ &+\langle\eta^\dagger_{(a}(x,\eta_1)\varphi^\dagger_{c)}(y,\eta_3)\rangle\cdot\langle\varphi_{(d}(y,\eta_3)\eta_{b)}(x,\eta_1)\rangle\rangle\Big),\end{aligned} \tag{2.99}$$

where round brackets (..) around indices denotes symmetrized indices. The two-point functions appearing above can be written explicitly in terms of fermion mode functions, which have the general form[9]

$$\begin{aligned}\langle\varphi_a^\dagger(x,\eta_1)\varphi_d(y,\eta_3)\rangle = \sum_\lambda\int\frac{\mathrm{d}^3k}{(2\pi)^3}\xi_a^\lambda(\mathbf{k})\xi_d^{\lambda\dagger}(\mathbf{k})e^{i\mathbf{k}\cdot(\mathbf{x}-\mathbf{y})}, \\ \times\Big[X_k^{-\lambda *}(\eta_1)X_k^{-\lambda}(\eta_3)-Y_k^{\lambda *}(\eta_1)Y_k^{\lambda}(\eta_3)\Big]\end{aligned} \tag{2.100}$$

$$\begin{aligned}\langle\eta_a^\dagger(x,\eta_1)\varphi_c^\dagger(y,\eta_3)\rangle = \sum_\lambda\int\frac{\mathrm{d}^3k}{(2\pi)^3}\xi_a^\lambda(\mathbf{k})\xi_c^{\lambda\dagger}(\mathbf{k})e^{i\mathbf{k}\cdot(\mathbf{x}-\mathbf{y})} \\ \times\Big[Y_k^{\lambda *}(\eta_1)X_k^{\lambda *}(\eta_3)-Y_k^{-\lambda *}(\eta_3)X_k^{-\lambda *}(\eta_1)\Big]\end{aligned} \tag{2.101}$$

[9] Using the relation $\xi^\lambda(\hat{k})=\xi^{-\lambda}(-\hat{k})$, which follows from the explicit form of the eigenspinors, given in [62].

On large scales we can expand the fermion mode functions as

$$X_k^+(k\tau) = -\left(\frac{m_\psi}{H}\Gamma(-2i\vartheta)\right)(1-i)\,2^{-1+i\vartheta}\,e^{ik\tau+\pi\vartheta}(-k\tau)^{i\vartheta}, \tag{2.102}$$

$$X_k^-(k\tau) = -(1+i)\,2^{-1+i\vartheta}\,e^{-ik\tau}(-k\tau)^{i\vartheta}, \tag{2.103}$$

$$Y_k^{+*}(k\tau) = -(1+i)\,2^{-1-i\vartheta}\,e^{-ik\tau}(-k\tau)^{-i\vartheta}, \tag{2.104}$$

$$Y_k^{-*}(k\tau) = -\left(\frac{m_\psi}{H}\Gamma(2i\vartheta)\right)(1-i)\,2^{-1-i\vartheta}\,e^{ik\tau-\pi\vartheta}(-k\tau)^{-i\vartheta}. \tag{2.105}$$

We then define the quantities:

$$\mathcal{A}_k^\lambda(\eta_i,\eta_j) = \left[X_k^{-\lambda *}(\eta_i)X_k^{-\lambda}(\eta_j) - Y_k^{\lambda *}(\eta_i)Y_k^{\lambda}(\eta_j)\right], \tag{2.106}$$

$$\mathcal{B}_k^\lambda(\eta_i,\eta_j) = \left[Y_k^{\lambda *}(\eta_i)X_k^{\lambda *}(\eta_j) - Y_k^{-\lambda *}(\eta_j)X_k^{-\lambda *}(\eta_i)\right]. \tag{2.107}$$

In general, neither A_k^λ, B_k^λ are nonzero, however we can order them for small m_ψ/H,

$$\mathcal{A}^+ \sim \mathcal{O}(1) \quad , \quad \mathcal{B}^\pm \sim \mathcal{O}\left(\frac{m}{H}\right) \quad , \quad \mathcal{A}^- \sim \mathcal{O}\left(\frac{m^2}{H^2}\right) \tag{2.108}$$

To lowest order in m_ψ/H, the fermion four-point function takes the form

$$\begin{aligned}\frac{1}{g^2}\langle J^\mu(x,\eta_1)J^\nu(y,\eta_3)\rangle = 2\overline{\sigma}^{\mu ab}\overline{\sigma}^{\nu cd}\int\frac{\mathrm{d}^3k_1}{(2\pi)^3}\frac{\mathrm{d}^3k_2}{(2\pi)^3}\mathcal{A}_{k_1}^+(\eta_1,\eta_3)\mathcal{A}_{k_2}^+(\eta_3,\eta_1) \\ \times\,\xi_a^+(\mathbf{k}_1)\xi_d^{+\dagger}(\mathbf{k}_1)\xi_c^+(\mathbf{k}_2)\xi_b^{+\dagger}(\mathbf{k}_2)e^{i(\mathbf{k}_1-\mathbf{k}_2)\cdot(\mathbf{x}-\mathbf{y})}\end{aligned} \tag{2.109}$$

where the next order correction is $\mathcal{O}(m/H)^2$. Therefore, the product appearing on the second line of (2.91) can be written in the form (now dropping the + superscript from the ξ's):

$$\begin{aligned}&\frac{1}{g^4}\langle J^\mu(x,\eta_1)J^\nu(y,\eta_3)\rangle\langle J_\mu(x,\eta_2)J_\nu(y,\eta_4)\rangle \\ &\quad= 4\overline{\sigma}^{\mu ab}\overline{\sigma}^{\nu cd}\overline{\sigma}_\mu^{rs}\overline{\sigma}_\nu^{tu}\int_0^{\vartheta aH}\frac{\mathrm{d}^3k_1}{(2\pi)^3}\frac{\mathrm{d}^3k_2}{(2\pi)^3}\frac{\mathrm{d}^3k_3}{(2\pi)^3}\frac{\mathrm{d}^3k_4}{(2\pi)^3} \\ &\quad\times\Bigg[\exp[i(\mathbf{k}_1-\mathbf{k}_2+\mathbf{k}_3-\mathbf{k}_4)\cdot(\mathbf{x}-\mathbf{y})] \\ &\quad\times\mathcal{A}_{k_1}^+(\eta_1,\eta_3)\mathcal{A}_{k_2}^+(\eta_3,\eta_1)\mathcal{A}_{k_3}^+(\eta_2,\eta_4)\mathcal{A}_{k_4}^+(\eta_4,\eta_2) \\ &\quad\times\xi_a(\mathbf{k}_1)\xi_d^\dagger(\mathbf{k}_1)\xi_c(\mathbf{k}_2)\xi_b^\dagger(\mathbf{k}_2)\xi_r(\mathbf{k}_3)\xi_u^\dagger(\mathbf{k}_3)\xi_t(\mathbf{k}_4)\xi_s^\dagger(\mathbf{k}_4)\Bigg]\end{aligned} \tag{2.110}$$

where the function $\mathcal{A}_k^+(\eta_1,\eta_2)$ can be explicitly written as

$$\mathcal{A}_k^+(\eta_1,\eta_2) = i\sin\left(k(\eta_1-\eta_2)\right)\exp\left[-i\vartheta\log\left(\frac{\eta_1}{\eta_2}\right)\right]. \tag{2.111}$$

Finally, the mode functions of the circular polarization (using the inflationary fermion mode functions and taking the lowest order in mass) are given by:

$$\begin{aligned}|\delta V_k|^2 =& 16g^4 f_h^2 \frac{1}{a^8(\tau)}\int\left(\prod_{j=1}^{4}\mathrm{d}\eta_j\, a(\eta_j)G'(\eta_j,\tau)\right)\int \mathrm{d}^3x \\ &\times\int_0^{\vartheta aH}\frac{\mathrm{d}^3k_1}{(2\pi)^3}\frac{\mathrm{d}^3k_2}{(2\pi)^3}\frac{\mathrm{d}^3k_3}{(2\pi)^3}\frac{\mathrm{d}^3k_4}{(2\pi)^3}\Bigg[\exp[i(\mathbf{k}_1-\mathbf{k}_2+\mathbf{k}_3-\mathbf{k}_4-\mathbf{k})\cdot\mathbf{x}] \\ &\times\sin\left(k_1(\eta_1-\eta_3)\right)\sin\left(k_2(\eta_1-\eta_3)\right)\sin\left(k_3(\eta_2-\eta_4)\right)\sin\left(k_4(\eta_2-\eta_4)\right) \\ &\times\xi(k_1)\overline{\sigma}^{\mu}\xi^{\dagger}(k_2)\cdot\xi(k_2)\overline{\sigma}^{\nu}\xi^{\dagger}(k_1)\cdot\xi(k_3)\overline{\sigma}_{\mu}\xi^{\dagger}(k_4)\cdot\xi(k_4)\overline{\sigma}_{\nu}\xi^{\dagger}(k_3)\Bigg].\end{aligned} \tag{2.112}$$

We can now perform the x-integration and one of the k_i-integrations. If we choose $i=4$, this sets $\mathbf{k}_4=\mathbf{k}_1-\mathbf{k}_2+\mathbf{k}_3-\mathbf{k}$. For $k/aH\ll 1$, the remaining k-integrals are dominated by the upper bound $k_i=\vartheta aH$.

$$\begin{aligned}|\delta V_k|^2 \approx& \frac{16g^4f_h^2}{a^8(\tau)}(\vartheta aH)^9\int\left(\prod_{j=1}^{4}\mathrm{d}\eta_j\, a(\eta_j)G'(\eta_j,\tau)\right)\sin\left(\vartheta aH(\eta_1-\eta_3)\right) \\ &\times\sin\left(\vartheta aH(\eta_1-\eta_3)\right)\sin\left(\vartheta aH(\eta_2-\eta_4)\right)\sin\left(\vartheta aH(\eta_2-\eta_4)\right) \\ &\times\int_{|k_i|=\vartheta aH}\mathrm{d}\theta_1\mathrm{d}\phi_1\mathrm{d}\theta_2\mathrm{d}\phi_2\mathrm{d}\theta_3\mathrm{d}\phi_3\xi(\theta_1,\phi_1)\overline{\sigma}^{\mu}\xi^{\dagger}(\theta_2,\phi_2) \\ &\times\xi(\theta_2,\phi_2)\overline{\sigma}^{\nu}\xi^{\dagger}(\theta_1,\phi_1)\cdot\xi(\theta_3,\phi_3)\overline{\sigma}_{\mu}\xi^{\dagger}(\mathbf{k}_4)\cdot\xi(\mathbf{k}_4)\overline{\sigma}_{\nu}\xi^{\dagger}(\theta_3,\phi_3),\end{aligned} \tag{2.113}$$

where the final line is an integral over the angular variables of the k_i at $|k_i|=\vartheta aH$, (recall that $\xi_\lambda(\mathbf{k})$ depends only on $\hat{k}$), and $\mathbf{k}_4\approx\mathbf{k}_1-\mathbf{k}_2+\mathbf{k}_3$ is evaluated at $|k_1|=|k_2|=|k_3|=\vartheta aH$. Again we note that all ξ's appearing above are ξ^+. This result has the schematic form,

$$|\delta V_k|^2 = \frac{16g^4f_h^2}{a^8(\tau)}(\vartheta aH)^9\,\mathcal{I}(\tau) \tag{2.114}$$

where $\mathcal{I}(\tau)$ is integral over Green's functions given above, and the angular integral over the helicity eigenspinors. As per the discussion in Section 2.4, the above $|\delta V_k|^2$ (valid on large scales) is k-independent.

Chapter 3

Oscillating Electric Dipole Moment

3.1 Introduction

While the idea of axionic dark matter is not new, the Invisible Axion and ALP have evaded detection in both astrophysical and Earth-based experiments. Some experiments have capitalized on enhancing detection in a resonant cavity with a strong external magnetic field [84, 85, 86]. Others have exploited the possibility of detecting the change in flux from a carefully oriented external magnetic field [87, 88]. Typically, these experiments rely on the modification to Maxwell's equations [24, 25, 89] by the axion-photon interaction of the form $\delta\mathcal{L} \propto \phi E \cdot B$. In contrast, we consider a new possibility of detecting the axion directly from its interaction with electrons.

Previously, various authors considered couplings of the axion to matter fields in the standard model [37, 90, 91, 92]. When considering the QCD axion, it is possible for the electron to have direct couplings and radiatively induced couplings to the axion. This interaction manifests by distinguishing the axion from the longitudinal Z^0 after spontaneously breaking electroweak symmetry [37]. The axion-electron effective interaction will then take the form of

$$\mathcal{L} \supset \frac{2X'_e m_e}{f_a}\phi\bar{\Psi}_e i\gamma^5\Psi_e, \tag{3.1}$$

where X'_e is related to the electron's Peccei-Quinn charge. Without restricting to a particular axion-like model, we will treat this coupling coefficient as an effective parameter.

As we will see, the relativistic axion-electron interaction will induce a non-relativistic interaction that involves an axion, electric field, electron coupling which will cause spin precession in the electron wave function; an electric dipole moment. This effect is similar to how a spin-magnetic field coupling can lead to spin precession. Similar mechanisms have been considered [93, 94] and find similar forms for an induced electron electric dipole moment. In this chapter, we consider new interactions and the quantum mechanics of electrons in the presence of axion dark matter and an external electric field. We will find that there is an induced change in magnetic flux that is in principle detectable for realistic background field values. Finally, we propose an idealized experiment, similar to [95], which may detect such a change in flux.

3.2 Non-relativistic Axion-Electron Dynamics

Consider dimension-four operators coupling a U(1) gauge field A_μ, fermion Ψ, and real pseudoscalar ϕ that retain gauge invariance and shift-symmetry. A simple example, analogous to the simplest realizations of Invisible Axion scenarios, contains an extra Higgs singlet is introduced whose phase is the axion $\Phi = \rho e^{i\phi/f}$. Yukawa couplings to quarks and leptons yield the following shift symmetric axion couplings:

$$\mathcal{L}_\phi = -\frac{1}{2}\partial_\mu\phi\partial^\mu\phi - \mu^4\left[1-\cos\left(\frac{\phi}{f}\right)\right] + \lambda f \sin\left(\frac{\phi}{f}\right)\bar{\Psi}i\gamma^5\Psi + ..., \tag{3.2}$$

where λ is the dimensionless Yukawa coupling of the singlet Φ and fermions Ψ, and μ is a parameter related to instanton effects. For a detailed description of low energy fermionic coupings for the QCD axion, see [96].

We will be studying ultra light axion dark matter solutions, given in Eq. (3.10), where $\phi \ll f$. This will reflect a symmetry breaking, where the axion acquires a mass by settling into one of the degenerate minima of its (effective) cosine potential. Without loss of generality, we assume the axion settles into $\phi = 0$ minima, and the small field expansion for ϕ/f is applied to the Lagrangian.

The resulting effective Lagrangian can be written as

$$\mathcal{L} = \bar{\Psi}\left(i\gamma^\mu D_\mu - m\right)\Psi - i\lambda\phi\bar{\Psi}\gamma^5\Psi + \mathcal{L}_{\text{kin}} \tag{3.3}$$

where D_μ is the U(1) gauge covariant derivative, and $\mathcal{L}_{\text{kin}}$ contains the kinetic terms for the pseudoscalar and the gauge field. In particular, we consider interactions between electromagnetism, electrons, and the axion. The equation of motion for the fermion field Ψ is found as

$$\left(i\gamma^\mu\partial_\mu - m + g\gamma^\mu A_\mu - i\lambda\phi\gamma^5\right)\Psi = 0. \tag{3.4}$$

We want to find a non-relativistic form of the equation of motion, analogous to the Schrodinger equation.

Working in the Dirac basis, define $A_0 = \varphi$ and decompose the Dirac fermion four-spinor Ψ into two component spinors. Then, the equation of motion gives coupled differential equations for the two-component spinors

$$(E + g\varphi - m)\,\Psi_e = -\left(-i\lambda\phi + \vec{\sigma}\cdot\left(\vec{p} + g\vec{A}\right)\right)\Psi_{\bar{e}}, \tag{3.5}$$

$$(E + g\varphi + m)\,\Psi_{\bar{e}} = \left(-i\lambda\phi - \vec{\sigma}\cdot\left(\vec{p} + g\vec{A}\right)\right)\Psi_e. \tag{3.6}$$

In taking the non-relativistic limit, the limit $g\varphi \ll m$ is imposed, as well as the usual approximation $E \approx m$. Taking these approximations, the equation for $\Psi_{\bar{e}}$ becomes

$$2m\Psi_{\bar{e}} \approx -\left(i\lambda\phi + \vec{\sigma}\cdot\vec{\pi}\right)\Psi_e, \tag{3.7}$$

where we have defined $\vec{\pi} = \vec{p} + g\vec{A}$. For $\lambda\phi \ll m$, the amplitude of the positron $\Psi_{\bar{e}}$ is suppressed when compared to the electron's amplitude Ψ_e. This condition naturally arises due to the small coupling between the axion dark matter and standard model fermions, and the small expectation value for the axion due to symmetry breaking.

After redefining the energy as the non-relativistic energy $E \to E + m$, solving for $\Psi_{\bar{e}}$ gives the uncoupled equation for Ψ_e can be found. Given that the fermion mass is the largest parameter in the problem, we expand the equation of motion in orders of $1/m$. To lowest order, the non-relativistic equation of motion is

$$\begin{aligned} E\Psi_e = &\left[\frac{1}{2m}\left(i\vec{\nabla} + g\vec{A}\right)^2 + 2\left(\frac{g}{2m}\right)\vec{S}\cdot\vec{B} - g\varphi\right]\Psi_e \\ &+ 2\left(\frac{g}{2m}\right)\left[\vec{S}\cdot\vec{\nabla}\left(\frac{\lambda}{g}\phi\right)\right]\Psi_e + \frac{(\lambda\phi)^2}{2m}\Psi_e. \end{aligned} \tag{3.8}$$

Written this way, it appears that spatial gradients of the axion field can act as an

effective magnetic field for the electrons with value $\vec{B}_{\text{eff}} = \frac{\lambda}{g}\vec{\nabla}\phi$.

Inclusion of the next order corrections introduces many important phenomena to the quantum mechanical description of the electron, including the spin-orbit coupling. Additionally, terms will appear in the non-relativistic Hamiltonian for an electron interacting with electromagnetic fields and axions. In particular, the new axion interaction terms, to second order, are given by

$$H_{axion} = \frac{\lambda}{m}\left(1 - \frac{g\varphi}{2m}\right)\left[\vec{S}\cdot\vec{\nabla}\phi + \frac{1}{2}\lambda\phi^2\right] + \left(\frac{g\lambda\phi}{2m^2}\right)\vec{S}\cdot\vec{\mathcal{E}}, \tag{3.9}$$

where the electric field is defined as $\vec{\mathcal{E}} = -\vec{\nabla}\varphi$.

We want to understand which is the dominant term. In the non-relavistic regime, $g\varphi \ll m$, hence the first term in H_{axion} can be looked at as simply the $1/m$ dependence. In other words, we want to compare the magnitudes of $\lambda\vec{\nabla}\phi$ and $\frac{g\lambda}{m}\phi\vec{\mathcal{E}}$. The first term is a quantity set by the axion field, which we cannot control. However, the second term depends on the external electric field. Hence, we want to find some condition on the electric field magnitude. We do not consider the $\lambda^2\phi^2$ term as it will only produce a uniform shift in the energy of the electron.

Consider a model where the axion ϕ is the principal component of our local dark matter energy density ρ_{DM}. We approximate the axion field, as in [97], by

$$\phi(t,x) \approx \frac{\sqrt{2\rho_{DM}}}{m_\phi}\cos\left[m_\phi\left(t - \vec{v}\cdot\vec{x}\right)\right] \tag{3.10}$$

where m_ϕ is the axion mass, $\vec{v}$ is the virial velocity in our galaxy $|\vec{v}| \sim 10^{-3}$. Then, the critical value of the electric field is

$$\mathcal{E} = \frac{m_e}{g}\frac{\nabla\phi}{\phi} \sim (3\times 10^9\ \text{V/m})\left(\frac{m_\phi}{1\ \text{eV}}\right). \tag{3.11}$$

Most dark matter model use values of $m_\phi \leq 10^{-6}$ eV, giving the $\mathcal{E} \sim 1$ kV/m. Above this value, the $\vec{S}\cdot\vec{\mathcal{E}}$ term is the dominant axion-electron interaction term. For the remainder of the calculation, we assume that we are above this critical electric field and consider only the additional term

$$H_{axion} = \left(\frac{g\lambda\phi}{2m_e^2}\right)\vec{S}\cdot\vec{\mathcal{E}}. \tag{3.12}$$

3.3 Spin-Precession and Electric Dipole Moment

For now, we consider what happens for a single electron subject to electromagnetic fields. The axion field term is considered to be a perturbative addition to the Hamiltonian, H_1. We ignore the spin-orbit coupling term for simplicity, however in the presence of a magnetic field, we expect this term will be at least as important as the axion correction term. Furthermore, we wish to isolate the effects of the new axion interaction by explicitly setting the magnetic field to zero. Written explicitly, we consider the following Hamiltonian for the electron:

$$H = -\frac{1}{2m_e}\nabla^2 - g\varphi + \frac{g\lambda}{2m_e^2}\vec{S}\cdot\vec{\mathcal{E}}\,\phi(\vec{x},t). \tag{3.13}$$

We take constant electric field $\vec{\mathcal{E}} = \mathcal{E}\hat{z}$. We want to find the commutator

$$\left[\frac{p^2}{2m_e} - g\varphi, \frac{g\lambda\mathcal{E}}{2m_e^2}S_z\phi(\vec{x},t)\right] = \frac{g\lambda\mathcal{E}}{4m_e^3}S_z\left[p^2,\phi(\vec{x},t)\right] \tag{3.14}$$

where we note the Hilbert space associated with the spin is disjoint from the spatial dependence. The remaining commutator is in general nonzero. Using the form of the axion field from Eq. (3.10), each spatial gradient of ϕ is suppressed by a factor $m_\phi v \ll 10^{-8}$ eV. As a result, we approximate the axion field as spatially homogeneous $\phi(\vec{x},t) = \langle\phi\rangle$, giving $\left[p^2,\phi(\vec{x},t)\right] = 0$. Therefore, we use a basis that simultaneously diagonalizes the Hamiltonian, $\psi_n(\vec{x})\,|\pm\rangle$ defined by

$$H_0\psi_n(\vec{x},t) = E_n\psi_n(\vec{x},t), \tag{3.15}$$

$$H_1\,|\pm\rangle = \pm\frac{g\lambda\mathcal{E}}{4m_e^2}\langle\phi\rangle\,|\pm\rangle\,. \tag{3.16}$$

The axion interaction Hamiltonian results in splitting in the electron energy spectrum. As an example, consider some initial state

$$\Psi(\vec{x},t=0) = \psi_n(\vec{x},0)\left(\frac{|+\rangle + |-\rangle}{\sqrt{2}}\right) \tag{3.17}$$

such that $\int |\psi_n(\vec{x},0)|^2 = 1$. The expectation values of spins in each direction at some later time t is given by

$$\langle S_x \rangle = \frac{1}{2}\cos\left(\frac{g\lambda\mathcal{E}\langle\phi\rangle}{2m_e^2}t\right), \quad \langle S_y \rangle = \frac{1}{2}\sin\left(\frac{g\lambda\mathcal{E}\langle\phi\rangle}{2m_e^2}t\right),$$
$$\langle S_z \rangle = 0. \tag{3.18}$$

We recognize this as a spin precession phenomena where the electric field is aligned in the $\hat{z}$-direction and the initial configuration of spins is in the $\hat{x}$-direction. The timescale for this spin precession, using the threshold electric field, given by Eq. (3.11), and local dark matter energy $\rho_{DM} \sim 0.3$ GeV/cm^3, is

$$\tau = \frac{2m_e^2}{g\lambda\mathcal{E}\langle\phi\rangle} \sim \frac{2m_e^2}{g\mathcal{E}}\left(\frac{m_\phi}{\lambda\sqrt{2\rho_{DM}}}\right) \sim \frac{10^{-4}s}{\lambda}. \tag{3.19}$$

Note, for a given constant electric field strength, there is still a linear dependence on the mass of the axion. The lighter the axion, the larger this effect should be.

Consider now a collection of N electrons all prepared in the $+\hat{x}$-direction, as the single electron case. We expect the coupling λ between the axion and electrons is small, then the timescale for the precession is large. The magnetic field in the $\hat{x}$-direction varies inversely to the square of the timescale, and thus is treated as constant. However, in the $\hat{y}$-direction, the magnetic moment of the electrons is

$$\mu_y \sim 2\mu_B N\langle S_y\rangle = \mu_B N \sin\left(\frac{t}{\tau}\right). \tag{3.20}$$

where μ_B is the Bohr magneton. We now imagine a loop of wire whose norm is in the $\hat{y}$-direction. If the loop is taken to be the same size as the collection of electrons with cross section A, then the magnetic flux through the loop of wire will be

$$\Phi_B(t) \sim \mu_B\mu_0 nA\sin\left(\frac{t}{\tau}\right) \tag{3.21}$$

with n number density of electrons. For non-interacting electrons, we must ensure the deBroglie wavelength is larger than the average distance between electrons. In particular, $n\lambda_{dB}^3 < 1$. Saturating the inequality gives a maximum number density

allowed. At some small time t relative to the timescale τ, the rate of change of flux is

$$\left.\frac{d\Phi_B}{dt}\right|_{t=0} = \frac{e\mu_B\mu_0}{2m_e^2}\left(\frac{\lambda\sqrt{2\rho_{DM}}}{m_\phi}\right) nA\cdot\mathcal{E}. \tag{3.22}$$

The changing flux will be inversely proportional to the timescale τ. We also assume that the electric field will not change the cross-sectional area of the collection of electrons. Dissipation of the electrons may provide an experimental problem. However, in the regime where the dissipation rate satisfies

$$\frac{dA}{dt} \ll \frac{A}{t}, \tag{3.23}$$

the flux change due to a decrease in number density is a subleading effect.

Including the axion-electron interaction results in a classical electric dipole moment for the electron, as seen in Eq. (3.12). In general, an electric dipole term can be written in the form [98]

$$H = \frac{d_e}{S}\vec{S}\cdot\vec{\mathcal{E}}. \tag{3.24}$$

The electric dipole moment induced by the axion can be found, by comparison, as

$$d_e = \frac{e\lambda}{m_e^2}\frac{\sqrt{2\rho_{DM}}}{m_\phi}\cos(m_\phi t) \tag{3.25}$$

While the Standard Model predicts a nonzero electron electric dipole moment due to loop correction, the current experimental bound is given $d_e \leq 8.7\times10^{-29} e\cdot$cm [99]. Converting this bound to one on the parameters λ, m_ϕ gives

$$\lambda\left(\frac{1\text{ eV}}{m_\phi}\right) \leq 10^{-10}. \tag{3.26}$$

Saturating the bound, the change in flux given by Eq. (3.22) can be found as

$$\frac{d\Phi_B}{dt} \sim 10^{-18}\text{ Wb}/s \tag{3.27}$$

for number density $n \sim 10^{21}$ m^{-3}, electric field $\mathcal{E} \sim 10^5$ V/m, and cross sectional area $A \sim 1$ m^2.

The frequency of oscillation of the electric dipole moment from Eq. (3.25) matches

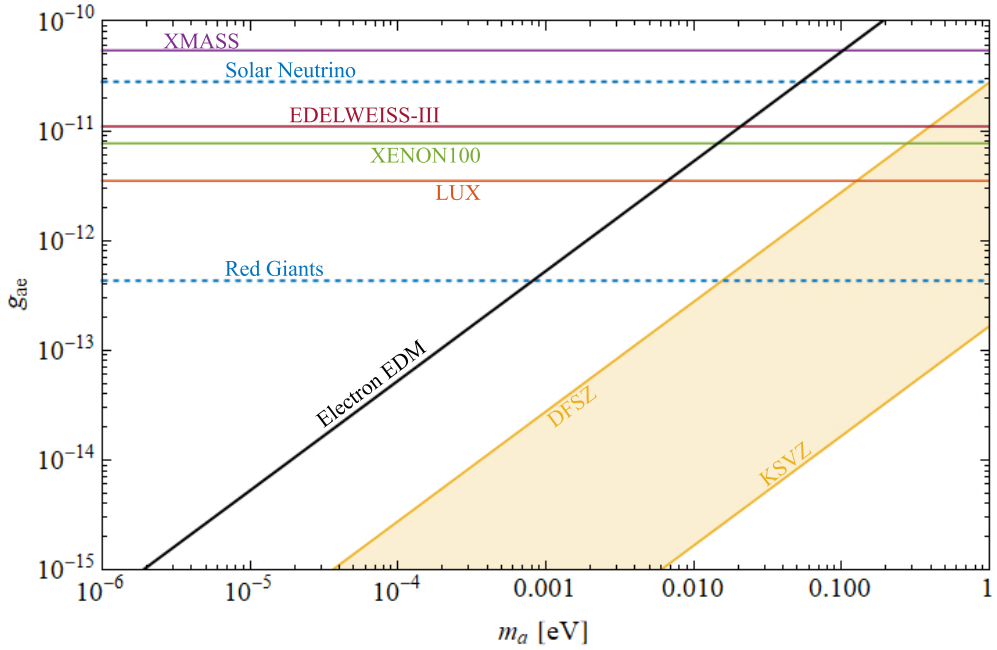

Figure 3.1: Low mass constraints (90% CL) on axion-electron coupling, $g_{ae} = \lambda$, from various solar axion experiments XMASS [102], EDELWEISS [103], XENON100 [104], and LUX [105]. The dashed blue lines indicate indirect astrophysical bounds from solar neutrinos [106] and red giants cooling [107]. The solid black line coincides with the electron electric dipole moment bound found in Eq.(3.26). The DFSZ (with $\cos\beta_{\rm DFSZ} = 1$) and KSVZ axions are darker yellow lines bounding the shaded region.

the previous results of [93], which rely on different interaction terms. This frequency is a universal feature of treating the axion as a classical oscillating field. In our analysis, however, we treat the pseudoscalar Yukawa interaction as a necessary term in the effective field theory. For axion models solving the strong CP problem, [96] provides a comprehensive analysis for finding the low energy interactions of the axion, including the particular value of λ.

More generally, the dimensionless coupling constant λ is determined by the particular ALP model. In string theory, where there are many axions $\lambda = C_{ie} m_e / f_{ai}$ where the index i denotes the number of axions [100]. In models of many axions this coupling could be larger than models of only one axion [27]. For example in the KSVZ and DFSZ model [37],

$$\lambda = \frac{2X'_e m_e}{f_a}, \qquad \text{with} \qquad X'_e \begin{cases} \approx 10^{-3} & \text{, KSVZ,} \\ \leq 0.2 & \text{, DFSZ.} \end{cases} \tag{3.28}$$

Evaluating the bound in Eq. (3.26) for the axion mass in Eq. (1.1), we find constraint

$X'_e \lesssim 3$. The current experimental limit on the electron's electric dipole moment are nearly one order of magnitude away from probing the standard QCD axion parameter range. Current axion-electron coupling constraints are shown in Fig. 3.1. In the low mass regime ($m_a \leq 10^{-2}$ eV), the electric dipole moment can provide more stringent constraints on the axion-electron coupling than modern (model-independent) solar axion detectors [101, 102, 103, 104, 105][1].

3.4 Discussion

A CP conserving interaction between the axion and electrons contributes multiple axion correction terms to the non-relativistic electron Hamiltonian. The prominent feature found is the emergence of a spin-electric field coupling that depends on the magnitude of the axion field. Contrary to other axion couplings, the presence of an interaction absent of derivatives proves robust against a wide range of axion masses. In particular, if the axion is a major component of the local dark matter energy density, experiments looking for axion-electron interactions can probe the lower spectrum of axion masses.

The dominant correction to the non-relativistic electron Hamiltonian, the electric dipole term given by Eq. (3.12), will result in a classical electric dipole moment. When subject to an external electric field, the dipole will exhibit spin precession. For reasonable values of physical parameters, the induced changing magnetic flux can be the same order as the sensitivity of SQUID magnetometers. Experiments measuring electron electric dipole moment, such as [99], use methods with heavy molecules to cause spin precession in the presence of both electric and magnetic fields. However, these experiments measure fluorescence emissions, not a direct detection the flux change due to precession.

We have primarily considered the resulting electron electric dipole moment, however this is not unique to axion-electron interactions. Many models, including the Standard Model, predict finite electric dipole moments due to quantum effects. Collider experiments and dark matter direct detection provide relativistic avenues to search for axion interactions. However, subleading terms in Eq. (3.9) provide additional predictions. In particular, the gradient of the axion need not be as small as previously stated. In general, the dark matter energy density will have fluctuations, possibly amplified due

[1] Better limits can be placed by these experiments when axions account for all of the local dark matter is axion, however these constraints are limited to keV axion masses.

to an astrophysical production of axions. These gradient terms can induce additional energy shifts of the electron as well as modifying the path of cosmic rays. Such experiments will introduce measurements with different dependencies on the parameters in the theory than what we have presented.

In particular, the axion solution in Eq. (3.10) is a background solution for cold dark matter axions, where interactions are treated as negligible perturbations. Adding the usual axion-photon coupling,

$$\mathcal{L} \supset \frac{\alpha}{f_a}\phi\vec{\mathcal{E}}\cdot\vec{B}, \tag{3.29}$$

with α the fine structure constant and f_a the energy cutoff for the effective field theory, the ambient electric and magnetic fields can induce an additional axion field gradient. Then the gradient term in the non-relativistic electron Hamiltonian becomes dominant when the ambient magnetic field projected in the direction of the electric field is above the cutoff

$$B_{||} = (10^{12}\text{ T})\left(\frac{1\text{ eV}}{m_\phi}\right)\left(\frac{1\text{ m}}{L}\right)\left(\frac{f_a}{M_{pl}}\right) \tag{3.30}$$

where M_{pl} is the Planck mass and L is the size of the experimental apparatus. For dark matter axion mass at 10^{-6} eV and the energy scale f_a for the Pontryagin term is taken to be 10^{15} GeV, the threshold magnetic field is $B \sim 10^{15}$ Tesla. Furthermore, the induced gradient only dominates the when $\vec{E}\cdot\vec{B} \geq 10^{30}$ T·V/m. Instead, we may also consider the situation where the axion field is screened by baryonic matter. In this case, $\phi \sim 0$ and the electric dipole moment term will be proportional to the perturbation of the axion field. The dominant term only depends on the electric field, similar to Eq. (3.11), differing only in an additional dependence on the size of the experimental apparatus. For small experimental setups, the electric field can be weaker for the dominant phenomena to be the electric dipole term. Again, unless the field strengths are large, such a situation will only further suppress the expected phenomena.

To achieve sufficiently large number for the predicted flux change in Eq. (3.27), as well as suppress external magnetic fields, superconductors may provide a useful test bed for experiments looking for the spin precession because magnetic fields should be suppressed. However, suppressing external magnetic fields may not be necessary to detect the precession due to the electric dipole moment. As an idealized example of differential measurement, in the presence of both electric and magnetic fields, the rotation

axis for the spin precession is given by the weighted (by dipole moments) average of the magnetic and electric fields. If these fields are constant and orthogonal to one another, there should be an observed change in flux in the direction of the magnetic field. This magnetic field can not be attributed to the magnetic spin precession. The observed flux change in the direction of the magnetic field will have the same magnitude as in Eq. (3.22), but it will oscillate with the frequency of the magnetic spin precession.

Because thermal fluctuations can induce a changing flux in the direction of the magnetic field, thermal effects will be important for similar experiments. Furthermore, a collection of electrons in a mixed state will not produce the desired spin precession. Therefore, the collection of electrons must be kept at a low temperature. For finite temperature, the number density of electrons in Eq. (3.21) can be replaced by the net number density of electrons.

Chapter 4

Gravitational Waves

4.1 Introduction

With the observation of black hole binary mergers [108, 109, 110, 111, 112] and a neutron star binary merger [113], gravitational wave astronomy is rapidly emerging as a powerful probe of fundamental physics [114]. These observations provide an exquisite confirmation of General Relativity in the extreme gravity regime, placing severe constraints on extra dimensions [115, 116, 117, 118], modifications to gravity [119], and ruling out large classes of dark energy models invoked to explain the current acceleration of the universe [120, 121, 122].

The connection of binary mergers to dark matter arises through the possibility that dark matter is gravitationally bound inside of neutron stars [123, 124, 125, 126, 127, 128, 129, 130, 131, 132, 133, 134, 135, 136, 137]. If the dark sector includes a light force mediator, then this naturally leads to an additional force between neutron stars, similar to that experienced by compact objects in scalar-tensor gravity, where the role of accumulated mass is played by a scalar field-dependent modulation of the inertial mass. This additional force modifies the gravitational wave signal from neutron star binary mergers, which can potentially probe the underlying dark matter model [138, 139, 140, 141, 142]. Probing these modifications by precise interferometer measurements requires building analytic templates of the modified waves and a detailed statistical analysis. In this chapter, we undertake precisely this task, focusing on modifications that induce a Yukawa-type modification to the gravitational potential, and with a particular focus on dark matter. We emphasize that this conclusion is *completely general* and it does not

depend on a specific dark matter model.

The amount of dark matter inside neutron stars is subject to considerable theoretical uncertainty, since this does depend, not only on the dark matter model, but also on the formation and entire lifetime of the neutron star. Estimates of the fraction of the neutron star mass in dark matter range from a few percent [143] to one part in 10^{15} [138]. Remarkably, we find that gravitational wave observations can probe dark matter even at mass fractions below the latter estimate.

4.2 Dark Matter Model

For the sake of concreteness, we here provide a specific example which produces modifications to the gravitational waveform. We emphasize, nonetheless, that the results presented in this paper are generic and not dependent of the specific features a particular dark matter model.

Consider then a model of asymmetric dark matter [144] coupled to an Abelian gauge field V^μ (the "dark photon"), as has been considered previously in [138, 145]. The dark sector Lagrangian[1] is given as

$$\mathcal{L}_{\rm DS} = -\frac{1}{4}V_{\mu\nu}V^{\mu\nu} + \frac{1}{2}m_v^2 V_\mu V^\mu + \bar{\chi}\left(i\gamma^\mu D_\mu - m_\chi\right)\chi, \tag{4.1}$$

where $D_\mu = \nabla_\mu + igV_\mu$ is the gauge covariant derivative, $V_{\mu\nu}$ is the dark photon field strength tensor, and the fermion χ has dark charge g and mass m_χ. The dark photon mass m_v can arise through a Higgs or Stueckelberg mechanism, but such completions of the theory will produce negligible effects on our analysis. Further, one can generalize this Lagrangian to non-Abelian gauge fields, but the lightest, massive gauge field will typically produce the most noticeable change in gravitational waves.

The range of dark photon masses that can be probed by gravitational waves are extremely light, $m_v \lesssim 10^{-10}$ eV, and gauge invariance is approximately conserved. This implies that a charge asymmetry for χ must be balanced by an opposite charge asymmetry for a second fermion, analogous to standard electromagnetism and the protons and electrons in our current universe. This opens up the possibility that some fraction of the dark matter will form neutral bound states, the precise value of which depends

[1] With the exception of the Lagrangian, we will use geometric units throughout our analysis.

sensitively on the value of the dark photon's fine structure constant [145]. Capture of these bounds states in compact objects will contribute to that object's dark dipole moment at lowest order, however we only consider the corrections due to its dark monopole moment here.

In order to produce a nonzero dark monopole moment, a net charge asymmetry will be required for neutron stars. Neutron stars can receive dark matter from two sources: (1) dark matter accreted from the surrounding halo, and (2) dark matter contained in the progenitor. The former has been studied in detail in [123, 124, 125, 126, 127, 128, 129, 130, 131, 132, 133, 134, 138, 143]. The latter has been argued to open up the possibility of anywhere from a few percent to an $\mathcal{O}(1)$ fraction of the mass of a neutron star to be dark matter, a so-called "Admixture Neutron Star" [146, 147].

If one considers only the accretion of dark matter by neutron stars, the number of dark matter particles[2] with $m_\chi \gtrsim 1$ GeV that are captured can be estimated as [128, 139],

$$N_\chi \simeq 2.3 \times 10^{44} \left(\frac{100 \text{ GeV}}{m_\chi}\right) \left(\frac{\rho_\chi}{10^3 \text{ GeV/cm}^3}\right) \left(\frac{\sigma_B}{2.1 \times 10^{-45} \text{ cm}^2}\right) \left(\frac{t_{NS}}{10^{10} \text{ yr}}\right), \quad (4.2)$$

where t_{NS} is the age of the neutron star, and σ_B is the lesser of the DM-neutron elastic scattering cross section σ_n and the effective geometric scattering cross section. For lighter dark matter, the number of accreted particles is independent of the dark matter mass [128]. Therefore, if there is a mass difference between the two dark matter fermions, and at least one is lighter than a GeV, a net charge can accumulate and the accretion is predominantly into the heavier χ fermions.

From the number of dark matter particles accreted, the fraction of the neutron star mass in the form of dark matter $f_{DM} = N_\chi m_\chi / m_{\rm NS}$ can be approximated to $f_{DM} \simeq 10^{-11}$ assuming standard parameters. Similar estimates have been made in the literature, with varying levels of precision. The most recent estimate is given by [138], which gives a more conservative bound of $f_{DM} \lesssim 10^{-15}$.

As we will show in Section 4.5.4, gravitational waves can still probe these small charge accumulations in compact objects. The relative strength of the dark photon's Yukawa interaction compared to gravity can compensate for the small dark matter fraction. This

[2] Considering a neutron star with mass $1.44 M_\odot$ and radius 10.6 km.

relative strength can be approximated as

$$\alpha \approx 1.18 \times 10^{33} g^2 f_{DM}^2 \left(\frac{100 \text{ GeV}}{m_\chi} \right)^2 . \tag{4.3}$$

Even using the conservative bound $f \sim 10^{-15}$, we see that the dark Yukawa interaction can remain relatively strong for weakly coupled ($g \ll 1$) dark fermions.

4.3 Modifications to Gravitational Wave Physics of Binary Inspirals

Given our simple dark matter model, we now consider the dynamic effects that manifest with a net dark charge on the binary system. During the early stages of the inspiral, the binary constituents are treated as point masses/charges. In this regime, the interaction between the two compact object via the dark photon can be approximated as a tree-level scattering. This interaction will manifest as a Yukawa correction to the potential energy of the binary system, given by

$$V_{\text{Yuk}}(r) = \alpha \frac{m^2 \eta}{r} e^{-r/\lambda}, \tag{4.4}$$

where $\lambda = m_v^{-1}$ is the length scale of the Yukawa interaction, $m = m_1 + m_2$ is the total mass of the binary, $\eta = m_1 m_2 / m^2$ is the symmetric mass ratio, r is the orbital separation, and the relative strength of the Yukawa potential α, from Eq. (4.3), can be defined in terms of the neutron star properties as

$$\alpha = \frac{q_1 q_2}{m_1 m_2} = \tilde{\text{q}}_1 \, \tilde{\text{q}}_2 \tag{4.5}$$

where $\tilde{\text{q}}_i = q_i / m_i$ is the dark charge to mass ratio of each star. For the asymmetric dark matter model we consider, both compact objects should acquire the same sign of net dark charge, thus we work in the regime where $\alpha > 0$[3].

This modification to the potential ultimately leads to a violation of Kepler's laws which will be functionally distinct from General Relativity corrections. For (nearly)

[3]For a scalar mediator, the argument presented would give $\alpha < 0$, i.e. an attractive interaction.

circular orbits, the modification will manifest as[4]

$$\omega^2 = \frac{1}{m\eta r}\frac{dV}{dr} = \frac{m}{r^3}\left[1 - \alpha\left(1 + \frac{r}{\lambda}\right)e^{-r/\lambda}\right]. \tag{4.6}$$

Furthermore, the potential is no longer a power law, hence the Virial theorem takes a more complicated form when evaluating the total energy of the binary. The latter can be calculated as

$$E_{\rm tot} = -\frac{m^2\eta}{2r}\left[1 - \alpha\left(1 - \frac{r}{\lambda}\right)e^{-r/\lambda}\right]. \tag{4.7}$$

The repulsive Yukawa potential results in both a decrease in the orbital frequency and magnitude of the total energy of the system at a given orbital separation.

These kinematic variables dictate the rate at which energy is radiated away from the system in the form of gravitational radiation. The power emitted in the form of gravitational radiation can be computed from the quadrupole moment as

$$P_{\rm GW} = \frac{D_L^2}{32\pi}\int {\rm d}\Omega\, \langle \dot{h}_{ij}^{TT}\dot{h}_{TT}^{ij}\rangle = \frac{32}{5}\eta^2 m^2\omega^6 r^4 = \frac{32}{5}\eta^2 v^{10}, \tag{4.8}$$

where the dot represents a time derivative, D_L is the luminosity distance, and $v = \omega r$ is the orbital velocity for a quasi-circular orbit.

When gravitational waves are the only form of emitted radiation, the balance law, $P_{\rm GW} = -\frac{d}{dt}E_{\rm tot}$, can be used to find the rate at which the orbital separation decreases as

$$\frac{dr}{dt} = -\frac{64\eta}{5}\left(\frac{m}{r}\right)^3 \frac{\left[1 - \alpha\left(1 + \frac{r}{\lambda}\right)e^{-r/\lambda}\right]^3}{1 - \alpha(1 + \frac{r}{\lambda} - \frac{r^2}{\lambda^2})e^{-r/\lambda}}. \tag{4.9}$$

While the power emitted in gravitational radiation is reduced due to the repulsive Yukawa interaction, this need not translate into a longer coalescence time than the Newtonian/General Relativity predictions. Instead, the decrease in energy of the system in Eq. (4.7) can overcompensate for this decrease in radiation leading to a quicker inspiral phase.

4.3.1 Dark dipole radiation

Up to this point, we have ignored the on-shell emission of the dark photon due to the orbital motion of the charged compact objects. However, this dipole radiation

[4] Our formula differs from [140] by an additional factor of the Yukawa term, agreeing with [138].

introduces an important, and potentially dominant, source of energy dissipation to the binary system. The effect of dipole radiation on the binary dynamics has been studied in [140, 148]. In our context, the additional power radiated is given by[5]

$$\begin{aligned} P_{\rm dark} &= \frac{2}{3}\gamma\eta^2 m^2\omega^4 r^2\left(1+\frac{1}{2(\lambda\omega)^2}\right)\left(1-\frac{1}{\lambda\omega}\right)^{\frac{1}{2}}, \\ &= \frac{2}{3}\gamma\eta^2 v^8\left(1+\frac{1}{2(\lambda\omega)^2}\right)\left(1-\frac{1}{\lambda\omega}\right)^{\frac{1}{2}}, \end{aligned} \tag{4.10}$$

where

$$\gamma \equiv (\tilde{q}_1 - \tilde{q}_2)^2 \tag{4.11}$$

is the squared difference between the charge-to-mass ratios of the binary stars[6]. Clearly, the effects of dipole radiation will only manifest when the dark matter mass fraction of the compact objects differ.

The other two functions of $\lambda\omega$ can be approximated as the Heaviside step function $\theta(\lambda\omega - 1)$, but note that the functional form is not actually of Heaviside form; Section 4.4.4 computes the corrections between the above functional form and the Heaviside approximation. The argument of the step function determines the activation of dipole radiation. This relation can be written in terms of the Yukawa length scale λ and the gravitational wave frequency f as

$$\lambda \geq 9.5\times 10^3 \text{ km}\left(\frac{10 \text{ Hz}}{f}\right). \tag{4.12}$$

For dipole radiation to be active, the Yukawa interaction must have a length scale much larger than the orbital separation of the binary. As we will see in Section 4.5.4, this will have important consequences in one's ability to place constraints on the parameters α and γ.

Taking the ratio of the power emitted between dark dipole radiation and the gravitational radiation,

$$\frac{P_{\rm dark}}{P_{\rm GW}} \approx \frac{5}{48}\left(\frac{\gamma}{v^2}\right)\theta(\lambda\omega - 1), \tag{4.13}$$

[5]Relative to [140], we include an additional factor of two for the vector mode dipole radiation, consistent with the results of [148].

[6]As further explained in Section 4.4.4, the dipole radiation power used here is for the emission of a vector mode. If the constraints in Section 4.5.4 are applied to a scalar mediator, one must account for an additional factor of two in the definition of γ. Explicitly, $\gamma = \gamma_V$ or $\gamma = 2\gamma_S$.

we see the dipole corrections will be largest early in the inspiral phase, immediately following the activation of the step function. This will manifest as a negative PN correction to the gravitational waveform.

The inclusion of dipole radiation will not change the orbital frequency or the total energy of the system. Instead, correcting the balance law to include the dark radiation $-\frac{d}{dt}E_{\rm tot} = P_{\rm GW} + P_{\rm dark}$ will introduce an additional factor to the evolution of the orbital separation in Eq. (4.9). Using Eq. (4.6), the equation for $\dot{r}$ can be rewritten as an equation for the time derivative of the orbital frequency. Including the dark dipole radiation term, $\dot{\omega}$ can be found in terms of the orbital separation

$$\omega\dot{\omega} = \frac{96\eta m^4}{5r^7}\left[1-\alpha\left(1+\frac{r}{\lambda}+\frac{r^2}{3\lambda^2}\right)e^{-r/\lambda}\right]\left(\frac{\left[1-\alpha\left(1+\frac{r}{\lambda}\right)e^{-r/\lambda}\right]^3}{1-\alpha(1+\frac{r}{\lambda}-\frac{r^2}{\lambda^2})e^{-r/\lambda}}\right) \times\left(1+\frac{5\gamma r}{48m}\frac{\theta(\lambda\omega-1)}{1-\alpha\left(1+\frac{r}{\lambda}\right)e^{-r/\lambda}}\right). \tag{4.14}$$

As we will see in Section 4.4, this equation for the orbital frequency evolution will be necessary when calculating the gravitational waveform. In particular, the waveform will acquire separate terms for the Yukawa corrections and the dipole radiation corrections, which can be used to constrain the parameters α and γ as a function of the Yukawa length scale.

4.3.2 Connection to Scalar-Tensor theory

While we have primarily consider the Yukawa potential and dipole radiation in the context of a dark matter model, the kinematic corrections described above are a general feature of most fifth force models. Scalar-tensor theories have received a lot of attention, in part due to its connection with string theory[149]. Scalar-tensor theories are a modification to general relativity where an additional scalar degree of freedom is coupled to the trace of the energy momentum tensor (in the Jordan frame), and have been shown [150, 151, 152] to produce the same Yukawa and dipole modification considered here.

In these theories, the "charge" accumulation is not due to the accretion of charged particles, but instead a scalar field dependent variation of the inertial mass $m_a(\phi)$ of the compact object [151]. When the scalar field theory is written in the Jordan frame [150, 151, 153, 154], the dipole radiation and Yukawa corrections can be written in terms

of the sensitivity of the body,

$$s_a = -\frac{\partial \log m_a}{\partial \phi}\Big|_{\phi_0}. \tag{4.15}$$

In particular, the γ parameter for dipole radiation can be written in terms of the sensitivities as

$$\gamma_{ST} = (s_1 - s_2)^2 \left[\frac{2\left(1 - \frac{s_1+s_2-2s_1s_2}{2+\omega_{BD}}\right)^2}{2+\omega_{BD}}\right], \tag{4.16}$$

where ω_{BD} is the Brans-Dicke coupling constant. One can recover General Relativity by taking $\omega_{BD} \to \infty$, and thus, using that $\omega_{BD} > 40,000$ from observations of the Shapiro time delay with the Cassini spacecraft [155], we can approximate

$$\gamma_{ST} \sim \frac{2(s_1 - s_2)^2}{\omega_{BD}}. \tag{4.17}$$

The additional factor in the square bracket arises from the sensitivity dependence in the gravitational constant, as well as a conversion between scalar "charge," defined in the Einstein frame and the sensitivities, defined in the Jordan frame.

4.4 The Gravitational Waveform

We now consider the gravitational waveform using the standard amplitude from General Relativity, and apply the results to the case of a binary system with some dark charge. In principle, corrections to the response function will also arise from additional gravitational wave polarizations that may be sourced by the dark sector we consider in this paper; however, since multiple detectors (or a space-based detector) are needed to detect such additional polarizations, we will neglect them here. We will follow the methods described in [156, 157].

The plus and cross polarizations of a gravitational wave in General Relativity are given by

$$h_+(t) = -\left(\frac{1+\cos^2\iota}{2}\right)\mathcal{A}(t)\cos\left(2\phi_c + 2\phi\left(t - t_c; m, \eta\right)\right), \tag{4.18}$$

$$h_\times(t) = -\left(\cos\iota\right)\mathcal{A}(t)\sin\left(2\phi_c + 2\phi\left(t - t_c; m, \eta\right)\right), \tag{4.19}$$

where the gravitational wave amplitude in the time domain is

$$\mathcal{A}(t) = \frac{4\eta m}{D_L}\omega^2(t)r^2(t)\,, \tag{4.20}$$

and where the prefactor is a geometric factor related to the inclination angle ι, i.e. the angle between the angular momentum of the binary and the observer, while t_c and ϕ_c are the time and phase of the binary at coalescence, with ϕ the orbital phase of the binary at some time, found by integrating the orbital frequency.

A given detector will have different response functions F_+ and $F_\times$ to the different plus- and cross-polarizations of gravitational waves, which will depend on some additional geometric factors. In the case of second-generation ground-based instruments, the timescale on which these functions change is much larger than the gravitational wave signal, and thus, they can be treated as constant. The strain induced on the detector is then given by

$$h(t) = F_+ h_+(t + t_c - t_0) + F_\times h_\times(t + t_c - t_0), \tag{4.21}$$

$$= -\mathcal{A}(t + t_c - t_0)\left[\left(\frac{1+\cos^2\iota}{2}\right)F_+\cos 2\bar{\phi}(t) + \cos\iota F_\times \sin 2\bar{\phi}(t)\right], \tag{4.22}$$

where t_0 is the time when the detector records the coalescence, and $\bar{\phi}(t) \equiv \phi_c + \phi(t - t_0)$. The strain can be rewritten as a single oscillating function by incorporating the geometric functions into a shift in the phase and a deviation in the luminosity distance:

$$D_{\text{eff}} = D_L\left[F_+^2\left(\frac{1+\cos^2\iota}{2}\right)^2 + F_\times^2\cos^2\iota\right]^{-1/2}, \tag{4.23}$$

$$\phi_0 = \phi_c - \arctan\left(\frac{2\cos\iota}{1+\cos^2\iota}\frac{F_\times}{F_+}\right). \tag{4.24}$$

The strain is then given as the function

$$h(t) = -\frac{4\eta m}{D_{\text{eff}}}\omega^2 r^2\cos\left(2\phi_0 + 2\phi\left(t - t_0; m, \eta\right)\right). \tag{4.25}$$

A matched filtering calculation requires that we compute the Fourier transform of the time-domain waveforms, which can be estimated in the stationary phase approximation.

The Fourier transform of the strain can be written as

$$\tilde{h}(f) = -\frac{2\eta m}{D_{\rm eff}} \int_{-\infty}^{\infty} \mathrm{d}t\, \omega^2 r^2 \left(e^{i(2\phi_0 + 2\phi(t) - 2\pi f t)} + e^{-i(2\phi_0 + 2\phi(t) + 2\pi f t)} \right), \tag{4.26}$$

where the cosine has been expanded in exponentials. We note that the orbital frequency is monotonically increasing and a positive function (for all cases we consider), properties inherited by $\phi(t)$.

The stationary point is defined as the time t_s when $\omega(t_s) \equiv \dot{\phi}(t_s) = \pi f$. The stationary phase approximation allows one to compute the integral as

$$\begin{aligned} \tilde{h}(f) = -\frac{2\eta m}{D_{\rm eff}} (\pi f)^2 r^2(t_s) \left(\frac{\pi}{|\dot{\omega}(t_s)|} \right)^{1/2} \\ \times \exp\left[-i \left(2\pi f t_s - 2\phi_0 - 2\phi(t_s) - \frac{\pi}{4} \mathrm{sgn}(\dot{\omega}(t_s)) \right) \right], \end{aligned} \tag{4.27}$$

where we expect $\mathrm{sgn}(\dot{\omega}(t_s)) = 1$ in all cases we consider. One is then required to find the functions $r(t_s), \phi(t_s)$, and t_s as a function of the Fourier frequency. To find the remaining functions in the phase, we define the quantity $\tau(\omega) = \omega/\dot{\omega}$. The functions ϕ and t can then be rewritten as

$$\phi(\omega) = \int^{\omega} \tau(\omega') \mathrm{d}\omega' \,, \qquad t(\omega) = \int^{\omega} \frac{\tau(\omega')}{\omega'} \mathrm{d}\omega' \,. \tag{4.28}$$

The binary's phase and time can then be found by $\phi(\omega(t_s)) = \phi(\pi f)$ and $t_s = t(\pi f)$. Therefore, once the functions $r(\omega)$ and $\dot{\omega}$ are computed for a given model, Eq. (4.27) can be applied to find the gravitational waveform.

4.4.1 Small deformation

Although the function $\dot{\omega}(r)$ is given in Eq. (4.14), the calculation of the orbital separation $r(\omega)$ requires the inversion of Eq. (4.6). The relative strength of the Yukawa potential α must be smaller than unity in order for the binary to merge. Furthermore, to remain consistent with the linear (in α) expansion of the potential in Eq. (4.4), we wish to find a solution for $r(\omega)$ to linear order in α. Such a solution will correspond to a small General Relativity deformation limit. This inversion can be done to find the separation,

and subsequently $\dot{\omega}(\omega)$, as

$$r(\omega) = \left(\frac{m}{\omega^2}\right)^{1/3}\left[1 - \frac{\alpha}{3}\left(1 + \frac{m}{\lambda}(m\omega)^{-2/3}\right)\exp\left(-\frac{m}{\lambda}(m\omega)^{-2/3}\right) + \mathcal{O}(\alpha^2)\right], \tag{4.29}$$

$$\begin{aligned}\dot{\omega} = \frac{96}{5}\mathcal{M}^{5/3}\omega^{11/3}\Bigg[1 + \frac{5\gamma}{48}(m\omega)^{-2/3}\theta(\lambda\omega - 1) \\ - \frac{2\alpha}{3}\left(1 + \frac{m}{\lambda}(m\omega)^{-2/3} + \frac{2m^2}{\lambda^2}(m\omega)^{-4/3}\right)\exp\left(-\frac{m}{\lambda}(m\omega)^{-2/3}\right)\Bigg],\end{aligned} \tag{4.30}$$

where $\mathcal{M} = \eta^{3/5}m$ is the chirp mass, and the time derivative of the orbital frequency is found by expanding Eq. (4.14) to linear order in α where the orbital separation is evaluated with Eq. (4.29).

In the inversion of Eq. (4.30), we have dropped terms of $\mathcal{O}(\alpha\gamma)$. Neutron stars should naturally accumulate relatively small charge-to-mass rations $\tilde{\mathrm{q}} \ll 1$, hence $\gamma \leq \tilde{\mathrm{q}}^2 \ll 1$. Explicitly, in order to expand the amplitude and phase of the waveform in Eq. (4.27) to linear order in γ, we will require

$$\gamma \ll 12.5\left(\frac{m}{M_\odot}\right)^{2/3}\left(\frac{\lambda}{1\text{ km}}\right)^{-2/3}, \tag{4.31}$$

so that the dipole radiation term is again a small correction to the General Relativity limit.

Under these conditions, Eq. (4.27) can be applied to give the Fourier space waveform:

$$\begin{aligned}\tilde{h}(f) = -\left(\frac{5\pi}{24}\right)^{\frac{1}{2}}\frac{\mathcal{M}^2}{D_{\text{eff}}}(\pi\mathcal{M}f)^{-\frac{7}{6}}\Bigg[1 - \frac{5\gamma}{96}(\pi mf)^{-\frac{2}{3}}\theta(\pi\lambda f - 1) \\ - \frac{\alpha}{3}\left(1 + \frac{m}{\lambda}(\pi mf)^{-\frac{2}{3}} - \frac{2m^2}{\lambda^2}(\pi mf)^{-\frac{4}{3}}\right)\exp\left(-\frac{m}{\lambda}(\pi mf)^{-\frac{2}{3}}\right)\Bigg]e^{-i\Psi},\end{aligned} \tag{4.32}$$

$$\begin{aligned}\Psi = 2\pi f t_0 - 2\phi_0 - \frac{\pi}{4} + \frac{3}{128}(\pi\mathcal{M}f)^{-5/3}\Bigg[1 + \frac{20\alpha}{3}F_3\left(\frac{m}{\lambda}(\pi mf)^{-2/3}\right) \\ - \frac{5\gamma}{84}(\pi mf)^{-\frac{2}{3}}\theta(\pi\lambda f - 1)\Bigg],\end{aligned} \tag{4.33}$$

where we have defined

$$F_3(x) = \left(\frac{180 + 180x + 69x^2 + 16x^3 + 2x^4}{x^4}\right)e^{-x} + \frac{21\sqrt{\pi}}{2x^{5/2}}\,\mathrm{erf}(\sqrt{x}), \tag{4.34}$$

and $\mathrm{erf}(x)$ is the error function[7].

We see that inclusion of dipole radiation manifests as a -1PN correction. The magnitude of this contribution can become very large at early times, however the step-function modulates this behavior by abruptly shutting off the contribution when Eq. (4.12) is not satisfied. In contrast, the Yukawa-type modifications to the waveform do not easily separate into a post-Newtonian expansion as a functions of $x = \frac{m}{\lambda}(\pi m f)^{-2/3}$. Both the amplitude and phase functions remain bounded for all positive (physical) values of x, thus these corrections remain well behaved throughout the binary inspiral.

4.4.2 Mass range of the dark photon

If we could observe the inspiral over its entire evolution (starting at infinite separation), $\frac{m}{\lambda}(m\omega)^{-2/3}$ would start arbitrarily large and eventually decay to the limit where $r \ll \lambda$. In this scenario, one needs to use the full waveform found in Eq. (4.32) and Eq. (4.33) in order to properly incorporate the non-perturbative behavior of the solutions. During the inspiral phase, however, the binary will emit gravitational waves at low frequencies for a longer period of time than at higher frequencies. For observations beginning at a gravitational wave frequency f_0, we can then look at the limiting behavior of the waveform when $x_0 \gg 1$ (the heavy limit) and when $x_0 \ll 1$ (the ultra-light limit), where we have defined $x_0 \equiv \frac{m}{\lambda}(\pi m f_0)^{-2/3}$. In these limiting studies, we ignore the dipole radiation term, as it remains uncoupled from the Yukawa corrections, and does not simplify in any limit involving x_0.

As we will see, degeneracies arise in the limiting regimes which are not present in the full waveform. These degeneracies will play an important role in our ability to constrain the relative Yukawa strength α in Section 4.5.4.

A heavy dark photon

For sufficiently large dark photon masses, $x_0 \gg 1$ throughout the observational window. In this case, the nonperturbative exponential functions suppress these corrections below any detectable range, as these terms remain proportional to e^{-x_0}. In this regime, the

[7] The error function can be represented approximately by

$$\mathrm{erf}(\sqrt{x}) \approx 1 - \left(1 + a_1 x^{1/2} + a_2 x + a_3 x^{3/2} + a_4 x^2\right)^{-4},$$

with $a_1 = 0.278393, a_2 = 0.230389, a_3 = 0.000972, a_4 = 0.078108$, if one wishes.

amplitude of the waveform, given by Eq. (4.32), does not acquire any corrections to linear order in α. The phase in Eq. (4.33) only receives linear α corrections from the error function. However, one can see from the integral definition,

$$\text{erf}\left(\sqrt{x_0}\right) = \frac{2}{\sqrt{\pi}} \int_0^{\sqrt{x_0}} e^{-t^2} dt \quad \rightarrow \quad 1 + \frac{2}{\sqrt{\pi}} e^{-x_0} + ... \tag{4.35}$$

that the only non-exponential correction from the error function will be a constant, degenerate with the phase ϕ_0. As a result, the Yukawa corrections for a heavy dark photon becomes completely degenerate with the General Relativity waveform.

An ultra-light dark photon

We now consider the case where observation of the binary begins after the binary has entered the range of the Yukawa interaction. In this case, $r \ll \lambda$, and the Yukawa potential can be Taylor expanded. Of course, this implies that we cannot take the infinite orbital separation limit and that the above condition will only be satisfied for a set of masses. This condition can be explicitly written in terms of the Yukawa length scale λ, or equivalently the dark photon mass, as

$$\lambda \gg (520 \text{ km}) \left(1 - \frac{\alpha}{6}\right) \left(\frac{f_0}{10 \text{ Hz}}\right)^{-\frac{2}{3}} \left(\frac{m}{M_\odot}\right)^{\frac{1}{3}}, \tag{4.36}$$

$$m_v \ll \left(3.8 \times 10^{-13} \text{ eV}\right) \left(1 + \frac{\alpha}{6}\right) \left(\frac{f_0}{10 \text{ Hz}}\right)^{\frac{2}{3}} \left(\frac{m}{M_\odot}\right)^{-\frac{1}{3}}. \tag{4.37}$$

Due to the extremely light mass required for the dark photon, we call this the *ultra-light dark photon* limit, corresponding to $x_0 \ll 1$. In this limit, the gravitational waveform can be written as

$$\begin{aligned} \tilde{h}_{\text{ul}}(f) = -\left(\frac{5\pi}{24}\right)^{\frac{1}{2}} \frac{\mathcal{M}^2}{D_{\text{eff}}} (\pi \mathcal{M} f)^{-\frac{7}{6}} \Bigg[1 - \frac{\alpha}{3} + \frac{5\alpha m^2}{6\lambda^2} (\pi m f)^{-\frac{4}{3}} \\ - \frac{7\alpha m^3}{9\lambda^3} (\pi m f)^{-2} + \mathcal{O}\left(\frac{m^4}{\lambda^4} (\pi m f)^{-\frac{8}{3}}\right)\Bigg] e^{-i\Psi_{\text{ul}}}, \end{aligned} \tag{4.38}$$

$$\begin{aligned} \Psi_{\text{ul}} = 2\pi f t_0 - 2\phi_0 - \frac{\pi}{4} + \frac{3}{128} (\pi \mathcal{M} f)^{-5/3} \Bigg[1 + \frac{2\alpha}{3} + \frac{10\alpha m^2}{27\lambda^2} (\pi m f)^{-\frac{4}{3}} \\ - \frac{200\alpha m^3}{693\lambda^3} (\pi m f)^{-2} + \mathcal{O}\left(\frac{m^4}{\lambda^4} (\pi m f)^{-\frac{8}{3}}\right)\Bigg]. \end{aligned} \tag{4.39}$$

The Fourier amplitude does not pick up any corrections to first order in the dark

photon mass. The two paramount functions for calculating the amplitude and phase, Eq. (4.6) and Eq. (4.14), only contain corrections of the form $\left(1+\frac{r}{\lambda}+\mathcal{O}\left(\frac{r}{\lambda}\right)^2\right)\exp\left(-\frac{r}{\lambda}\right)$. Taking the $r \ll \lambda$ expansion of these equations will result in no linear order correction. This property is inherited by the separation function during the inversion of Eq. (4.6) due to the term-by-term matching of the perturbative series.

The leading order correction in both the phase and amplitude appears at -2PN, with corrections to this appearing at *more negative post-Newtonian orders*. This is consistent again with the expansion requirements of this section, namely $r \ll \lambda$. One can for example check that the -2PN order term is actually larger than the -3PN order term because $\frac{m}{\lambda} \ll (\pi m f)^{2/3} \sim v^2 \sim m/r$. Therefore, when including λ corrections, the usual post-Newtonian order counting is not applicable. Instead, the model presented above is a *bivariate expansion* in both $v \ll 1$ and $r \ll \lambda$.

We note that the first correction to both the amplitude and phase of the waveform is independent of λ. This introduces a degeneracy between the chirp mass and the Yukawa strength parameter α. It is ultimately this degeneracy that is explored in [140]. This degeneracy is lifted by the -2PN correction. However, both amplitude and phase depend only on the quantity $\alpha m^{2/3}\lambda^{-2}$, which implies there is a 100% degeneracy between α and λ. This degeneracy is again lifted when we include the -3PN correction, which depends on a different combination of α and λ. This is analogous to the degeneracy between the component mass m_1 and m_2 in General Relativity at Newtonian order, which is lifted when one includes 1PN corrections.

4.4.3 Relative magnitude of Yukawa and dipole corrections

We now consider the region of parameter space where the dipole radiation modifications of the waveform dominate over the Yukawa modifications. Due to the particular sensitivity of gravitational wave interferometers to the phase of the gravitational wave, we focus on the phase modifications presented in Eq. (4.33). The dipole radiation modifications will be dominant under the condition

$$\frac{5\gamma}{84\alpha v^2}\theta\left(\frac{\lambda}{m}v^3-1\right) \geq \frac{20}{3}F_3\left(\frac{m}{\lambda v^2}\right). \tag{4.40}$$

The requirement of a valid post-Newtonian expansion ($v \ll 1$) can be combined with the requirement that the step-function condition is satisfied to find

$$\frac{m}{\lambda v^2} \leq v \ll 1, \tag{4.41}$$

which corresponds to the ultra-light dark photon limit. Therefore, after removing boundary terms, the dipole corrections to the waveform are only present in the waveform from Eq. (4.38) and Eq. (4.39). The condition that dipole radiation dominates over the Yukawa modifications can be rewritten as

$$v^2 \leq \frac{5\gamma}{56\alpha} + \mathcal{O}\left(\frac{m^2}{\lambda^2 v^4}\right), \quad \text{and} \quad v^3 \geq \frac{m}{\lambda}. \tag{4.42}$$

The second of these conditions is precisely the condition in Eq. (4.12), requiring the step-function to be active. The only significant deviations from these approximate requirements come when the orbital velocity approaches unity, which also allows the minimum λ/m to approach unity. In this regime, of course, the post-Newtonian expansion is valid no longer and a full numerical analysis is required.

4.4.4 Corrections to dipole radiation step function

We now consider how the corrections to the Heaviside step function in the activation of dipole radiation modifies the gravitational waveform, for both a scalar and vector mediator. We begin with the time-averaged power radiated through dipole emission of a vector or scalar source given by [148]:

$$\langle \dot{E}_S \rangle = \frac{1}{3}\eta^2 m^2 \omega^4 r^2 g_S(m_S, e)(\tilde{\mathrm{q}}_1 - \tilde{\mathrm{q}}_2)^2, \tag{4.43}$$

$$\langle \dot{E}_V \rangle = \frac{2}{3}\eta^2 m^2 \omega^4 r^2 g_V(m_V, e)(\tilde{\mathrm{q}}_1 - \tilde{\mathrm{q}}_2)^2, \tag{4.44}$$

where $\tilde{\mathrm{q}}_i$ is the charge-to-mass ratio of the compact object, and the g_i functions are dependent on the eccentricity e of the orbit and the mass of the additional degree of

freedom. Explicitly written,

$$g_S(m_S,e)=\sum_{n=1}^{\infty}2n^2\left[\mathcal{J}_n'^2(ne)+\left(\frac{1-e^2}{e^2}\right)\mathcal{J}_n^2(ne)\right]\times\left[1-\left(\frac{m_S}{n\omega}\right)^2\right]^{3/2}, \tag{4.45}$$

$$\begin{aligned} g_V(m_V,e)=\sum_{n=1}^{\infty}2n^2&\left[\mathcal{J}_n'^2(ne)+\left(\frac{1-e^2}{e^2}\right)\mathcal{J}_n^2(ne)\right] \\ &\times\left[1-\left(\frac{m_V}{n\omega}\right)^2\right]^{1/2}\left[1+\frac{1}{2}\left(\frac{m_V}{n\omega}\right)^2\right], \end{aligned} \tag{4.46}$$

where $\mathcal{J}_n$ is the nth order Bessel function. By taking the $e\to 0$ limit (circular orbits), we can use the identity

$$\lim_{e\to 0}\left[\mathcal{J}_n'^2(ne)+\left(\frac{1-e^2}{e^2}\right)\mathcal{J}_n^2(ne)\right]=\frac{1}{2}\delta_{n,1}, \tag{4.47}$$

to rewrite the time-averaged power radiated in the simple form

$$\langle\dot{E}_S\rangle=\frac{1}{3}\eta^2m^2\omega^4r^2(\tilde{\mathrm{q}}_1-\tilde{\mathrm{q}}_2)^2\theta\left(\omega-m_S\right)\left(\frac{\omega^2-m_S^2}{\omega^2}\right)^{3/2}, \tag{4.48}$$

$$\langle\dot{E}_V\rangle=\frac{2}{3}\eta^2m^2\omega^4r^2(\tilde{\mathrm{q}}_1-\tilde{\mathrm{q}}_2)^2\theta\left(\omega-m_V\right)\left(\frac{\omega^2-m_V^2}{\omega^2}\right)^{1/2}\left(\frac{\omega^2+m_V^2}{2\omega^2}\right). \tag{4.49}$$

Note that if we ignore the "corrections" to the Heaviside step-function θ at high angular orbital frequencies ($\omega\gg m_{S,V}$), dipole radiation of a vector mode emits twice that of a scalar mode, but has the same functional form.

We now calculate the waveform including the dipole radiation term for either scalar or vector modes. A more useful form will be as a ratio of P_{GW}:

$$\frac{\langle\dot{E}_S\rangle}{P_{GW}}=\frac{5(\tilde{\mathrm{q}}_1-\tilde{\mathrm{q}}_2)^2}{96m^{2/3}\omega^{2/3}}\left(\frac{\lambda_S^2\omega^2-1}{\lambda_S^2\omega^2}\right)^{3/2}, \tag{4.50}$$

$$\frac{\langle\dot{E}_V\rangle}{P_{GW}}=\frac{5(\tilde{\mathrm{q}}_1-\tilde{\mathrm{q}}_2)^2}{48m^{2/3}\omega^{2/3}}\left(\frac{\lambda_V^2\omega^2-1}{\lambda_V^2\omega^2}\right)^{1/2}\left(\frac{2\lambda_V^2\omega^2+1}{2\lambda_V^2\omega^2}\right), \tag{4.51}$$

where $\lambda_i=m_i^{-1}$ is the length scale associated with the additional scalar or vector degree of freedom. The introduction of dipole radiation will manifest as an additional factor in the equation for $\dot{\omega}$. In particular, we assume $(\tilde{\mathrm{q}}_1-\tilde{\mathrm{q}}_2)^2\ll 1$ so that dipole radiation is a small correction to the usual gravitational radiation. Then,

$$\dot{\omega}^{-1}=\frac{5}{96}\mathcal{M}^{-5/3}\omega^{-11/3}\left(1-\frac{\langle\dot{E}_i\rangle}{P_{GW}}\right). \tag{4.52}$$

In order to calculate the phase of the gravitational waveform, we must integrate the function

$$\begin{aligned} 2\omega t - 2\phi &= 2\int^{\omega} \frac{\omega - \omega'}{\dot{\omega}'} d\omega' \\ &= \frac{5}{48}\mathcal{M}^{-5/3}\int^{\omega} (\omega - \omega')\omega'^{-11/3}\left(1 - \frac{\langle \dot{E}_i \rangle}{P_{GW}}\right) d\omega'. \end{aligned} \tag{4.53}$$

Including the corrections to the Heaviside step function, the dipole term results can be integrated in terms of hypergeometric functions. However, we wish to find a power series expansion for the integral. We expand each function as

$$\frac{\langle \dot{E}_i \rangle}{P_{GW}} = C_i \theta\left(\lambda\omega - 1\right) \sum_{n=0}^{\infty} (-1)^n a_i(n) \left(\lambda_i \omega\right)^{-2n}, \tag{4.54}$$

where $i = S, V$ denote the type of dipole radiation, and

$$C_s = \frac{5(\tilde{\mathrm{q}}_1 - \tilde{\mathrm{q}}_2)^2}{96 m^{2/3}}, \tag{4.55}$$

$$C_v = \frac{5(\tilde{\mathrm{q}}_1 - \tilde{\mathrm{q}}_2)^2}{48 m^{2/3}}, \tag{4.56}$$

$$a_s(n) = \frac{3\sqrt{\pi}}{4\Gamma[\frac{5}{2} - n]\Gamma[n+1]}, \tag{4.57}$$

$$a_v(n) = \frac{3\sqrt{\pi}(1-n)}{4\Gamma[\frac{5}{2} - n]\Gamma[n+1]}. \tag{4.58}$$

The integral in Eq. (4.53) is then evaluated as

$$\begin{aligned} 2\omega t - 2\phi = {} & 2\omega\left[t_0 - \delta t_0 \theta(\lambda_i\omega - 1)\right] - 2\left[\phi_0 - \delta\phi_0\theta(\lambda_i\omega - 1)\right] + \frac{3}{128}(\mathcal{M}\omega)^{-5/3} \\ & \times \left[1 - 20 C_i \omega^{-2/3}\theta(\lambda_i\omega - 1)\sum_{n=0}^{\infty} \frac{(-1)^n a_i(n)}{(3n+5)(6n+7)}\left(\lambda_i\omega\right)^{-2n}\right]. \end{aligned} \tag{4.59}$$

We note, the corrections to the coalescence time t_0 and inspiral phase ϕ_0 include non-trivial frequency dependence through the step function. In principle, these additional step function corrections can be important for the matched filter process. However, these corrections enter at 2.5PN and 4PN order for the phase and coalescence time, respectively, and should be small for most observations.

Finally, the waveform is written as

$$\tilde{h}(f) = -\left(\frac{5\pi}{24}\right)^{1/2} \frac{\mathcal{M}^2}{D_{\rm eff}} (\pi\mathcal{M}f)^{-7/6} e^{-i\Psi} \times \left[1 - \frac{1}{2} C_i (\pi f)^{-2/3} \theta(\pi\lambda_i f - 1) \sum_{n=0}^{\infty} (-1)^n a_i(n) \, (\pi\lambda_i f)^{-2n}\right], \tag{4.60}$$

$$\Psi = 2\omega \left[t_0 - \delta t_0 \theta(\pi\lambda_i f - 1)\right] - 2\left[\phi_0 - \delta\phi_0 \theta(\pi\lambda_i f - 1)\right] - \frac{\pi}{4} + \frac{3}{128}(\pi\mathcal{M}f)^{-5/3} \times \left[1 - 20 C_i (\pi f)^{-2/3} \theta(\pi\lambda_i f - 1) \sum_{n=0}^{\infty} \frac{(-1)^n a_i(n)}{(3n+5)(6n+7)} \, (\pi\lambda_i f)^{-2n}\right]. \tag{4.61}$$

Due to the step function, $1 \leq \pi\lambda_i f$, the infinite sum converges (to the same hypergeometric functions stated before) for both scalar and vector modes. In the case of vector mode dipole radiation, $a_v(1) = 0$, hence the first correction to the step function occurs at second order, $(\pi\lambda_i f)^{-4}$. Then, the -1PN correction to the waveform from the step-function dipole term is modified by a small -7PN correction for vector mode radiation or a -4PN correction for scalar mode radiation (small in the sense that $(\pi\lambda_i f)^{-2n} \leq 1$).

4.5 Constraints on Dark Matter Model Parameters

4.5.1 Fisher analysis basics

The Fisher information matrix is a standard statistical tool used to estimate the accuracy to which parameters can be measured in gravitational wave physics in the large signal-to-noise ratio limit [158, 159]. The inverse of the Fisher information provides a lower bound on the error of any unbiased estimator (the Cramer-Rao bound), and hence provides an optimistic set of forecasted constraints, as compared to a Bayesian analysis. The appeal of this approach is the computational efficiency; it requires orders of magnitude less computing power then a Markov-Chain Monte Carlo analysis.

The Fisher information matrix Γ_{ab} is defined as a weighted inner product of derivatives of the waveform with respect to parameters θ^a and θ^b. That is,

$$\Gamma_{ab} \equiv \left(\frac{\partial h}{\partial\theta^a} \middle| \frac{\partial h}{\partial\theta^b}\right), \tag{4.62}$$

where the inner product is defined as

$$(h_1|h_2) \equiv 2\int_{f_{\rm low}}^{f_{\rm high}} \frac{\tilde{h}_1\tilde{h}_2^* + \tilde{h}_1^*\tilde{h}_2}{S_n(f')}{\rm d}f', \tag{4.63}$$

with $S_n(f)$ the spectral noise density of the detector, and $\tilde{h}(f)$ the Fourier transform of the time-domain response $h(t)$. From this definition, one can quickly see that the signal to noise ratio (SNR) is given by

$$\rho^2 \equiv (h|h) = 4\int {\rm dlog}f\ \frac{f|\tilde{h}|^2}{S_n(f)}. \tag{4.64}$$

The bounds of integration in Eq. (4.63) are discussed in detail in Section 4.5.2.

The Fisher matrix is equivalent to evaluating the second derivative of the likelihood $\mathcal{L}$

$$\Gamma_{ab} = -{\rm E}\left[\frac{\partial^2\mathcal{L}}{\partial\theta^a\partial\theta^b}\right], \tag{4.65}$$

at the maximum likelihood estimate for θ^a, where $\mathcal{L}$ is given by

$$\mathcal{L}(\theta) = \exp\left[-\frac{1}{2}\left(s-h(\theta)|s-h(\theta)\right)\right], \tag{4.66}$$

given a signal s and a gravitational waveform h. Hence, the inverse of the Fisher matrix can alternatively be viewed as the frequentist error of the maximum likelihood estimator. A third interpretation of the Fisher information matrix is a Bayesian one: the inverse Fisher matrix is the covariance of the posterior probability distribution of the true parameters, as would be inferred by a Bayesian analysis of a single experiment, assuming constant prior probabilities, a high SNR, and Gaussian noise.

From these definitions, one can estimate the sensitivity of a detector to a given parameter. The root-mean-squared (1σ) error on a parameter θ^a can be estimated by,

$$\Delta\theta^a \leq \sqrt{\Sigma^{aa}}, \tag{4.67}$$

where Σ^{aa} is defined as the (a,a) component of the covariance matrix $\Sigma^{ij} \equiv (\Gamma_{ij})^{-1}$. In this work we will use Eqs. (4.62) and (4.63) to compute the above error, which we interpret as the projected sensitivity of a given detector to a parameter θ^a. To prevent (numerically) singular Fisher matrices, we follow the method of [114], where we use a

working precision of one hundred decimal places and invert the Fisher matrix by the Cholesky decomposition.

4.5.2 Range of frequency integration

The limits of integration in the Fisher analysis dictate the range over which our waveform in Eq. (4.32) remains valid and detectable above detector noise. For the detectors we consider (see Section 4.5.3), typical binary neutron star and mixed black hole-neutron star inspirals will merge within the detector's frequency window. The high frequency limit will then remain independent of the particular detector, given instead by physical quantities of the binary. However, the low frequency limit will depend on the sensitivity of a particular detector.

For the low frequency limit, we follow [114], defining

$$f_{\rm low} = \max\left[f_{\rm low-cut}, f_{\rm lratio}\right], \tag{4.68}$$

where $f_{\text{low-cut}}$ is a detector dependent cutoff frequency given as 1 Hz for the Einstein Telescope (ET), and 5 Hz for the remaining detectors we consider in Section 4.5.3. The frequency $f_{\rm lratio}$ is defined as the lowest frequency where the amplitude of the gravitational wave signal is 10% of the detector noise spectrum. Below this frequency, the integrand in Eq. (4.64) is less than $\mathcal{O}(10^{-2})$, and can thus we neglected when computing the signal-to-noise ratio.

At high frequencies, our waveform becomes invalid [160, 161] due to a lack of stable circular orbits, assumed in the orbital frequency in Eq. (4.6) and the complete breakdown of the post-Newtonian approximation. The frequency of gravitational waves [162] emitted at the innermost stable circular orbit (ISCO) (for a test particle in a Schwarzschild spacetime of mass m) is given by

$$f_{\rm ISCO} = (4.4 \times 10^3 \text{ Hz}) \left(\frac{m}{M_\odot}\right)^{-1}. \tag{4.69}$$

However, when the binary contains a neutron star, the waveform must be terminated before contact. The contact frequency [163] can be approximated as the gravitational

wave frequency at which the separation is equal to the sum of the radii of the two stars:

$$f_{\rm contact} = (4.4 \times 10^3 \text{ Hz}) \left(\frac{m}{M_\odot}\right)^{-1} (6\tilde{C})^{3/2} \tag{4.70}$$

$$\tilde{C}^{-1} = \frac{m_1}{mC_1} + \frac{m_2}{mC_2}, \tag{4.71}$$

where C_i is the compactness of the ith star[8], and $\tilde{C}$ acts as an effective compactness for the binary. The high frequency limit must be taken as the minimum between these two frequencies,

$$f_{\rm high} = \min\left[f_{\rm contact}, f_{\rm ISCO}\right]. \tag{4.72}$$

As discussed in [164], enforcing this high frequency cut-off can lead to incorrect results for the accuracy of parameter-estimation. This particularly affects parameters that depend sensitively on the merger time, such as the total mass, and thus is particularly relevant for higher mass systems. In contrast, the accuracy to which dipole and Yukawa modifications can be constrained builds up during the early inspiral phase, and further, in this work we study only low mass systems. Hence we do not expect parameter-estimation to depend sensitively on the merger phase.

We can further simply $f_{\rm high}$ as follows. Stable neutron stars have roughly the same radius $R_{\rm NS}$, given by their equation of state [165], and therefore the compactness of the individual star is given by $C_i \approx m_i/R_{\rm NS}$. The effective compactness $\tilde{C}_{\text{NS-NS}}$ can then be rewritten as

$$6\tilde{C}_{\text{NS-NS}} \approx \frac{3m}{R_{\rm NS}} = 0.44 \left(\frac{m}{M_\odot}\right) \left(\frac{R_{\rm NS}}{10 \text{ km}}\right)^{-1}. \tag{4.73}$$

Similarly, we take the black hole compactness to be $C = \frac{1}{2}$, so the effective compactness for a black hole - neutron star binary can be written as

$$6\tilde{C}_{\text{BH-NS}} \approx \frac{6m}{2m_{\rm BH} + R_{\rm NS}}. \tag{4.74}$$

For a particular neutron star equation of state, the effective compactness for various binaries systems can be calculated. Figure 4.1 displays the range of $6\tilde{C}$ for various neutron star equations of state. We see that the effective compactness is greater than unity for all but low mass binary neutron stars.

[8] For a non-rotating black holes, the compactness is taken as $C = \frac{1}{2}$, while neutron stars have the upper bound $C \leq \frac{4}{9}$. For stable neutron stars, the compactness [165] is typically in the range $C \in (0.1, 0.2)$.

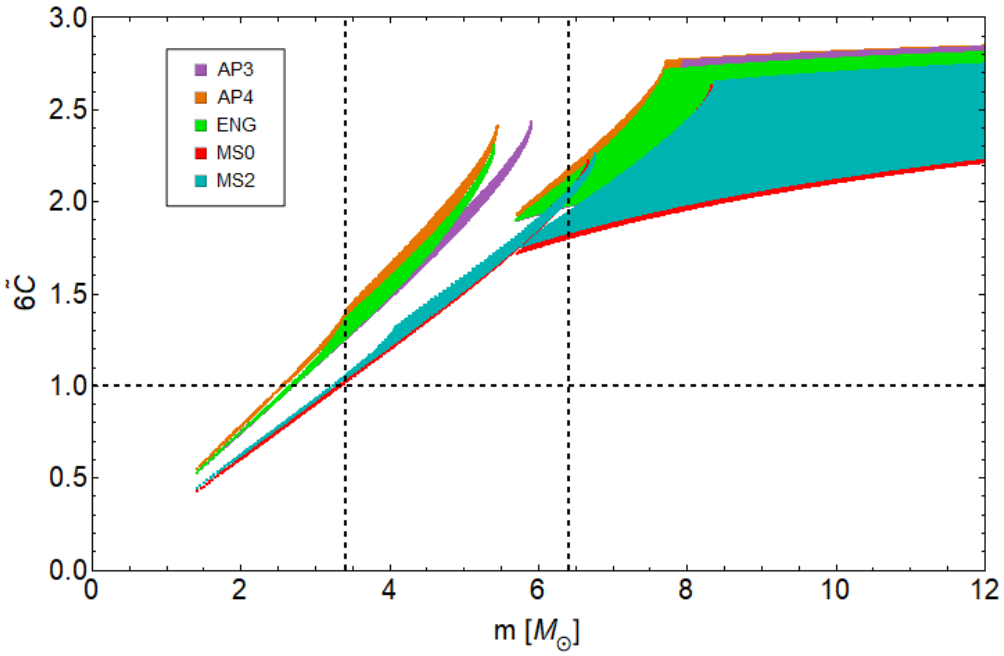

Figure 4.1: Effective compactness of neutron star binaries and mixed black hole-neutron star binaries, for various neutron star equations of state [165]. We have taken the minimum black hole mass as $5M_\odot$. The vertical, dashed black lines correspond to the total masses we will consider in Section 4.5.4. In both cases, we see that $6\tilde{C} \geq 1$.

When $6\tilde{C} > 1$, the contact frequency occurs after $f_{\rm ISCO}$. Therefore, the high frequency limit is written as

$$f_{\rm high} = (4.4 \times 10^3 \text{ Hz}) \left(\frac{m}{M_\odot}\right)^{-1} (6\mathcal{C})^{3/2}, \tag{4.75}$$

$$\mathcal{C} = \min\left[\tilde{C}, \frac{1}{6}\right]. \tag{4.76}$$

For the binaries we consider in Section 4.5.4, $6\mathcal{C} = 1$, thus our analysis will always take the high frequency limit as $f_{\rm ISCO}$.

The mass-radius relations of neutron stars used in Fig. 4.1 does not include the effects of a dark matter core. However, recent work [143] has shown that for a particular equation of state, the same total mass neutron star will typically have a smaller radius when a dark core is included. This implies that including dark matter will increase the compactness of a particular neutron star, further increasing the effective compactness $6\tilde{C}$. Therefore, $f_{\rm high} = f_{\rm ISCO}$ remains valid for the binary systems of interest.

4.5.3 Future detectors and sensitivity curves

In this work we compute forecasted constraints on dark sector modifications for a set of 10 ground-based detectors: aLIGO at design sensitivity [166], aLIGO with squeezing (A+/A++ [167]), Voyager [167], VRT [167, 168], Cosmic Explorer 1 (CE1) and 2 narrow-band and wide-band configurations (CE2n and CE2w respectively) [167], and the Einstein Telescope in its single interferometer configuration (ET-B) and in "xylophone" configuration ET-D [169, 170].

For a detailed overview of the detector sensitivities we refer the reader to [171]. Here we briefly summarize the salient details of each detector:

A+, A++: Upgrades to LIGO to minimize quantum and thermal noise, operational starting around 2020.

Voyager: An upgrade to LIGO, which replaces glass mirrors and suspensions with silicon parts, and will operate at a cryogenic temperature of 123K. To be operational in 2027.

Vrt: The same as Voyager, but operated at room temperature, instead of at cryogenic temperatures.

Cosmic Explorer: Aims to observe binaries at high redshift ($z > 1$), using 40km long detectors. CE1 is built on A+ technology, while CE2 (in narrow band and wide band configurations) is built on Voyager technology. Projected start date of 2035.

Einstein Telescope: Designed to improve upon low-frequency ($f < 10$ Hz) noise levels. To be built underground, operational in 2030-2035.

For each of these detectors, we find an analytic fit to the tabulated projected sensitivities. These fitting functions will greatly accelerate the computation of Fisher matrix elements. The functional form we use is

$$\frac{1}{2}\log S_n(f) = \sum_{i=1}^{9} p_i \left(\frac{x - p_{10}}{p_{11}}\right)^{9-i} + \frac{p_{12}}{\sqrt{(x - p_{13})^2 + p_{14}^2}} \tag{4.77}$$

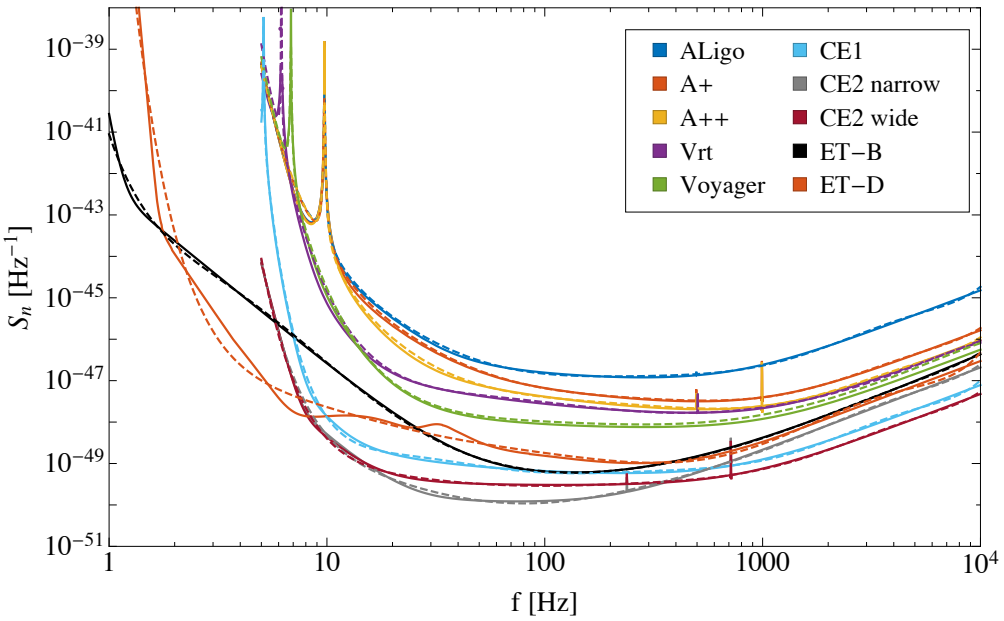

Figure 4.2: Projected spectral noise density (solid) and analytic fits (dashed) for each detector we consider. The curves are truncated at the particular detector's cutoff frequency $f_{\text{low-cut}}$.

where $x \equiv \log f$. The final term is only included when the detector obtains a large resonance at small frequencies near $f_{\text{low-cut}}$. This resonance does not occur in CE2 (narrow and wide) and the Einstein Telescope, hence we set $p_{12} = 0$ for these four fit functions. While the shift and rescaling parameters p_{10}, p_{11} are redundant in this expansion, p_{10} will manifest as a "characteristic" frequency, similar to previous work [150]. The fitting parameters are given explicitly in Table 4.2. The tabulated and analytic fit sensitivity curves are shown in Fig. 4.2.

4.5.4 Constraints on dark sectors

We now apply the Fisher analysis discussed in Sec. 4.5.1 to the most general waveform, calculated in Eq. (4.32), and include the General Relativity corrections, up to 2PN order, calculated in [172]. In particular, we will look at a binary neutron star and a mixed black hole-neutron star binary, evaluated at the parameters found in Table 4.1. The maximal list of parameters we consider is given by

$$\boldsymbol{\theta} = \{\log \mathcal{A}, t_c, \phi_c, \log \mathcal{M}_c, \log \eta, \chi_s, \chi_a, \alpha, \gamma\}\,, \tag{4.78}$$

Name	$m_1[M_\odot]$	$m_2[M_\odot]$	(χ_1, χ_2)	$D_{\rm eff}$ [Mpc]	SNR (aLIGO)
NSNS	2.0	1.4	(0.01, 0.02)	100	25
BHNS	5.0	1.4	(0.2 , 0.02)	150	25

Table 4.1: Representative systems used in our Fisher analysis. The signal-to-noise ratio is given for Adv. LIGO at design sensitivity.

where $\chi_s = (\chi_1 + \chi_2)/2$, $\chi_a = (\chi_1 - \chi_2)/2$, and χ_i is the dimensionless spin parameter for the ith star. Our Fisher analysis, thus, will include all covariances between the parameters listed above. We also note that our set of parameters does not include spin precession or tidal parameters, as these enter at higher PN order.

When projecting future constraints, we will assume that future gravitational wave observations are consistent with General Relativity. This implies that when computing the Fisher matrix elements, we will take the General Relativity limit $\Gamma_{ab}|_{\alpha,\gamma\to 0}$. A by-product of this is that we lose the ability to constrain the length scale of the Yukawa interaction λ separately, and thus, this parameter does not appear in Eq. (4.78). This can be seen directly in Eq. (4.32), noticing that any derivative with respect to λ is proportional to either α or γ. Instead, the constraints placed on each of these parameters will have a functional dependence on the Yukawa length scale. This has the added benefit that the Fisher analysis will not have numerical errors due to the sharp features manifesting from derivatives of the Heaviside function in dipole radiation.

In the case of the mixed binary, the black hole should not be charged under the massive dark photon [173], and thus we expect $\alpha = 0$. For this reason, we do not include α in the list of parameters when considering the mixed binary in a Fisher analysis. This parameter, however, could be included in the future as a test of black hole no-hair theorems. While nonzero α can also be attributed to a dark matter cloud surrounding the black hole, tidal effects may become relevant before the $f_{\rm high}$ considered here.

Similarly, when dipole emission is not present in the waveform, the parameter γ will be removed from the parameter list. This occurs when Eq. (4.12) is not satisfied, forcing the step function to vanish and removing the dipole radiation terms from the waveform. The parameter γ can only be constrained when the step-function is active sometime before the end of the observation, given by the frequency $f_{\rm high}$. Using the definition of

f_{high} in Eq. (4.75), we find the minimum length scale as

$$\lambda \geq (22 \text{ km}) (6\mathcal{C})^{-3/2} \left(\frac{m}{M_\odot} \right), \tag{4.79}$$

for which we include γ as a parameter in the Fisher analysis.

Under these considerations, we estimated projected constraints for γ from both binary systems, as shown in Fig. 4.3. The earlier dipole radiation activates, the more significant its contribution becomes to the signal-to-noise ratio. Thus, as the Yukawa length scale increases, the constraint on γ becomes more stringent, until $\lambda \sim \mathcal{O}\left(10^4 - 10^5 \text{ km}\right)$. At this length scale, the step function is activated before the low frequency bound, given by Eq. (4.12). Approximating the low frequency limit as $f_{\text{low-cut}}$, we find this critical length scale to be $\lambda \approx 10^5$ km for ET, and $\lambda \approx 2 \times 10^4$ km for the remaining detectors. Above this length scale, the length scale λ only enters the waveform through the Yukawa-corrections. For BHNS binaries, we have no Yukawa corrections, thus the constraint is independent of the length scale. For NSNS binaries, these Yukawa corrections maintain a (weak) lambda dependence, causing the constrain to asymtote to a particular (detector-dependent) value.

The relative Yukawa strength α can also be constrained from future binary neutron star observations, as shown in Fig. 4.4. We find that significant constraints can be placed on the relative Yukawa strength above $\lambda \sim 5$ km. Below this length scale, the exponential suppression of the Yukawa interaction leads to minuscule corrections to the waveform through the inspiral. Surprisingly, even when the Yukawa length scale is comparable to the radius of the neutron star ($R_{NS} \sim 13$ km), we are still able to constrain $\alpha \leq 10^{-2}$. Once one crosses into the ultra-light regime, $\lambda \gtrsim \mathcal{O}(10^3 \text{ km})$, we again see a rapid decline in the strength of the constraint due to the small Yukawa corrections shown in Eq. (4.38). It is during this regime that the dipole radiation terms can begin to dominate for a significant period of the inspiral phase. Again, once dipole radiation activates throughout the entire detection window, α is only constrained below the consistency bound $\alpha < 1$ by the more sensitive CE and ET detectors.

In the ultra-light regime, $\lambda \gtrsim \mathcal{O}(10^3 \text{ km})$, all previous figures show an increase in the variance of estimated parameters, see e.g. the variance of α in Fig. 4.4. The variance of the estimated astrophysical parameters, like the chirp mass, also increases in this regime,

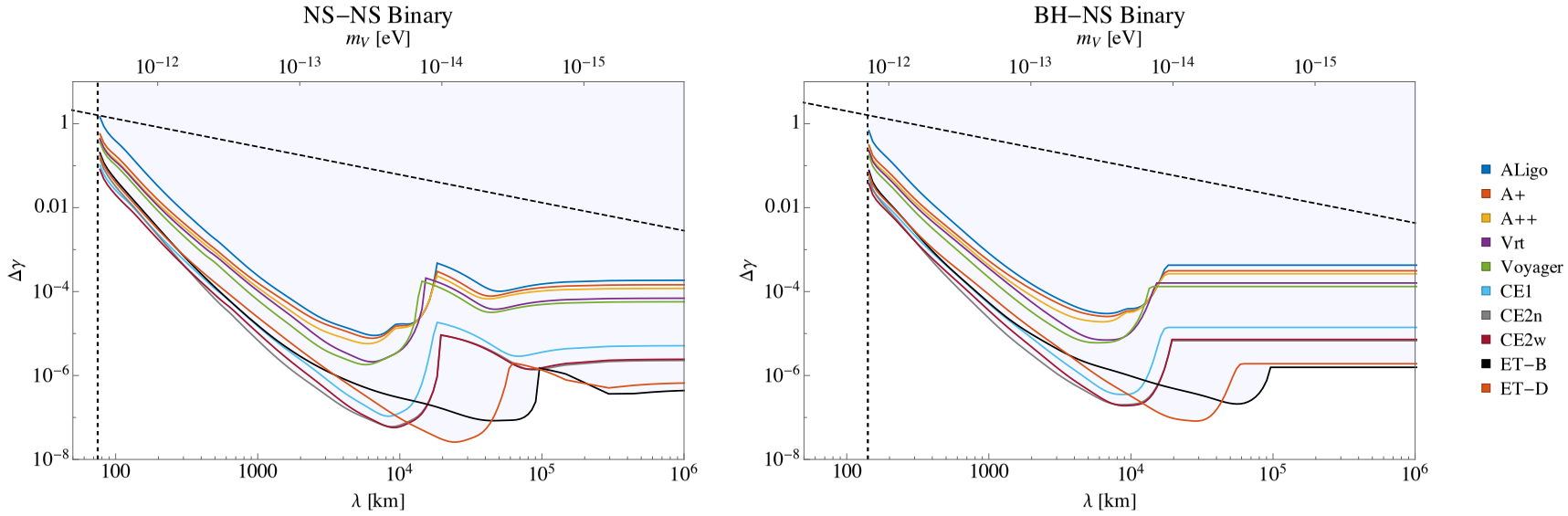

Figure 4.3: Projected constraints on the charge asymmetry γ with future neutron star binary (NSNS) and mixed black hole-neutron star binary (BHNS) observations. The vertical dashed line denotes the activation of dipole radiation at some point before $f_{\rm ISCO}$. The diagonal dashed line gives the consistency requirement of the waveform, given by Eq. (4.31). All detectors considered are able to constrain γ from our waveform until $\lambda \sim 10^8$ km.

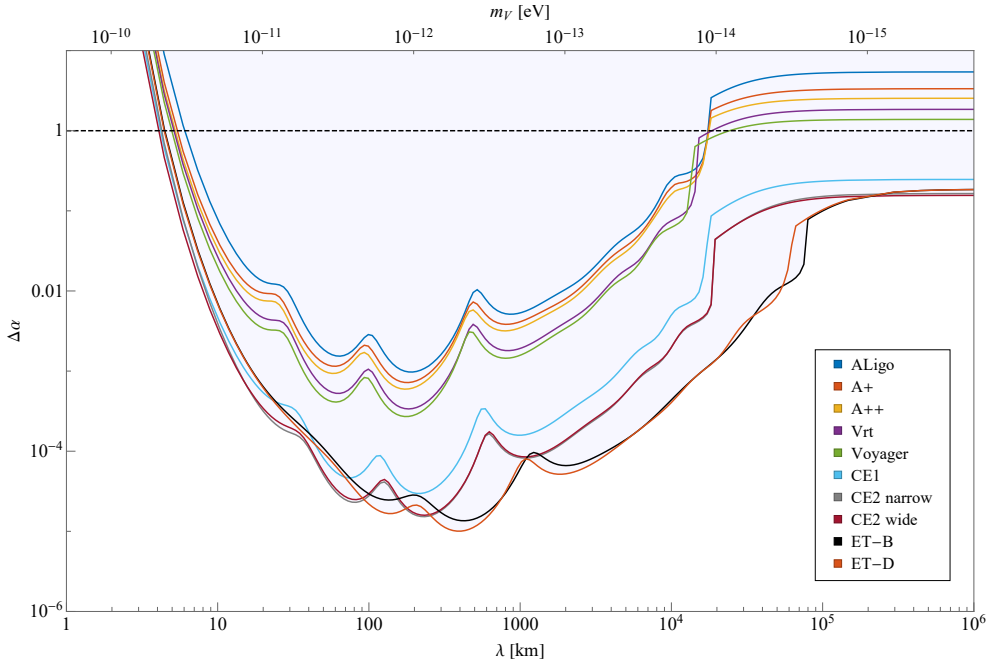

Figure 4.4: Projected constraints on the relative strength of the Yukawa interaction α between neutron stars. The dashed line at $\alpha = 1$ corresponds to the physical requirement that the total energy in Eq. (4.7) remains negative throughout the inspiral.

as we can see in Fig. 4.5, which for illustrative purposes focuses on a NSNS merger. The reason for this increase in the variance is a similar increase in the correlation between the α parameter and the chirp mass; we have indeed verified that this element of the correlation matrix approaches unity as $\lambda \gtrsim \mathcal{O}(10^3 \text{ km})$. We can see the growth of this correlation analytically in Eq. (4.39): as λ becomes large, the $1/\lambda^2$ and the $1/\lambda^3$ terms in the Fourier phase become small, and the leading order term in the phase depends not on just the chirp mass, but rather the product of the chirp mass and a $(1 + 2\alpha/3)$ factor. This makes the Fisher matrix nearly degenerate, which then leads to a very large variance upon inversion. In this regime, parameter estimation with GR templates could be subject to "fundamental theoretical bias" [174].

We now return to dark matter. One can convert the bounds on α, γ into an upper bound on the charge to mass ratio $\tilde{\mathrm{q}}$ of the neutron star via

$$\tilde{\mathrm{q}} \leq \frac{\sqrt{\gamma_b} + \sqrt{\gamma_b + 4\alpha_b}}{2}, \tag{4.80}$$

where α_b, γ_b are the bounding functions given in Figs. 4.3 and 4.4 for a particular detector. This relation follows straightforwardly from the definitions of α and γ. We

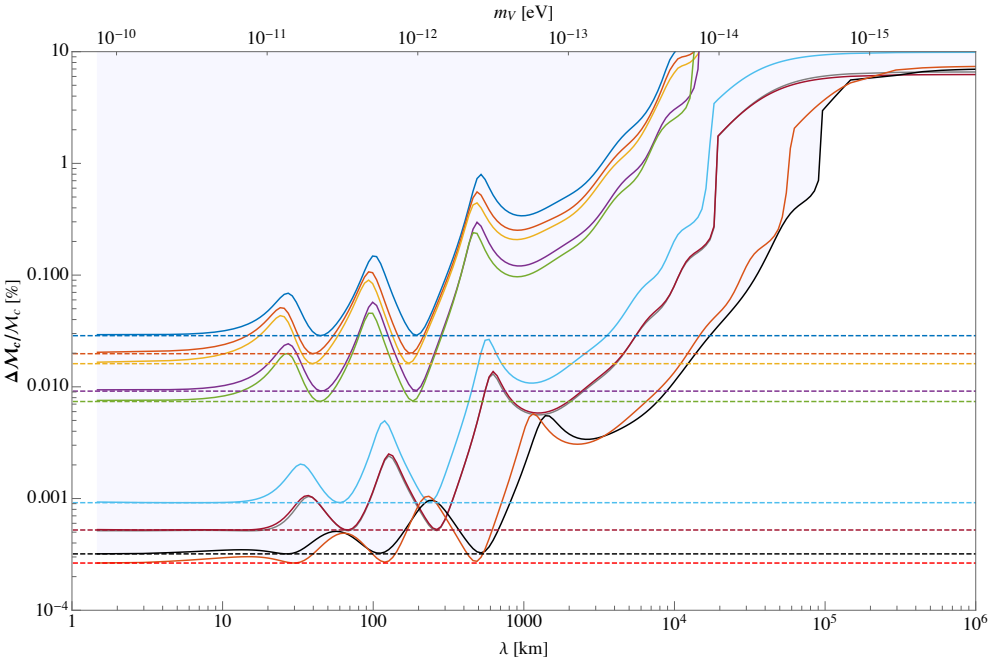

Figure 4.5: Projected sensitivity to the chirp mass in a binary neutron star merger, with and without dark sector modifications. Dashed lines are the sensitivity predicted by the GR waveform, while the solid lines are the sensitivity once dark sectors are included. Colors are as in previous plots.

note, that for the mixed black hole-neutron star system, the assumption that $\alpha = 0$ provides the stronger constraints $\tilde{\mathrm{q}} \leq \sqrt{\gamma_b}$. To date, no gravitational wave observations have been made of a mixed binary, so we will focus on the binary neutron star case below instead.

Using the dark matter model described in Sec. 4.2, the constraint on the charge-to-mass ratio can further be converted into a more useful constraint on the dark matter mass fraction of the neutron star

$$\tilde{\mathrm{q}} \equiv 1.22 \times 10^{17} f_{DM} \left(\frac{g^2}{4\pi}\right)^{1/2} \left(\frac{100\ \mathrm{GeV}}{m_\chi}\right). \tag{4.81}$$

The value of the self-interaction $g^2/4\pi$ is constrained primarily by astrophysical constraints on dark matter self-interactions, e.g. morphology of galactic halos. In particular, the ellipticity of large halos constrains $g^2/4\pi \lesssim 10^{-3}$ [145]. Saturating this bound, we see from Fig. 4.6 that for sub-TeV mass dark matter, gravitational waves can probe even the extreme dark matter mass fraction $f_{DM} \sim 10^{-15}$ predicted in [138].

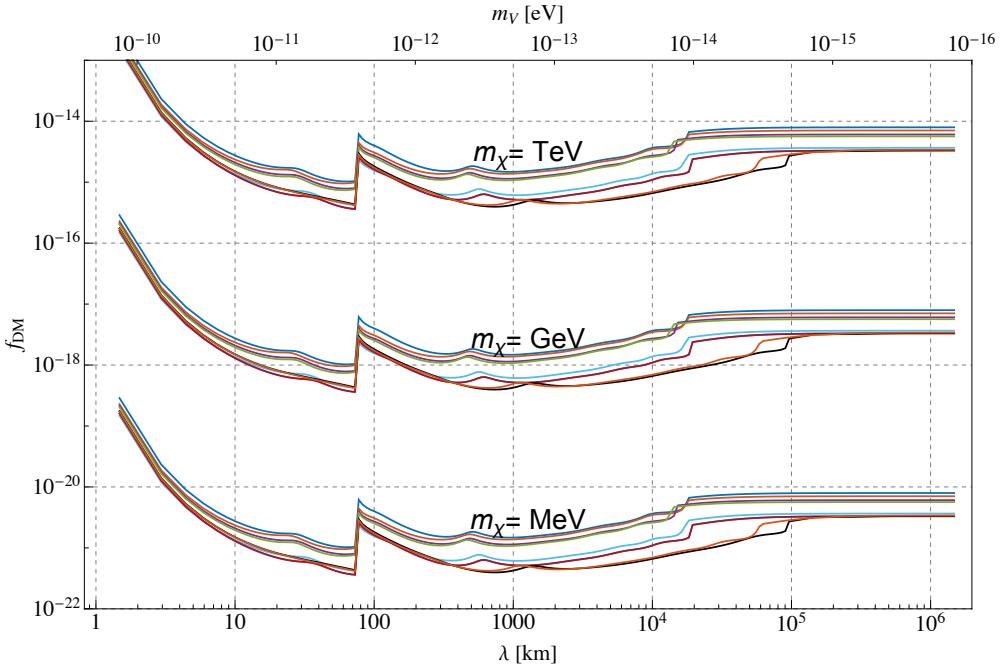

Figure 4.6: Projected sensitivity to dark matter mass fraction from an NSNS binary merger, found from Eq. (4.80), with $g^2/4\pi = 10^{-3}$ and for varying mass m_χ. Colors are as in previous figures. At length scales below $\lambda \sim 70$ km, dipole radiation is not activated, and Eq. (4.80) provides no constraint on the dark matter mass fraction. One can provide optimistic constraints below this regime by assuming the mass fraction for the two neutron stars are comparable ($\gamma \ll \alpha$).

4.6 Discussion

Current gravitational wave interferometers have been a remarkable success, and the observations of black-hole binary mergers [108, 109, 110, 111, 112] and a neutron star binary merger [113] have already place strong constraints on fundamental physics. The third generation of detectors will improve on LIGO sensitivity by up to two orders of magnitude, which provides ample cause for excitement at the prospect of further probing fundamental physics with gravitational waves from binary mergers.

In this work we have quantified these expectations, and have studied dark sector modifications to the gravitational waves emitted in binary inspirals. We have considered Yukawa corrections to the gravitational potential, and the associated dipole emission, as both arise in dark matter models with massive gauge bosons, and any modification of gravity that introduces a new scalar degree of freedom. We have explicitly computed the waveform, and performed a Fisher information matrix analysis to compute projected sensitivities of ten next generation gravitational wave detectors.

The projected sensitivities to the Yukawa interaction coupling α and the dipole emission parameter γ are shown in Figs. 4.3 and 4.4. The Einstein Telescope is found to be the most sensitive to such dark sector modifications, with sensitivity as good as $\mathcal{O}(10^{-5})$ and $\mathcal{O}(10^{-7})$ for α and γ respectively. We project that constraints can be placed provided the Yukawa length scale $\lambda > \mathcal{O}(10)$ km, and they are optimal when $\lambda \sim 10^2 - 10^3$ km and $\sim 10^4$ km for α and γ respectively. The degree to which we can constraint these parameters is dependent on the signal-to-noise ratio of the gravitational wave detection. Thus, parameters such as the masses of the binary constituents and the effective luminosity distance will play a significant role in the ability to constrain α, γ. Because the dark sector corrections considered here are not degenerate with higher PN corrections of GR, the spin parameters will not noticeably change the constraints.

We emphasize that for a large range in λ, the Einstein Telescope gives the most stringent constraints for both α, γ parameters, due to the increased frequency range in the integration of the Fisher elements. One may expect that the use of lower frequency detectors, such as LISA, may significantly improve these constraints. But these space-based detectors will observe near-monochromatic binaries, so it is not clear whether these detectors will be effective at constraining dark sector modifications.

When written as a constraint on a specific dark matter model, we find these observations can detect even a minuscule amount of dark matter stored in neutron stars. For a GeV dark matter candidate with a gauge coupling $g^2/4\pi = 10^{-3}$, the bound on the fraction of the NS mass in dark matter can easily be better than 1 part in 10^{15}, as shown in Fig. 4.6. More generally, the constraints on α and γ, shown in Figs. 4.3 and 4.4, probe dark photon masses in the range $m_v \lesssim 10^{-10}$ eV, with optimal constraints around $m_v \sim 10^{-12}$ eV.

We interpret these results as quantitative confirmation that gravitational wave astronomy is a powerful probe of fundamental physics. However, the work is not over, and there are indeed new directions for future work in every step on this analysis. In particular, one could improve upon theoretical estimates of the dark matter fraction of neutron stars, extend the statistical analysis to include space-based detectors such as LISA (using extreme mass-ratio inspirals that include a neutron star component), and recompute the projected sensitivities by performing a full Markov-chain Monte-Carlo analysis. The last of these is a necessary step to properly quantify the degeneracy with

astrophysical parameters, as well as the 'fundamental theoretical bias' [174] introduced by the use of GR waveforms and neglecting the modifications studied here.

	ALIGO	A+	A++	VRT	Voyager	CE1	CE2w	CE2n	ET-B	ET-D
p_1	0.1136	9.235×10^{-2}	7.22×10^{-2}	-1.379×10^{-2}	-1.149×10^{-5}	0.2076	0.1111	0.1021	0.1132	0.3328
p_2	-3.296×10^{-2}	-5.346×10^{-2}	-1.006×10^{-4}	-4.705×10^{-2}	4.806×10^{-4}	-0.2575	-0.1297	-0.1333	-0.194	-0.3963
p_3	-0.5891	-0.4692	-0.3896	0.2288	-7.609×10^{-3}	-0.8017	-0.4107	-0.3544	-0.4398	-1.122
p_4	-4.839×10^{-3}	8.376×10^{-2}	-0.2102	-0.1593	4.603×10^{-2}	0.7220	0.2321	0.3786	0.9275	0.6489
p_5	1.141	0.9587	0.9982	-0.2686	0.1295	1.0520	0.6513	0.4214	8.287×10^{-2}	1.568
p_6	-6.951×10^{-2}	-0.1183	0.2691	0.5208	-3.569	-0.4328	3.022×10^{-2}	-0.6310	-1.428	0.2107
p_7	0.2893	0.3372	7.438×10^{-2}	0.6479	21.42	0.2003	0.2179	0.8405	2.767	0.3309
p_8	7.484×10^{-2}	-0.3580	-0.4025	-0.3940	-57.99	0.2033	0.2460	1.238	-0.5816	-0.9473
p_9	-54	-54.6	-54.79	-54.96	6.253	-56.66	-56.98	-57.2	-56.63	-56.12
p_{10}	5.536	5.536	5.536	5.536	0	5.445	5.41	5.41	4.605	4.605
p_{11}	2.144	2.144	2.144	2.144	1	2.174	2.196	2.196	2.66	2.66
p_{12}	4.003×10^{-2}	4.395×10^{-2}	4.771×10^{-2}	1.762×10^{-2}	3.153×10^{-2}	1.429×10^{-2}	0	0	0	0
p_{13}	2.275	2.275	2.275	1.821	1.921	1.633	–	–	–	–
p_{14}	9.254×10^{-3}	1.020×10^{-2}	1.108×10^{-2}	2.954×10^{-3}	7.960×10^{-3}	3.879×10^{-3}	–	–	–	–

Table 4.2: Fitting parameters for noise curves.

Chapter 5

Concluding Remarks

In this thesis, we consider three potentially observable signals from beyond Standard model particles. While each field is introduced to solve a specific problem, such as the Strong CP problem or the naturalness of the inflationary potential, the breadth of theoretical uncertainty associated with these additional fields manifests as a large energy gap between the different effects. Yet central to the resolutions are axion-like particles. Furthermore, taking advantage of the pseudoscalar couplings provides unique avenues to probe these ALP models.

In the context of natural inflation, interactions between the inflaton, charged fermions, and photons lead to a large deposition of energy into a particular handedness of photons. As a result, large amounts of V-mode polarization should exist in universe following reheating. Using standard computational techniques for inflationary perturbations, we are able to find the spectral tilt of the primordial V-mode power spectrum. In order to make contact with observation, modes drawing from this initial spectrum must be transferred to the CMB. Without introducing additional sources to the Boltzmann equation, the initial circular polarization will be exponentially damped due to the high conductivity of the early universe. Thus, any detection of circular polarization would pose a difficult problem of disentangling the initial circular polarization from new interactions.

Alternatively, the possibilitiy of axion-like dark matter prompts the investigation of effective interactions between ALP and standard model particles. We show that the axion-electron coupling gives rise an oscillating electric dipole moment for the electron. While experiments such as EDELWEISS and XMASS can provide model-independent constraints on the axion-electron current, more stringent constraints can be placed for

low-mass axion by the amplitude of the electron's electric dipole moment. Within a factor of two improvement in current experimental techniques, electric dipole constrains will probe into the QCD axion regime. However, these experiments do not utilize the oscillating nature of the axion-induced electric dipole moment.

Finally, we consider the capture of axions (more generally, some dark matter particle) into neutron stars and black holes. In a binary system, long range interactions between the collections of dark matter will modify the total energy and orbital angular frequency of the binary. During the inspiral and merger phase of the system, these kinetic modifications will manifest in the gravitational waveform emitted. Calculating these corrections, we perform a Fisher analysis to generically constrain dark matter interactions as a function of the light mediator's mass. However, with the detection of gravitational waves from a neutron star binary, more sophisticated techniques, such as Markov-chain Monte Carlo simulations can be applied in the future using the template calculated.

Bibliography

[1] N. Aghanim *et al.* [Planck Collaboration], *Planck 2018 results. VI. Cosmological parameters*, arXiv:1807.06209 [astro-ph.CO].

[2] G. E. Addison, D. J. Watts, C. L. Bennett, M. Halpern, G. Hinshaw and J. L. Weiland, *Elucidating ΛCDM: Impact of Baryon Acoustic Oscillation Measurements on the Hubble Constant Discrepancy*, Astrophys. J. **853**, no. 2, 119 (2018) [arXiv:1707.06547 [astro-ph.CO]].

[3] J. L. Bernal, L. Verde and A. G. Riess, *The trouble with H_0*, JCAP **1610**, no. 10, 019 (2016) doi:10.1088/1475-7516/2016/10/019 [arXiv:1607.05617 [astro-ph.CO]].

[4] J. Martin, *Everything You Always Wanted To Know About The Cosmological Constant Problem (But Were Afraid To Ask)*, Comptes Rendus Physique **13**, 566 (2012) [arXiv:1205.3365 [astro-ph.CO]].

[5] M. A. Troxel *et al.* [DES Collaboration], *Dark Energy Survey Year 1 results: Cosmological constraints from cosmic shear*, Phys. Rev. D **98**, no. 4, 043528 (2018) [arXiv:1708.01538 [astro-ph.CO]].

[6] F. Kahlhoefer, *Review of LHC Dark Matter Searches*, Int. J. Mod. Phys. A **32**, no. 13, 1730006 (2017) [arXiv:1702.02430 [hep-ph]].

[7] T. M. Undagoitia and L. Rauch, *Dark matter direct-detection experiments*, J. Phys. G **43**, no. 1, 013001 (2016) [arXiv:1509.08767 [physics.ins-det]].

[8] J. M. Gaskins, *A review of indirect searches for particle dark matter*, Contemp. Phys. **57**, no. 4, 496 (2016) [arXiv:1604.00014 [astro-ph.HE]].

[9] V. Khachatryan *et al.* [CMS Collaboration], *Search for dark matter in proton-proton collisions at 8 TeV with missing transverse momentum and vector boson tagged jets*, JHEP **1612**, 083 (2016) Erratum: [JHEP **1708**, 035 (2017)] [arXiv:1607.05764 [hep-ex]].

[10] T. Cohen, T. Golling, M. Hance, A. Henrichs, K. Howe, J. Loyal, S. Padhi and J. G. Wacker, *SUSY Simplified Models at 14, 33, and 100 TeV Proton Colliders*, JHEP **1404**, 117 (2014) [arXiv:1311.6480 [hep-ph]].

J. Fan, P. Jaiswal and S. C. Leung, *Jet Observables and Stops at 100 TeV Collider*, Phys. Rev. D **96**, no. 3, 036017 (2017) [arXiv:1704.03014 [hep-ph]].

[11] R. D. Peccei and H. R. Quinn, *CP Conservation in the Presence of Instantons*, Phys. Rev. Lett. **38**, 1440 (1977).

[12] S. Weinberg, *A New Light Boson?*, Phys. Rev. Lett. **40**, 223 (1978).

[13] F. Wilczek, *Problem of Strong P and T Invariance in the Presence of Instantons*, Phys. Rev. Lett. **40**, 279 (1978).

[14] G. 't Hooft, *Symmetry Breaking Through Bell-Jackiw Anomalies*, Phys. Rev. Lett. **37**, 8 (1976).

[15] G. 't Hooft, *Computation of the Quantum Effects Due to a Four-Dimensional Pseudoparticle*, Phys. Rev. D **14**, 3432 (1976) Erratum: [Phys. Rev. D **18**, 2199 (1978)].

[16] M. Dine, W. Fischler and M. Srednicki, *A Simple Solution to the Strong CP Problem with a Harmless Axion*, Phys. Lett. **104B**, 199 (1981).

[17] A. R. Zhitnitsky, *On Possible Suppression of the Axion Hadron Interactions.* (In Russian), Sov. J. Nucl. Phys. **31**, 260 (1980) [Yad. Fiz. **31**, 497 (1980)].

[18] J. E. Kim, *Weak Interaction Singlet and Strong CP Invariance*, Phys. Rev. Lett. **43**, 103 (1979).

[19] M. A. Shifman, A. I. Vainshtein and V. I. Zakharov, *Can Confinement Ensure Natural CP Invariance of Strong Interactions?*, Nucl. Phys. B **166**, 493 (1980).

[20] A. Ringwald, *Axions and Axion-Like Particles*, arXiv:1407.0546 [hep-ph].

[21] P. Svrcek and E. Witten, *Axions In String Theory*, JHEP **0606**, 051 (2006) [hep-th/0605206].

[22] A. Arvanitaki, S. Dimopoulos, S. Dubovsky, N. Kaloper and J. March-Russell, *String Axiverse*, Phys. Rev. D **81**, 123530 (2010) [arXiv:0905.4720 [hep-th]].

[23] K. Freese, J. A. Frieman and A. V. Olinto, *Natural inflation with pseudo - Nambu-Goldstone bosons*, Phys. Rev. Lett. **65**, 3233 (1990).

[24] J. Preskill, M. B. Wise and F. Wilczek, *Cosmology of the Invisible Axion*, Phys. Lett. **120B** (1983) 127.

[25] L. F. Abbott and P. Sikivie, *A Cosmological Bound on the Invisible Axion*, Phys. Lett. **120B**, 133 (1983).

[26] D. J. E. Marsh, *Axion Cosmology*, Phys. Rept. **643**, 1 (2016) [arXiv:1510.07633 [astro-ph.CO]].

[27] K. R. Dienes and B. Thomas, *Dynamical Dark Matter: I. Theoretical Overview*, Phys. Rev. D **85**, 083523 (2012) [arXiv:1106.4546 [hep-ph]].

[28] Y. Akrami *et al.* [Planck Collaboration], *Planck 2018 results. I. Overview and the cosmological legacy of Planck*, arXiv:1807.06205 [astro-ph.CO].

[29] A. G. Riess *et al.* [Supernova Search Team], *Observational evidence from supernovae for an accelerating universe and a cosmological constant*, Astron. J. **116**, 1009 (1998) [astro-ph/9805201].

[30] W. Rindler, *Visual horizons in world-models*, Gen. Rel. Grav. **34**, 133 (2002) [Mon. Not. Roy. Astron. Soc. **116**, 662 (1956)].

[31] A. H. Guth, *The Inflationary Universe: A Possible Solution to the Horizon and Flatness Problems*, Phys. Rev. D **23**, 347 (1981) [Adv. Ser. Astrophys. Cosmol. **3**, 139 (1987)].

[32] T. S. Bunch and P. C. W. Davies, *Quantum Field Theory in de Sitter Space: Renormalization by Point Splitting*, Proc. Roy. Soc. Lond. A **360**, 117 (1978).

[33] Y. Akrami *et al.* [Planck Collaboration], *Planck 2018 results. X. Constraints on inflation*, arXiv:1807.06211 [astro-ph.CO].

[34] A. Ringwald, *Exploring the Role of Axions and Other WISPs in the Dark Universe*, Phys. Dark Univ. **1**, 116 (2012) [arXiv:1210.5081 [hep-ph]].

[35] D. Cadamuro and J. Redondo, *Cosmological bounds on pseudo Nambu-Goldstone bosons*, JCAP **1202**, 032 (2012) [arXiv:1110.2895 [hep-ph]].

[36] P. Arias, D. Cadamuro, M. Goodsell, J. Jaeckel, J. Redondo and A. Ringwald, *WISPy Cold Dark Matter*, JCAP **1206**, 013 (2012) [arXiv:1201.5902 [hep-ph]].

[37] M. Srednicki, *Axion Couplings to Matter. 1. CP Conserving Parts*, Nucl. Phys. B **260**, 689 (1985).

[38] P. W. Graham, I. G. Irastorza, S. K. Lamoreaux, A. Lindner and K. A. van Bibber, *Experimental Searches for the Axion and Axion-Like Particles*, Ann. Rev. Nucl. Part. Sci. **65**, 485 (2015) [arXiv:1602.00039 [hep-ex]].

[39] S. Alexander, E. McDonough and R. Sims, *V-mode Polarization in Axion Inflation and Preheating*, Phys. Rev. D **96**, no. 6, 063506 (2017) [arXiv:1704.00838 [gr-qc]].

[40] S. Alexander and R. Sims, *Detecting axions via induced electron spin precession*, Phys. Rev. D **98**, no. 1, 015011 (2018) [arXiv:1702.01459 [hep-ph]].

[41] S. Alexander, E. McDonough, R. Sims and N. Yunes, *Hidden-Sector Modifications to Gravitational Waves From Binary Inspirals*, Class. Quant. Grav. **35**, 235012 (2018) [arXiv:1808.05286 [gr-qc]].

[42] J. Kovac, E. M. Leitch, C. Pryke, J. E. Carlstrom, N. W. Halverson and W. L. Holzapfel, *Detection of polarization in the cosmic microwave background using DASI,* Nature **420**, 772 (2002) [astro-ph/0209478].

N. Aghanim *et al.* [Planck Collaboration], *Planck 2015 results. XI. CMB power spectra, likelihoods, and robustness of parameters,* Astron. Astrophys. **594**, A11 (2016) [arXiv:1507.02704 [astro-ph.CO]].

[43] F. Finelli and M. Galaverni, *Rotation of Linear Polarization Plane and Circular Polarization from Cosmological Pseudo-Scalar Fields,* Phys. Rev. D **79**, 063002 (2009) [arXiv:0802.4210 [astro-ph]].

[44] A. Kosowsky, *Cosmic microwave background polarization*, Annals Phys. **246**, 49 (1996) [astro-ph/9501045].

[45] M. Giovannini, *The V-mode polarization of the Cosmic Microwave Background*, Phys. Rev. D **80**, 123013 (2009) [arXiv:0909.3629 [astro-ph.CO]].

[46] S. Alexander, D. Jyoti, A. Kosowsky and A. Marciano, *Dynamics of Gauge Field Inflation*, JCAP **1505**, 005 (2015) [arXiv:1408.4118 [hep-th]].

[47] A. Maleknejad and M. M. Sheikh-Jabbari, *Gauge-flation: Inflation From Non-Abelian Gauge Fields*, Phys. Lett. B **723**, 224 (2013) [arXiv:1102.1513 [hep-ph]].

[48] P. Adshead and M. Wyman, *Chromo-Natural Inflation: Natural inflation on a steep potential with classical non-Abelian gauge fields*, Phys. Rev. Lett. **108**, 261302 (2012) [arXiv:1202.2366 [hep-th]].

[49] M. M. Anber and L. Sorbo, *Naturally inflating on steep potentials through electromagnetic dissipation*, Phys. Rev. D **81**, 043534 (2010) [arXiv:0908.4089 [hep-th]].

[50] P. Adshead, J. T. Giblin, T. R. Scully and E. I. Sfakianakis, *Gauge-preheating and the end of axion inflation,* JCAP **1512**, no. 12, 034 (2015) [arXiv:1502.06506 [astro-ph.CO]].

[51] E. McDonough, H. Bazrafshan Moghaddam and R. H. Brandenberger, *Preheating and Entropy Perturbations in Axion Monodromy Inflation,* JCAP **1605**, no. 05, 012 (2016) [arXiv:1601.07749 [hep-th]].

[52] P. Adshead, J. T. Giblin, T. R. Scully and E. I. Sfakianakis, *Magnetogenesis from axion inflation*, JCAP **1610**, 039 (2016) [arXiv:1606.08474 [astro-ph.CO]].

[53] P. Adshead and E. I. Sfakianakis, *Fermion production during and after axion inflation,* JCAP **1511**, no. 11, 021 (2015) [arXiv:1508.00891 [hep-ph]].

[54] P. Adshead and E. I. Sfakianakis, *Leptogenesis from left-handed neutrino production during axion inflation*, Phys. Rev. Lett. **116**, no. 9, 091301 (2016) [arXiv:1508.00881 [hep-ph]].

[55] S. Alexander, S. Cormack and R. Sims, *Chirality and Circular Polarization in Models of Inflation,* arXiv:1606.05357 [astro-ph.CO].

[56] W. Hu, *CMB temperature and polarization anisotropy fundamentals*, Annals Phys. **303**, 203 (2003) doi:10.1016/S0003-4916(02)00022-2 [astro-ph/0210696].

[57] D. H. Lyth and A. R. Liddle, *The primordial density perturbation: Cosmology, inflation and the origin of structure*, Cambridge, UK: Cambridge Univ. Pr. (2009) 497 p

[58] S. T. Staggs and D. Barkats and J. O. Gundersen and M. M. Hedman and C. P. Herzog and J. J. McMahon and B. Winstein, *Calibrating CMB polarization telescopes*, AIP Conference Proceedings, 609 1 (2002)

[59] P. A. R. Ade *et al.* [Planck Collaboration], *Planck 2015 results. XX. Constraints on inflation*, Astron. Astrophys. **594**, A20 (2016) [arXiv:1502.02114 [astro-ph.CO]].

[60] F. Marchesano, G. Shiu and A. M. Uranga, *F-term Axion Monodromy Inflation*, JHEP **1409**, 184 (2014) [arXiv:1404.3040 [hep-th]].

[61] D. Baumann, *TASI Lectures on Inflation,* arXiv:0907.5424 [hep-th].

[62] J. F. Koksma and T. Prokopec, *Fermion Propagator in Cosmological Spaces with Constant Deceleration,* Class. Quant. Grav. **26**, 125003 (2009) [arXiv:0901.4674 [gr-qc]].

[63] L. J. Dixon, *A brief introduction to modern amplitude methods*, arXiv:1310.5353 [hep-ph].

[64] M. D. Schwartz, *Quantum Field Theory and the Standard Model*, ISBN-9781107034730.

[65] P. De Causmaecker, R. Gastmans, W. Troost and T. T. Wu, *Multiple Bremsstrahlung in Gauge Theories at High-Energies. 1. General Formalism for Quantum Electrodynamics*, Nucl. Phys. B **206**, 53 (1982).

[66] F. A. Berends, R. Kleiss, P. De Causmaecker, R. Gastmans, W. Troost and T. T. Wu, *Multiple Bremsstrahlung in Gauge Theories at High-Energies. 2. Single Bremsstrahlung*, Nucl. Phys. B **206**, 61 (1982).

[67] N. Barnaby, E. Pajer and M. Peloso, *Gauge Field Production in Axion Inflation: Consequences for Monodromy, non-Gaussianity in the CMB, and Gravitational Waves at Interferometers,* Phys. Rev. D **85**, 023525 (2012) [arXiv:1110.3327 [astro-ph.CO]];
N. Barnaby, R. Namba and M. Peloso, *Phenomenology of a Pseudo-Scalar Inflaton: Naturally Large Nongaussianity,* JCAP **1104**, 009 (2011) [arXiv:1102.4333 [astro-ph.CO]];
N. Barnaby and M. Peloso, *Large Nongaussianity in Axion Inflation,* Phys. Rev. Lett. **106**, 181301 (2011) [arXiv:1011.1500 [hep-ph]].

[68] Y. Shtanov, J. H. Traschen and R. H. Brandenberger, *Universe reheating after inflation,* Phys. Rev. D **51**, 5438 (1995) [hep-ph/9407247].

[69] J. H. Traschen and R. H. Brandenberger, *Particle Production During Out-of-equilibrium Phase Transitions,* Phys. Rev. D **42**, 2491 (1990).

[70] L. Kofman, A. D. Linde and A. A. Starobinsky, *Reheating after inflation,* Phys. Rev. Lett. **73**, 3195 (1994) [hep-th/9405187].

[71] L. Kofman, A. D. Linde and A. A. Starobinsky, *Towards the theory of reheating after inflation,* Phys. Rev. D **56**, 3258 (1997) [hep-ph/9704452].

[72] R. Allahverdi, R. Brandenberger, F. Y. Cyr-Racine and A. Mazumdar, *Reheating in Inflationary Cosmology: Theory and Applications,* Ann. Rev. Nucl. Part. Sci. **60**, 27 (2010) [arXiv:1001.2600 [hep-th]].

[73] M. A. Amin, M. P. Hertzberg, D. I. Kaiser and J. Karouby, *Nonperturbative Dynamics Of Reheating After Inflation: A Review,* Int. J. Mod. Phys. D **24**, 1530003 (2014) [arXiv:1410.3808 [hep-ph]].

[74] P. B. Greene and L. Kofman, *Preheating of fermions*, Phys. Lett. B **448**, 6 (1999) [hep-ph/9807339].

P. B. Greene and L. Kofman, *On the theory of fermionic preheating*, Phys. Rev. D **62**, 123516 (2000) [hep-ph/0003018].

[75] M. Peloso and L. Sorbo, *Preheating of massive fermions after inflation: Analytical results*, *JHEP* **0005** (2000) 016, [hep-ph/0003045].

J. Garcia-Bellido, S. Mollerach, and E. Roulet, *Fermion production during preheating after hybrid inflation*, *JHEP* **0002** (2000) 034, [hep-ph/0002076].

S. Tsujikawa, B. A. Bassett, and F. Viniegra, *Multifield fermionic preheating*, *JHEP* **0008** (2000) 019, [hep-ph/0006354].

[76] J. M. Nagy *et al.* [SPIDER Collaboration], *A New Limit on CMB Circular Polarization from SPIDER*, [arXiv:1704.00215 [astro-ph.CO]].

[77] R. Mainini *et al.*, *An improved upper limit to the CMB circular polarization at large angular scales*, JCAP **1308**, 033 (2013) [arXiv:1307.6090 [astro-ph.CO]].

[78] R. H. Brandenberger, A. Nayeri, S. P. Patil and C. Vafa, *Tensor Modes from a Primordial Hagedorn Phase of String Cosmology*, Phys. Rev. Lett. **98**, 231302 (2007) [hep-th/0604126].

R. H. Brandenberger, A. Nayeri and S. P. Patil, *Closed String Thermodynamics and a Blue Tensor Spectrum*, Phys. Rev. D **90**, no. 6, 067301 (2014) [arXiv:1403.4927 [astro-ph.CO]].

[79] Y. F. Cai, J. O. Gong, S. Pi, E. N. Saridakis and S. Y. Wu, *On the possibility of blue tensor spectrum within single field inflation*, Nucl. Phys. B **900**, 517 (2015) [arXiv:1412.7241 [hep-th]].

A. Ashoorioon, K. Dimopoulos, M. M. Sheikh-Jabbari and G. Shiu, *Non-Bunch-Davies initial state reconciles chaotic models with BICEP and Planck*, Phys. Lett. B **737**, 98 (2014) [arXiv:1403.6099 [hep-th]].

Y. Wang and W. Xue, *Inflation and Alternatives with Blue Tensor Spectra*, JCAP **1410**, no. 10, 075 (2014) [arXiv:1403.5817 [astro-ph.CO]].

[80] R. Namba, M. Peloso, M. Shiraishi, L. Sorbo and C. Unal, *Scale-dependent gravitational waves from a rolling axion*, JCAP **1601**, no. 01, 041 (2016) [arXiv:1509.07521 [astro-ph.CO]].

[81] A. Kandus, K. E. Kunze and C. G. Tsagas, *Primordial magnetogenesis*, Phys. Rept. **505**, 1 (2011) [arXiv:1007.3891 [astro-ph.CO]].

R. Durrer and A. Neronov, *Cosmological Magnetic Fields: Their Generation, Evolution and Observation*, Astron. Astrophys. Rev. **21**, 62 (2013) [arXiv:1303.7121 [astro-ph.CO]].

K. Subramanian, *The origin, evolution and signatures of primordial magnetic fields*, Rept. Prog. Phys. **79**, no. 7, 076901 (2016) [arXiv:1504.02311 [astro-ph.CO]].

[82] A. Challinor, *Microwave background polarization in cosmological models*, Phys. Rev. D **62**, 043004 (2000) [astro-ph/9911481].

[83] R. R. Caldwell, V. Gluscevic and M. Kamionkowski, *Cross-Correlation of Cosmological Birefringence with CMB Temperature*, Phys. Rev. D **84**, 043504 (2011) [arXiv:1104.1634 [astro-ph.CO]].

[84] P. Sikivie, *Experimental Tests of the Invisible Axion*, Phys. Rev. Lett. **51**, 1415 (1983) Erratum: [Phys. Rev. Lett. **52**, 695 (1984)].

[85] S. J. Asztalos *et al.* [ADMX Collaboration], *Large scale microwave cavity search for dark matter axions*, Phys. Rev. D **64**, 092003 (2001).

[86] R. Barbieri *et al.*, *Searching for galactic axions through magnetized media: the QUAX proposal*, Phys. Dark Univ. **15**, 135 (2017) [arXiv:1606.02201 [hep-ph]].

[87] S. J. Asztalos *et al.* [ADMX Collaboration], *A SQUID-based microwave cavity search for dark-matter axions*, Phys. Rev. Lett. **104**, 041301 (2010) [arXiv:0910.5914 [astro-ph.CO]].

[88] Y. Kahn, B. R. Safdi and J. Thaler, *Broadband and Resonant Approaches to Axion Dark Matter Detection*, Phys. Rev. Lett. **117**, no. 14, 141801 (2016) [arXiv:1602.01086 [hep-ph]].

[89] M. Dine and W. Fischler, *The Not So Harmless Axion*, Phys. Lett. **120B**, 137 (1983).

[90] J. E. Kim, *Weak Interaction Singlet and Strong CP Invariance*, Phys. Rev. Lett. **43**, 103 (1979).

[91] M. A. Shifman, A. I. Vainshtein and V. I. Zakharov, *Can Confinement Ensure Natural CP Invariance of Strong Interactions?*, Nucl. Phys. B **166**, 493 (1980).

[92] M. Dine, W. Fischler and M. Srednicki, *A Simple Solution to the Strong CP Problem with a Harmless Axion*, Phys. Lett. **104B**, 199 (1981); A. R. Zhitnitsky, *On Possible Suppression of the Axion Hadron Interactions.* (In Russian), Sov. J. Nucl. Phys. **31**, 260 (1980) [Yad. Fiz. **31**, 497 (1980)].

[93] C. T. Hill, *Axion Induced Oscillating Electric Dipole Moments*, Phys. Rev. D **91**, no. 11, 111702 (2015) [arXiv:1504.01295 [hep-ph]]; C. T. Hill, *Axion Induced Oscillating Electric Dipole Moment of the Electron*, Phys. Rev. D **93**, no. 2, 025007 (2016) [arXiv:1508.04083 [hep-ph]].

[94] C. Cao and A. Zhitnitsky, *Axion detection via Topological Casimir Effect*, arXiv:1702.00012 [hep-ph].

[95] D. Budker, P. W. Graham, M. Ledbetter, S. Rajendran and A. Sushkov, *Proposal for a Cosmic Axion Spin Precession Experiment (CASPEr)*, Phys. Rev. X **4**, no. 2, 021030 (2014) [arXiv:1306.6089 [hep-ph]].

[96] H. Georgi, D. B. Kaplan and L. Randall, *Manifesting the Invisible Axion at Low-energies*, Phys. Lett. **169B**, 73 (1986).

[97] A. Arvanitaki, S. Dimopoulos and K. Van Tilburg, *Sound of Dark Matter: Searching for Light Scalars with Resonant-Mass Detectors*, Phys. Rev. Lett. **116**, no. 3, 031102 (2016) [arXiv:1508.01798 [hep-ph]].

[98] M. Pospelov and A. Ritz, *Electric dipole moments as probes of new physics*, Annals Phys. **318**, 119 (2005) [hep-ph/0504231].

[99] J. Baron *et al.* [ACME Collaboration], *Order of Magnitude Smaller Limit on the Electric Dipole Moment of the Electron*, Science **343**, 269 (2014) [arXiv:1310.7534 [physics.atom-ph]].

[100] M. Cicoli, M. Goodsell and A. Ringwald, *The type IIB string axiverse and its low-energy phenomenology*, JHEP **1210**, 146 (2012) [arXiv:1206.0819 [hep-th]].

[101] A. V. Derbin, I. S. Drachnev, A. S. Kayunov and V. N. Muratova, *Constraints on the axion-electron coupling constant for solar axions appearing owing to bremsstrahlung and the Compton process*, JETP Lett. **95**, 339 (2012) [Pisma Zh. Eksp. Teor. Fiz. **95**, 379 (2012)] [arXiv:1206.4142 [hep-ex]].

[102] K. Abe *et al.*, *Search for solar axions in XMASS, a large liquid-xenon detector*, Phys. Lett. B **724**, 46 (2013) [arXiv:1212.6153 [astro-ph.CO]].

[103] E. Armengaud *et al.*, *Axion searches with the EDELWEISS-II experiment*, JCAP **1311**, 067 (2013) [arXiv:1307.1488 [astro-ph.CO]].

E. Armengaud *et al.* [EDELWEISS Collaboration], *Searches for electron interactions induced by new physics in the EDELWEISS-III Germanium bolometers*, Phys. Rev. D **98**, no. 8, 082004 (2018) [arXiv:1808.02340 [hep-ex]].

[104] E. Aprile *et al.* [XENON100 Collaboration], *First Axion Results from the XENON100 Experiment*, Phys. Rev. D **90**, no. 6, 062009 (2014) Erratum: [Phys. Rev. D **95**, no. 2, 029904 (2017)] [arXiv:1404.1455 [astro-ph.CO]].

[105] D. S. Akerib *et al.* [LUX Collaboration], *First Searches for Axions and Axionlike Particles with the LUX Experiment*, Phys. Rev. Lett. **118**, no. 26, 261301 (2017) [arXiv:1704.02297 [astro-ph.CO]].

[106] P. Gondolo and G. Raffelt, *Solar neutrino limit on axions and keV-mass bosons*, Phys. Rev. D **79**, 107301 (2009) [arXiv:0807.2926 [astro-ph]].

[107] N. Viaux, M. Catelan, P. B. Stetson, G. Raffelt, J. Redondo, A. A. R. Valcarce and A. Weiss, *Neutrino and axion bounds from the globular cluster M5 (NGC 5904)*, Phys. Rev. Lett. **111**, 231301 (2013) [arXiv:1311.1669 [astro-ph.SR]].

[108] B. P. Abbott *et al.* [LIGO Scientific and Virgo Collaborations], *Observation of Gravitational Waves from a Binary Black Hole Merger*, Phys. Rev. Lett. **116**, no. 6, 061102 (2016) [arXiv:1602.03837 [gr-qc]].

[109] B. P. Abbott *et al.* [LIGO Scientific and Virgo Collaborations], *GW151226: Observation of Gravitational Waves from a 22-Solar-Mass Binary Black Hole Coalescence*, Phys. Rev. Lett. **116**, no. 24, 241103 (2016) [arXiv:1606.04855 [gr-qc]].

[110] B. P. Abbott *et al.* [LIGO Scientific and Virgo Collaborations], *GW170814: A Three-Detector Observation of Gravitational Waves from a Binary Black Hole Coalescence*, Phys. Rev. Lett. **119**, no. 14, 141101 (2017) [arXiv:1709.09660 [gr-qc]].

[111] B. P. Abbott *et al.* [LIGO Scientific and Virgo Collaborations], *GW170608: Observation of a 19-solar-mass Binary Black Hole Coalescence*, Astrophys. J. **851**, no. 2, L35 (2017) [arXiv:1711.05578 [astro-ph.HE]].

[112] B. P. Abbott *et al.* [LIGO Scientific and VIRGO Collaborations], *GW170104: Observation of a 50-Solar-Mass Binary Black Hole Coalescence at Redshift 0.2*, Phys. Rev. Lett. **118**, no. 22, 221101 (2017) [arXiv:1706.01812 [gr-qc]].

[113] B. P. Abbott *et al.* [LIGO Scientific and Virgo Collaborations], *GW170817: Observation of Gravitational Waves from a Binary Neutron Star Inspiral*, Phys. Rev. Lett. **119**, no. 16, 161101 (2017) [arXiv:1710.05832 [gr-qc]].

[114] K. Chamberlain and N. Yunes, *Theoretical Physics Implications of Gravitational Wave Observation with Future Detectors*, Phys. Rev. D **96**, no. 8, 084039 (2017) [arXiv:1704.08268 [gr-qc]].

[115] C. Deffayet and K. Menou, *Probing Gravity with Spacetime Sirens*, Astrophys. J. **668**, L143 (2007) [arXiv:0709.0003 [astro-ph]].

[116] L. Visinelli, N. Bolis and S. Vagnozzi, *Brane-world extra dimensions in light of GW170817*, Phys. Rev. D **97**, no. 6, 064039 (2018) [arXiv:1711.06628 [gr-qc]].

[117] K. Pardo, M. Fishbach, D. E. Holz and D. N. Spergel, *Limits on the number of spacetime dimensions from GW170817*, JCAP **1807**, no. 07, 048 (2018) [arXiv:1801.08160 [gr-qc]].

[118] B. P. Abbott *et al.* [LIGO Scientific and Virgo Collaborations], arXiv:1811.00364 [gr-qc].

[119] N. Yunes, K. Yagi and F. Pretorius, *Theoretical Physics Implications of the Binary Black-Hole Mergers GW150914 and GW151226*, Phys. Rev. D **94**, no. 8, 084002 (2016) [arXiv:1603.08955 [gr-qc]].

[120] J. M. Ezquiaga and M. Zumalacarregui, *Dark Energy After GW170817: Dead Ends and the Road Ahead*, Phys. Rev. Lett. **119**, no. 25, 251304 (2017) [arXiv:1710.05901 [astro-ph.CO]].

[121] P. Creminelli and F. Vernizzi, *Dark Energy after GW170817 and GRB170817A*, Phys. Rev. Lett. **119**, no. 25, 251302 (2017) [arXiv:1710.05877 [astro-ph.CO]].

[122] J. Sakstein and B. Jain, *Implications of the Neutron Star Merger GW170817 for Cosmological Scalar-Tensor Theories*, Phys. Rev. Lett. **119**, no. 25, 251303 (2017) [arXiv:1710.05893 [astro-ph.CO]].

[123] I. Goldman and S. Nussinov, *Weakly Interacting Massive Particles and Neutron Stars*, Phys. Rev. D **40**, 3221 (1989).

[124] C. Kouvaris, *WIMP Annihilation and Cooling of Neutron Stars*, Phys. Rev. D **77**, 023006 (2008) [arXiv:0708.2362 [astro-ph]].

[125] C. Kouvaris and P. Tinyakov, *Can Neutron stars constrain Dark Matter?*, Phys. Rev. D **82**, 063531 (2010) [arXiv:1004.0586 [astro-ph.GA]].

[126] A. de Lavallaz and M. Fairbairn, *Neutron Stars as Dark Matter Probes*, Phys. Rev. D **81**, 123521 (2010) [arXiv:1004.0629 [astro-ph.GA]].

[127] C. Kouvaris and P. Tinyakov, *Constraining Asymmetric Dark Matter through observations of compact stars*, Phys. Rev. D **83**, 083512 (2011) [arXiv:1012.2039 [astro-ph.HE]].

[128] S. D. McDermott, H. B. Yu and K. M. Zurek, *Constraints on Scalar Asymmetric Dark Matter from Black Hole Formation in Neutron Stars*, Phys. Rev. D **85**, 023519 (2012) [arXiv:1103.5472 [hep-ph]].

[129] T. Güver, A. E. Erkoca, M. Hall Reno and I. Sarcevic, *On the capture of dark matter by neutron stars*, JCAP **1405**, 013 (2014) [arXiv:1201.2400 [hep-ph]].

[130] J. Bramante, K. Fukushima and J. Kumar, *Constraints on bosonic dark matter from observation of old neutron stars*, Phys. Rev. D **87**, no. 5, 055012 (2013) [arXiv:1301.0036 [hep-ph]].

[131] N. F. Bell, A. Melatos and K. Petraki, *Realistic neutron star constraints on bosonic asymmetric dark matter*, Phys. Rev. D **87**, no. 12, 123507 (2013) [arXiv:1301.6811 [hep-ph]].

[132] J. Bramante, K. Fukushima, J. Kumar and E. Stopnitzky, *Bounds on self-interacting fermion dark matter from observations of old neutron stars*, Phys. Rev. D **89**, no. 1, 015010 (2014) [arXiv:1310.3509 [hep-ph]].

[133] J. Bramante, A. Delgado and A. Martin, *Multiscatter stellar capture of dark matter*, Phys. Rev. D **96**, no. 6, 063002 (2017) [arXiv:1703.04043 [hep-ph]].

[134] J. Bramante, T. Linden and Y. D. Tsai, *Searching for dark matter with neutron star mergers and quiet kilonovae*, Phys. Rev. D **97**, no. 5, 055016 (2018) [arXiv:1706.00001 [hep-ph]].

[135] H. Zheng, K. J. Sun and L. W. Chen, *Old neutron stars as probes of isospin-violating dark matter*, Astrophys. J. **800**, no. 2, 141 (2015) [arXiv:1408.2926 [nucl-th]].

[136] F. Sandin and P. Ciarcelluti, *Effects of mirror dark matter on neutron stars*, Astropart. Phys. **32**, 278 (2009) [arXiv:0809.2942 [astro-ph]].

[137] N. Raj, P. Tanedo and H. B. Yu, *Neutron stars at the dark matter direct detection frontier*, Phys. Rev. D **97**, no. 4, 043006 (2018) [arXiv:1707.09442 [hep-ph]].

[138] J. Kopp, R. Laha, T. Opferkuch and W. Shepherd, *Cuckoo's Eggs in Neutron Stars: Can LIGO Hear Chirps from the Dark Sector?*, arXiv:1807.02527 [hep-ph].

[139] A. Nelson, S. Reddy and D. Zhou, *Dark halos around neutron stars and gravitational waves*, arXiv:1803.03266 [hep-ph].

[140] D. Croon, A. E. Nelson, C. Sun, D. G. E. Walker and Z. Z. Xianyu, *Hidden-Sector Spectroscopy with Gravitational Waves from Binary Neutron Stars*, Astrophys. J. **858**, no. 1, L2 (2018) [arXiv:1711.02096 [hep-ph]].

[141] J. Ellis, A. Hektor, G. Hütsi, K. Kannike, L. Marzola, M. Raidal and V. Vaskonen, *Search for Dark Matter Effects on Gravitational Signals from Neutron Star Mergers*, Phys. Lett. B **781**, 607 (2018) [arXiv:1710.05540 [astro-ph.CO]].

[142] J. Huang, M. C. Johnson, L. Sagunski, M. Sakellariadou and J. Zhang, *Prospects for axion searches with Advanced LIGO through binary mergers*, arXiv:1807.02133 [hep-ph].

[143] J. Ellis, G. Hütsi, K. Kannike, L. Marzola, M. Raidal and V. Vaskonen, *Dark Matter Effects On Neutron Star Properties*, Phys. Rev. D **97**, no. 12, 123007 (2018) [arXiv:1804.01418 [astro-ph.CO]].

[144] K. Petraki and R. R. Volkas, *Review of asymmetric dark matter*, Int. J. Mod. Phys. A **28**, 1330028 (2013) [arXiv:1305.4939 [hep-ph]].

[145] K. Petraki, L. Pearce and A. Kusenko, *Self-interacting asymmetric dark matter coupled to a light massive dark photon*, JCAP **1407**, 039 (2014) [arXiv:1403.1077 [hep-ph]].

[146] Z. Rezaei, *Double dark-matter admixed neutron star*, arXiv:1807.01781 [astro-ph.HE].

[147] S. C. Leung, M. C. Chu and L. M. Lin, *Dark-matter admixed neutron stars*, Phys. Rev. D **84**, 107301 (2011) [arXiv:1111.1787 [astro-ph.CO]].

[148] D. Krause, H. T. Kloor and E. Fischbach, *Multipole radiation from massive fields: Application to binary pulsar systems*, Phys. Rev. D **49**, 6892 (1994).

[149] T. Damour and A. M. Polyakov, *String theory and gravity*, Gen. Rel. Grav. **26**, 1171 (1994) [gr-qc/9411069].

[150] C. M. Will, *Testing scalar - tensor gravity with gravitational wave observations of inspiraling compact binaries*, Phys. Rev. D **50**, 6058 (1994) [gr-qc/9406022].

[151] J. Alsing, E. Berti, C. M. Will and H. Zaglauer, *Gravitational radiation from compact binary systems in the massive Brans-Dicke theory of gravity*, Phys. Rev. D **85**, 064041 (2012) [arXiv:1112.4903 [gr-qc]].

[152] L. Sagunski, J. Zhang, M. C. Johnson, L. Lehner, M. Sakellariadou, S. L. Liebling, C. Palenzuela and D. Neilsen, *Neutron star mergers as a probe of modifications of general relativity with finite-range scalar forces*, Phys. Rev. D **97**, no. 6, 064016 (2018) [arXiv:1709.06634 [gr-qc]].

[153] E. Berti, K. Yagi and N. Yunes, *Extreme Gravity Tests with Gravitational Waves from Compact Binary Coalescences: (I) Inspiral-Merger*, Gen. Rel. Grav. **50**, no. 4, 46 (2018) [arXiv:1801.03208 [gr-qc]].

[154] S. Mirshekari and C. M. Will, *Compact binary systems in scalar-tensor gravity: Equations of motion to 2.5 post-Newtonian order*, Phys. Rev. D **87**, no. 8, 084070 (2013) [arXiv:1301.4680 [gr-qc]].

[155] B. Bertotti, L. Iess and P. Tortora, *A test of general relativity using radio links with the Cassini spacecraft*, Nature **425**, 374 (2003).

[156] B. Allen, W. G. Anderson, P. R. Brady, D. A. Brown and J. D. E. Creighton, *FINDCHIRP: An Algorithm for detection of gravitational waves from inspiraling compact binaries*, Phys. Rev. D **85**, 122006 (2012) [gr-qc/0509116].

[157] N. Yunes, K. G. Arun, E. Berti and C. M. Will, *Post-Circular Expansion of Eccentric Binary Inspirals: Fourier-Domain Waveforms in the Stationary Phase Approximation*, Phys. Rev. D **80**, no. 8, 084001 (2009) Erratum: [Phys. Rev. D **89**, no. 10, 109901 (2014)] [arXiv:0906.0313 [gr-qc]].

[158] E. K. Porter and N. J. Cornish, *Fisher versus Bayes: A comparison of parameter estimation techniques for massive black hole binaries to high redshifts with eLISA*, Phys. Rev. D **91**, no. 10, 104001 (2015) [arXiv:1502.05735 [gr-qc]].

[159] M. Vallisneri, *Use and abuse of the Fisher information matrix in the assessment of gravitational-wave parameter-estimation prospects*, Phys. Rev. D **77**, 042001 (2008) [gr-qc/0703086 [GR-QC]].

[160] P. Ajith *et al.*, *A Template bank for gravitational waveforms from coalescing binary black holes. I. Non-spinning binaries*, Phys. Rev. D **77**, 104017 (2008) Erratum: [Phys. Rev. D **79**, 129901 (2009)] [arXiv:0710.2335 [gr-qc]].

[161] B. P. Abbott *et al.* [LIGO Scientific and Virgo Collaborations], *The basic physics of the binary black hole merger GW150914*, Annalen Phys. **529**, no. 1-2, 1600209 (2017) doi:10.1002/andp.201600209 [arXiv:1608.01940 [gr-qc]].

[162] G. F. Giudice, M. McCullough and A. Urbano, *Hunting for Dark Particles with Gravitational Waves*, JCAP **1610**, no. 10, 001 (2016) [arXiv:1605.01209 [hep-ph]].

[163] L. Lehner, S. L. Liebling, C. Palenzuela, O. L. Caballero, E. O'Connor, M. Anderson and D. Neilsen, *Unequal mass binary neutron star mergers and multimessenger signals*, Class. Quant. Grav. **33**, no. 18, 184002 (2016) [arXiv:1603.00501 [gr-qc]].

[164] I. Mandel, C. P. L. Berry, F. Ohme, S. Fairhurst and W. M. Farr, *Parameter estimation on compact binary coalescences with abruptly terminating gravitational waveforms*, Class. Quant. Grav. **31**, 155005 (2014) [arXiv:1404.2382 [gr-qc]].

[165] K. Yagi and N. Yunes, *I-Love-Q Relations in Neutron Stars and their Applications to Astrophysics, Gravitational Waves and Fundamental Physics*, Phys. Rev. D **88**, no. 2, 023009 (2013) [arXiv:1303.1528 [gr-qc]].

[166] B. P. Abbott *et al.* [KAGRA and LIGO Scientific and VIRGO Collaborations], *Prospects for Observing and Localizing Gravitational-Wave Transients with Advanced LIGO, Advanced Virgo and KAGRA*, Living Rev. Rel. **21**, 3 (2018) [Living Rev. Rel. **19**, 1 (2016)] [arXiv:1304.0670 [gr-qc]].

[167] L. S. Collaboration, *LIGO-T15TBI: Instrument Science White Paper.*

[168] R. X. Adhikari, Rev. Mod. Phys. **86**, 121 (2014) doi:10.1103/RevModPhys.86.121 [arXiv:1305.5188 [gr-qc]].

[169] Available at http://www.et-gw.eu/index.php/etsensitivities

[170] S. Hild, S. Chelkowski, A. Freise, J. Franc, N. Morgado, R. Flaminio and R. DeSalvo, *A Xylophone Configuration for a third Generation Gravitational Wave Detector*, Class. Quant. Grav. **27**, 015003 (2010) [arXiv:0906.2655 [gr-qc]].

[171] B. P. Abbott *et al.* [LIGO Scientific Collaboration], *Exploring the Sensitivity of Next Generation Gravitational Wave Detectors*, Class. Quant. Grav. **34**, no. 4, 044001 (2017) [arXiv:1607.08697 [astro-ph.IM]].

[172] S. Khan, S. Husa, M. Hannam, F. Ohme, M. Pürrer, X. Jiménez Forteza and A. Bohé, *Frequency-domain gravitational waves from nonprecessing black-hole binaries. II. A phenomenological model for the advanced detector era*, Phys. Rev. D **93**, no. 4, 044007 (2016) [arXiv:1508.07253 [gr-qc]].

[173] J. D. Bekenstein, *Nonexistence of baryon number for static black holes*, Phys. Rev. D **5**, 1239 (1972);

J. D. Bekenstein, *Nonexistence of baryon number for black holes. ii*, Phys. Rev. D **5**, 2403 (1972).

[174] N. Yunes and F. Pretorius, *Fundamental Theoretical Bias in Gravitational Wave Astrophysics and the Parameterized Post-Einsteinian Framework*, Phys. Rev. D **80**, 122003 (2009) [arXiv:0909.3328 [gr-qc]].